Politecnico di Milano

SCHOOL OF INDUSTRIAL AND INFORMATION ENGINEERING
Dep. of Aerospace Science and Technology
M.Sc. Degree in Aeronautical Engineering

POLITECNICO
MILANO 1863

Impact of yaw-based wind farm control on wind turbines

Supervisor
Prof. Alessandro Croce

Co-Supervisor
PhD. Luca Sartori

Author:
Paride De Fidelibus – 883172

Academic Year 2018 – 2019

Ringraziamenti

Nell'iniziare questi Tesi, è doveroso ringraziare tutte le persone che hanno partecipato attivamente al lavoro. Per questo motivo, il mio primo enorme ringraziamento va al Professore Alessandro Croce per avermi offerto la bellissima opportunità di far parte, anche solo da studente, del team POLI-WIND, fonte di enorme conoscenza scientifica ma anche di crescita personale. Ringrazio infinitamente anche Luca Sartori, verso cui nutro una profonda stima, che grazie alla sua genialità mi ha guidato passo dopo passo alla realizzazione dello studio. Un sentito grazie anche a Stefano Cacciola, che con i suoi preziosi consigli ha aiutato a chiarire molti dei miei dubbi. Ringrazio infine anche Gabriele, con cui ho condiviso non solo tutta la magistrale ma soprattutto l'esperienza in galleria del vento.

Una dedica speciale va però a tutti i miei amici che hanno avuto un peso rilevante nel conseguimento di questo risultato che rappresenta da un lato, un punto di arrivo, ma dall'altro, un nuovo punto di partenza. Grazie per aver condiviso con me questo percorso, sia dentro, ma soprattutto fuori l'università. Grazie per tutti gli splendidi momenti passati insieme. Non ci separereremo mai.

Vorrei però spendere in particolare due parole per Simone, con cui ho condiviso tutta l'esperienza milanese e universitaria: sono convinto che senza di te questo traguardo sarebbe stato molto più difficile. Grazie per tutto quello che hai fatto. Potrai sempre contare su di me.

Un accenno speciale va anche al mio amico di sempre, Stefano, con cui ho passato tutti i momenti più belli della mia vita. Grazie per l'immancabile sostegno e per essere stato sempre al mio fianco, anche nelle difficoltà, nonostante la distanza. Che tu possa raggiungere i tuoi obiettivi e i tuoi sogni.

Dulcis in fundo, vorrei ringraziare la mia famiglia: senza di loro tutto questo non sarebbe stato possibile. In particolare i miei genitori, che non mi hanno mai fatto mancare nulla supportando ogni mia scelta; mia sorella Lara che mi accudisce affettuosamente e infine mio fratello Giovanni per la stima che nutre nei miei confronti. Questo risultato è anche vostro.

Sommario

Negli ultimi decenni la questione dell'inquinamento da combustibili fossili è diventata più importante, portando a un crescente interesse per le energie rinnovabili. Sebbene il vento sia una delle risorse energetiche più economiche, le istituzioni accademiche e industriali stanno cercando di trovare soluzioni per utilizzare gli impianti eolici nel modo più ottimizzato possibile, cercando di ridurre maggiormente il costo dell'energia. In questa prospettiva, il controllo coordinato dei parchi eolici può essere una delle soluzioni per ottenere una produzione di energia complessiva più elevata e una vita più lunga delle turbine. Tuttavia, l'uso di queste tecniche di controllo del parco eolico richiede un'analisi accurata per quanto riguarda i carichi massimi e a fatica sperimentati da una singola turbina, sia se quest'ultima costituisce la macchina su cui opera il controllo, o sia se questa sia la macchina interessata dal controllo attivo. In quest'ottica, questa analisi è di importanza cruciale perché stabilisce se il controllo scelto può essere applicato direttamente alle turbine eoliche esistenti o se, al contrario, è possibile progettarli ottimizzando tale controllo. Questa Tesi si concentrerà sulla comprensione degli effetti dell'applicazione di una di queste strategie su macchine esistenti, al fine di chiarirne la reale fattibilità negli attuali parchi eolici, attraverso metodologie basate su modelli numerici altamente dettagliati. In particolare, analizziamo con precisione il comportamento di una singola macchina posta a monte, che mira attivamente a guidare la scia sfruttando il disallineamento dell'angolo di imbardata. Pertanto, in questo lavoro studiamo in dettaglio l'incidenza di questa strategia sugli indicatori chiave di prestazione della turbina in termini di produzione di energia, carichi finali e di fatica attraverso un'analisi parametrica effettuata su due turbine di diverse caratteristiche e taglia con l'obiettivo di osservare se si possono trovare punti comuni. Successivamente, con una maggiore conoscenza del fenomeno, forniamo una configurazione strutturalmente fattibile di un rotore di una turbina eolica da 10 MW in grado di soddisfare i requisiti dettati dal controllo scelto. Gli esiti dello studio mostreranno che una possibile implementazione del disallineamento dell'imbardata per guidare le scie deve essere valutata attentamente in modo da evitare carichi eccessivi che possano compromettere l'integrità strutturale delle turbine.

Parole chiave: energia eolica, aerogeneratore, controllo di wind farm, reindirizzamento della scia, disallineamento di imbardata, analisi dei carichi, costo dell'energia, design della pala

Abstract

Over the last decades, the issue of fossil fuel pollution has become more important leading to an increasing interest in renewable energy. Although wind is one of the lowest-priced energy resource, academic and industrial institutions are trying to find solutions to use wind plants in an optimised manner trying to further reduce the cost of energy. In this perspective, coordinated wind farms control may be one of the solutions to obtain a higher overall power production and a longer lifetime of turbines. However, the use of these wind farm control techniques requires an accurate analysis for what concerns the maximum and fatigue loads experienced by a single wind turbine, whether the latter may constitute the machine on which the control operates or the machine which is affected by the active control. This analysis is of crucial importance because it establishes whether the chosen control can be directly applied to existing wind turbines or, on the contrary, it is possible to design them by optimising such a control. This Thesis will focus on understanding the effects of the application of a specific control on existing machines, in order to clarify the real feasibility of the application of these strategies on current wind farms, through methodologies based on highly detailed numerical models. In particular, we analyse accurately the impact of this control on a single upwind machine which aims to actively control the wake by yaw-misalignment. Therefore, in this work we investigate in detail the incidence of this strategy on the key performance indicators in terms of power production, ultimate and fatigue loads through a parametric analysis carried out on two turbines of different characteristics and sizes with the objective to search for potential analogies. Subsequently, with a higher knowledge of the phenomenon, we provide a structurally-feasible configuration of a 10MW wind turbine rotor able to satisfy the requirements dictated by the active control. Results of the study will show that a possible implementation of yaw-misalignment to steer the wakes must be carefully evaluated to avoid excessive loadings which may compromise the structural integrity of the turbines.

Keywords: wind energy, wind turbine, wind farm control, wake steering, yaw-misalignment, loads analysis, cost of energy, blade design

Contents

List of Figures

List of Tables

Chapter 1

Introduction

Over the last decades, since the issue of fossil fuel pollution of the lower atmospheric layers has become more important, an increasing interest in alternative, renewable and clean energy production has been found. In this perspective, nations are moving toward generating more energy from sustainable and environmentally friendly resources in order not to contribute to climate change. In fact, non-renewable sources are expected to run out within the next centuries and are responsible for the accumulation of carbon dioxide in the atmosphere, giving rise to dramatic consequence for the planet. In this light, wind energy intends to play a key-role as a major source of alternative energy, being one of those which has more advantages compared to disadvantages [1]. Although it is one of the lowest-priced energy resources available today, academic and industrial institutions are trying to find solutions to progressively reduce the cost of energy (CoE) through many investments in the sector, so that it is accounted for 63% of Europe's investments in renewable energy in 2018 [2]. A possible solution to

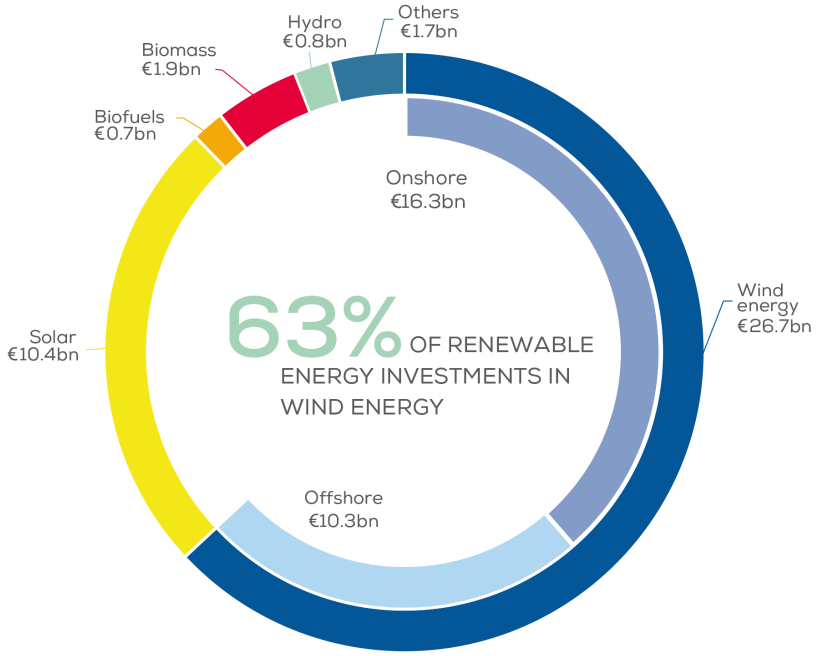

Figure 1.1. Investments in renewable energy. Credit to Wind Europe [2].

harvest the most wind energy possible is developing field, known as wind farm, where

single turbines are grouped together to generate bulk electrical power. Actual wind plants operate in non-optimal conditions, since they are not controlled as elements of a global system. In particular, current practice is that each machine relies only on the available information of its own measurements without interfacing with other turbines. For this reason, nowadays an increasing number of projects aim at developing and testing open and closed loop control algorithms to increase the performances of wind farms, reducing overall costs and improving efficiency and reliability of whole farms [3]. However, it is necessary to quantify the impact of these strategies on single turbine in order to understand if machines installed in existing wind farms are able to exploit these innovative techniques. In this context, we investigate the effect of yaw-based wind farm control on the leader turbine evaluating the loads induced on the whole machine and its overall performance. Furthermore, this work aims to show the consequences of the use of this strategy on the design of the turbine trying to clarify in which case a redesign is essential.

1.1 Scope and methodology

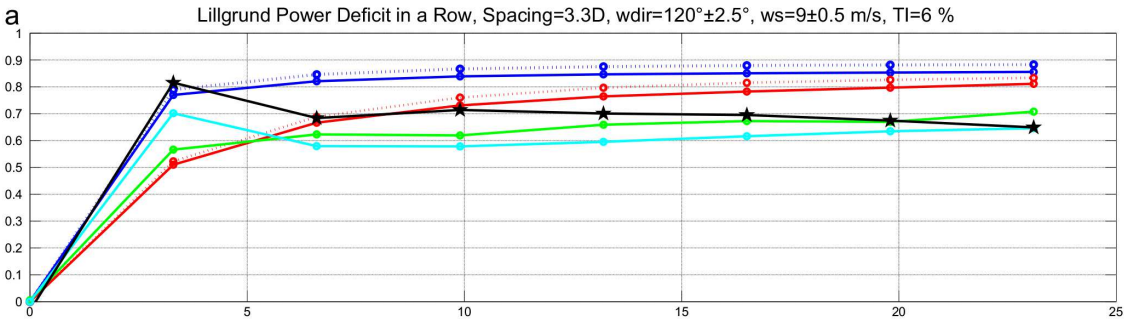

Figure 1.2. An example of power deficit at Lillgrund wind plant. Thanks to Göçmen [4]

One of the most promising solutions to reduce the cost of energy (CoE) and Operation and Maintenance costs is to group together wind turbines in farms. Particularly, wind plants guarantee reduced deployment costs of the electricity grid, reduce use of terrains or water and increase power capture per unit area. However, the formation of wakes, regions of turbulent air flow, downwind of turbines, risks compromising these benefits and leading to higher degradation of the structure. For example, as illustrated in Fig 1.2, Lillgrund offshore wind farm shows losses in power capture up to 23% compared to individually placed turbines [5] while Barthelmie et al. [6] report an average energy production loss of 12%. For this reason, modern farm control techniques aim to mitigate wake losses by intelligently steering the flow, improving the total farm's power quality and turbine lifetimes. In fact, one of these methods misaligns turbines from the incoming flow to deflect their wakes away from downstream turbines, as shown in Figure 1.3 [8]. In this regard, research has shown that with certain misalignments the overall production of a wind plant can increase, even though the misaligned turbines experience an individual power loss [9]. Even though potential benefits have been found, it is fundamental to discover the real feasibility of the application of this strategy on existing turbines. In fact, machines

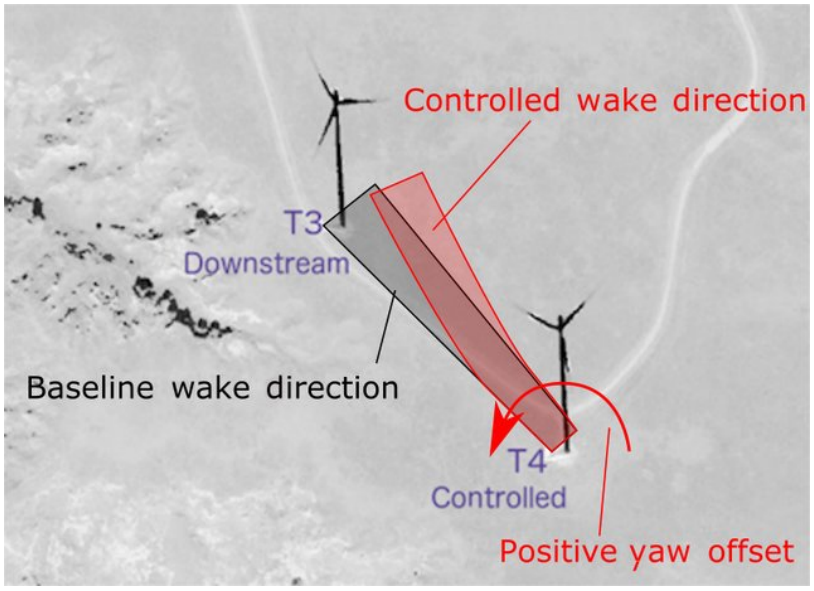

Figure 1.3. Yaw-based wake steering strategy. Credit to Fleming et al. [7].

installed in current wind farms are sized to use traditional controls and it may be interesting to determine if they could be controlled with innovative approaches without the need to dramatically reconsider how wind turbines are designed and operated. As a consequence, the purpose of this work is a rigorous investigation of the impact of wake steering by yaw-misalignment through a study able to understand its incidence on the ultimate and fatigue loads of an upstream single turbine which aims to actively control the wake, eventually verifying if a re-design of the machine is necessary. To carry out the study, we have employed tools representing the state of the art for what concerns the wind turbine design to get the most realistic and accurate results possible. In this regard, we have performed a parametric analysis on two reference wind turbines with different sizes and characteristics to observe how the investigated wind farm (WF) control impacts their performances, with particular regard to maximum and fatigue loads, for a given set of yaw angles. In this way, we have analysed if possible common trends exist between the two models and if it would be possible to draw generalised conclusions from this study. However, although the work has been conducted with methodologies able to take into account the international certification standards for an individual turbine, currently, there are no defined guidelines which rule the wind farm design. Hence, it would be also interesting to understand if current certification standards could remain a reliable tool to drive the analysis and design, as the focus shifts from a single machine towards the design at wind-farm level. To reach the goal, the study has been organized following this workflow: first of all, to correctly implement such strategies, it is necessary to use specific controller tools which are natively developed for the use on wind farms. However, such controllers are relatively new and their use in highly-detailed numerical models is still fairly unexplored. For this reason, we have decided to initiate this work by observing its response comparing it with a benchmark controller to evaluate and validate its performance. Subsequently, we have conducted a parametric analysis on the two turbines to study the effects of yaw-misalignment. At this stage, we have quantified its impact on key performance

indicators including power production, ultimate loads, displacements and fatigue loads. In this way, we have been able to get a better knowledge of the phenomenon to identify what are the main issues which may occur to an existing wind turbine. In a last step, we have performed a complete structural redesign of a 10MW wind turbine rotor with and without the WF control to understand if and how such control impacts on the structural integrity of the design. At this level, we want to establish whether the chosen WF control can be directly applied to existing wind turbines or if, on the contrary, a certain turbine must account for the controller from the beginning. At the end, we have shown a comparison between the two solutions to evidence the main structural difference with the aim of observing what characteristics must be considered to design a wind turbine using wake redirection through yaw-misalignment.

1.2 Outline of the work

This Thesis is organized following this outline: Chapter 2 provides a brief overview of the modern strategy of wind farm control to point out the context of this work. We discuss how and why this work can represent a breakthrough in current scientific research. In Chapter 3, we present the work-environment including the tools and the models employed to conduct the study. Furthermore, we show a complete validation of the controller used to implement innovative wind farm control techniques. Chapter 4 represents the core of the Thesis. In fact, here, we perform a detailed parametric analysis to investigate the impact of yaw-based wake steering on two turbines providing the key performance indicators for each of the yaw angles under analysis. In particular, we show possible benefits and drawbacks which must be accounted for potential applications of this technique. In Chapter 5, we illustrate a rigorous redesign process in which the 10MW turbine is sized to fulfil the constraints imposed by the wind farm control strategy implemented. Lastly, Chapter 6 draws the summary of the achievements of this research and presents potential future developments.

Chapter 2

Wind farm control strategies

The Intergovernmental Panel on Climate Change (IPCC) has claimed that the current rates of emissions will result in a noticeable temperature rise by 2040 [10]. Meanwhile, recent studies have predicted that the Paris Climate Agreement will fail to keep warming below the stated goal of 2°C [11]. As a further matter, the Special Report 15 has established that coal-based electricity generation should decrease from actual rates of 40% of global energy production to 1–7%. For this reason, renewable energy should compensate for this transition, increasing from 20% of energy generation in 2018 to 67% by 2050 [10]. Wind might be one of the best candidates to lead this conversion thanks to its numerous advantages with respect to other sources of alternative energy. However, although recent studies have shown wind energy to be economically favourable compared with traditional sources, such estimates are specific to sites with robust and reliable wind resource [12]. To achieve the objectives of the Paris Climate Agreement, wind farms must significantly increase in number, extending therefore to sites with less certain wind resource [13]. In this regard, methods to increase wind farm efficiency must be found to meet these increasingly stringent requirements. In fact, in current industrial applications, turbines are still controlled to maximise their own individual performance, without considering their mutual interactions through wakes [14]. Wake is a region of altered fluid which arises behind the body around which the fluid flows and extends for some distance. It is generally associated with some characteristics which are space-, time- and parameters-dependent such as:

- velocity deficit, caused by the energy extraction of the turbines;
- increased turbulence intensity, as a result of the turbine blade's rotation or vortex tips;
- recovery, i.e. the phenomenon during which, downwind, the wind velocity recovers the free stream velocity due to mixing;
- meandering, i.e. is a stochastic phenomenon in which the wake centre shows horizontal and vertical oscillations;
- expansion, occurring at long distance from the turbine and can be explained by the mass conservation and the assumption of flow incompressibility;

- deflection, in fact the wake can diverge because the rotor might be not oriented perpendicular with respect to the incoming wind;
- vertical wind shear, in fact the properties of the flow field varies vertically inside the wake.

Focusing on our field, these features provoke side effect on wind turbines which can be summarised in two main concerns: energy production losses and increases of both ultimate and fatigue loads. As far as the first issue is concerned, studies have shown a total loss of approximately 3.7$ million due to wake effects [15] or a reduction from 10 to 20% of power production in an entire year [6]. As for the second problem, researches have discovered that operating in wake gives important increase in loads even for long distance from the upwind turbine [16]. For such reasons, there has recently been much interest in trying to minimise these effects through modern strategy of wind farm control. Instead of allowing each turbine to behave selfishly, achieving the best combination of energy production and loading, the wind farm controller coordinates the operations of the single machine in order to achieve the best performance for the entire wind plant. This means that in any particular wind condition, the performance of some turbines is sacrificed to improve the performance of others, in order to optimise the overall performance of the wind farm. Although many solutions have been proposed and discussed for several years, the recent need of improving efficiency and thus cost of energy has now started to arise commercial interest. Different approaches to the control of wake interactions are possible and some of them are summarized in the Table 2.1.

Control Type	Control Action	Objective	Effect on controlled turbine	Overall Effect
Traditional	Switch off upstream turbine	Avoid wake effects	Complete loss of production but low loads	Reduced loads but dramatic loss of production
Induction Control	Reduce power of some turbines	Reduce thrust to decrease wake effects	Partial loss of production but low loads	Reduced loads but likely increase in production
Wake steering	Yaw misalignment of some turbines	Deflect wake away from downstream turbines	Partial loss of production but high loads	Reduced loads but likely increase in production

Table 2.1. Groups of wind farm control techniques.

The first technique has been used for many years on wind farms where wake effects are sometimes problematic. This involves the shutdown of heavily-wake affected turbines in order to prevent excessive fatigue loading or vibrations from causing structural deteriorations. Clearly, this results in a significant loss of production and

does not represent the optimal solution. However, a better understanding of the wake interactions can be used to determine a priori a reasonable schedule of shutdowns avoiding dramatic loss of energy production. Instead, the other techniques reported in the table aforementioned make use of active strategies for wake control and, thus, are more interesting from a scientific point of view. In this regard, they will be better described in the next sections.

2.1 Induction control

Basically, this strategy implies a change of the axial induction of an upstream turbine in order to reduce its thrust-force, and thus the wake effect. A turbine downstream will experience surely increased power production, but this must be balanced against the reduced energy generation of the upstream machine operating far from optimal conditions. In this optic, a trade-off between these two contrasting effects might be found making this task not so trivial. Anyway, the downstream turbine will see an increased wind speed with lower turbulence resulting in uncertainty about the increase or decrease of overall loads while the upstream machine loads will decrease since operating in sub-optimal status. There are different options to reduce the axial induction:

- altering the pitch angle maintaining the same tip speed ratio;
- changing directly the tip speed ratio.

The change in pitch can be obtained in different ways: below the rated speed, the wind farm controller might change the pitch settings of the turbine to achieve the desired thrust change. However, this does not work in full-load operations where the rated power can be reduced by an amount equal to the desired reduction. For this reason, clearly, some mechanism is necessary to manage the transition between the two regions. A possible workaround is the use of delta control, able to work across the whole operative conditions of the turbine. In fact, at any wind speed, a power reduction (delta) is calculated to provide the desired thrust reduction. Then, using a wind speed estimator, the turbine controller calculates the power normally produced, and demands a lower power output by the amount of the commanded delta. This would result in increasing rotor speed: but above rated, the normal pitch control loop corrects this, and below rated, the controller computes an increased pitch in order to maintain the correct speed. Changing the tip speed ratio (TSR) is the other strategy which can be exploited to obtain a reduction of the rotor thrust. However, this solution is rarely used because of increased difficulty in implementation. Several studies have been conducted to analyse axial induction control achieving contradictory results. A series of researchers such as Horvat and Lee et al. [17, 18] has used engineering wake models which contain numerous simplifications to test these techniques providing total efficiency improvements. Later, Annoni et al. [19] have disclosed some discrepancies between such a simplified model and an higher-order wake based on LES computations getting similar results to Bart et al. [20] which have carried out an experimental study using the two above-mentioned strategies. In his work he hasn't found significant overall increase in power output because the added kinetic energy in the wake diffuses into the free-stream and cannot be recovered by the downstream turbines anymore.

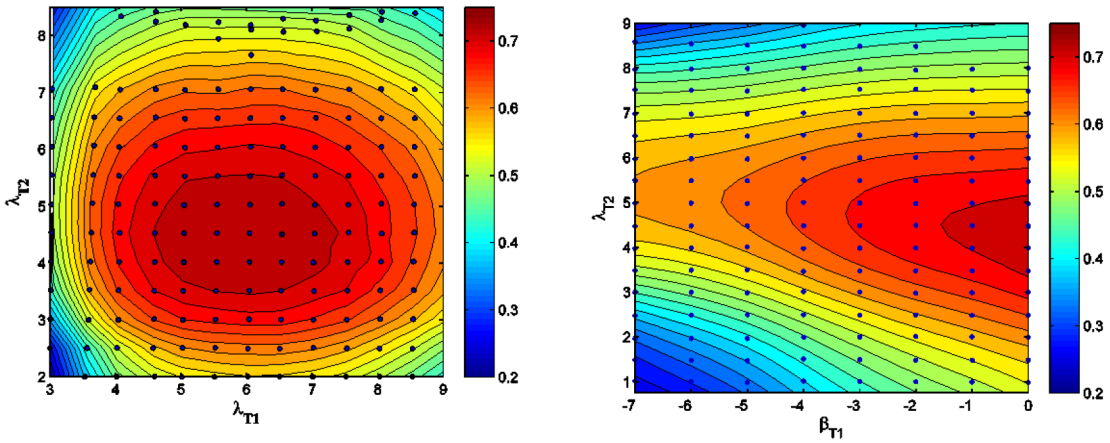

(a) Map of the combined farm efficiency of the two turbines setup at a separation distance of x/D=3 in dependence of upstream turbine tip speed ratio λ_{T1} at constant pitch angle $\beta_{T1} = 0°$

(b) Map of the combined farm efficiency of the two turbines setup at a separation distance of x/D=3 in dependence of upstream constant pitch β_{T1} at constant tip speed ratio $\lambda_{T1} = 6$

Figure 2.1. Maps of the combined farm efficiency for both ways of reducing thrust. Thanks to Bart et al. [20]

Figure 2.1 displays that the array efficiency is rather constant in both maps, so considering the measurement uncertainty, no significant increase in efficiency has been provided. This means that the same amount of energy lost by the upstream rotor is recovered by a downstream turbine at distance of $x/D = 3$. It must be noted that, in a wind farm, the distance between up and downwind turbines is typically around $7D$ [20]. Hence, the power that is purposely not captured by the upwind turbine will not completely be captured by the downwind turbines because of the deviation of the upwind machine wake caused by:

- Wind direction;
- Relative position of turbines;
- Wake meandering;
- Atmospheric conditions;
- Wake expansion.

The former contributes to the deflection and skewing of the wake making it overlap less with the downwind rotor. Secondly, the wind direction is never exactly perpendicular to the rotor, and therefore there will always be a deviation of the upwind turbine wake from the downwind rotor. Moreover, when using pitch offsets, majority of the power passed by the upwind turbine is located outer of the wake. This complicates the axial induction control, since it becomes more difficult for the downstream to capture this energy because of wake expansion. Interestingly, Santoni et al. [21] have demonstrated that axial induction control can be employed to reduce turbine loading while maintaining equivalent power production. However, new more effective approaches are being studied among researchers. They are all based on adaptive

scheme in a closed-loop environment where information about wake is exploited by downstream turbines to optimise their performance via gradient-based methods.

2.2 Wake Steering

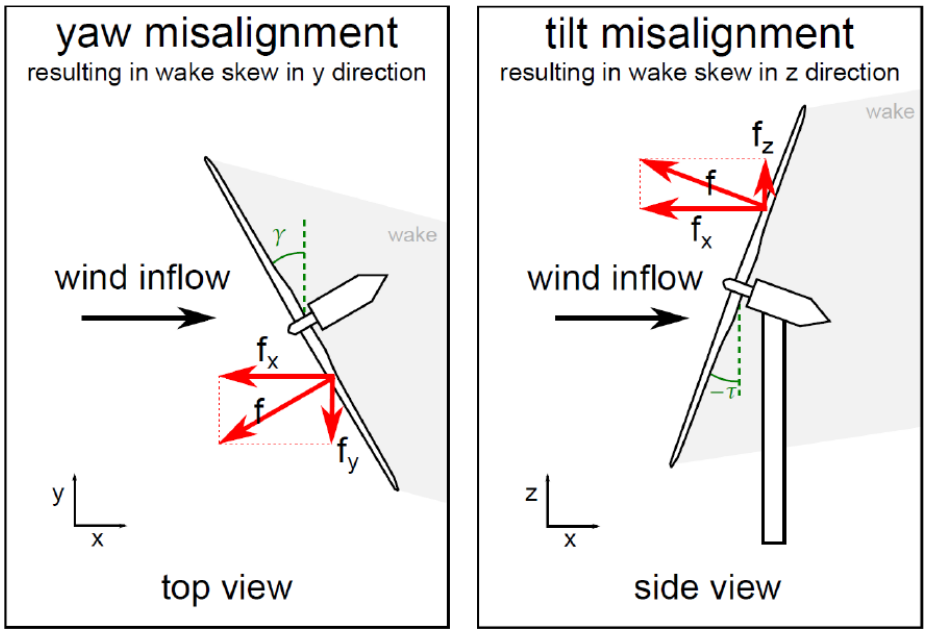

Figure 2.2. Demonstration of the yaw and tilt misalignments for wake steering. Credit to Gebraad et al. [22].

Any misalignment of the turbine leads to the generation of lateral or vertical force on it. Therefore, the conservation of momentum makes the wake deflect, without impinging directly upon a downstream turbine. Moreover, changing the yaw or tilt angle of a machine clearly modifies the axial induction of the rotor. This trivial concept is the basis of wake steering control, a novel technique of wind farm control which is being investigated by several researchers interested in wind energy. At first, mainly open-loop strategies have been used: in this light, advantages have been found in comparison to applying the common "greedy" control in which each turbine is optimized without taking account mutual interactions among turbines. Such a similar approach has shown to have great potential in CFD simulations : for example, Fleming et Al. [23] have found an overall increase of power production after modifying the yaw and tilt angles of an upstream turbine.

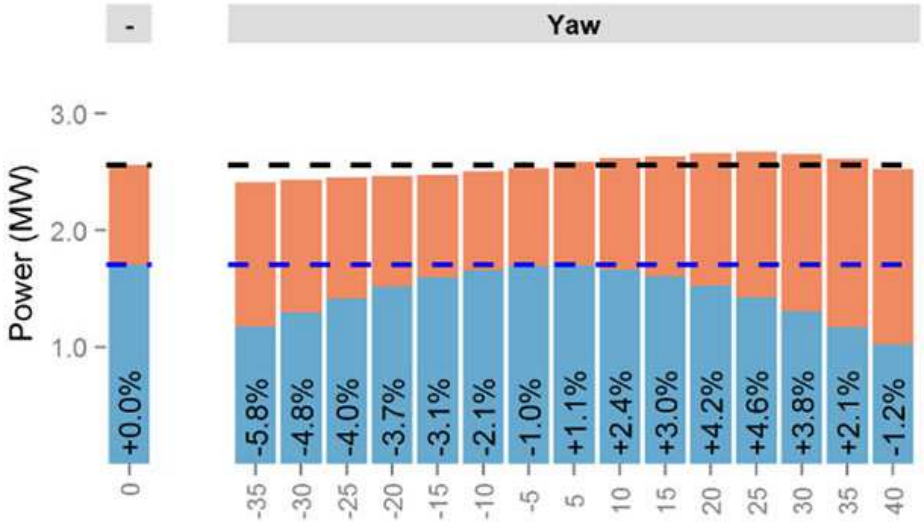

(a) Combined power output for yaw misalignment compared with the baseline case. Turbine 1 is blue, turbine 2 is orange.

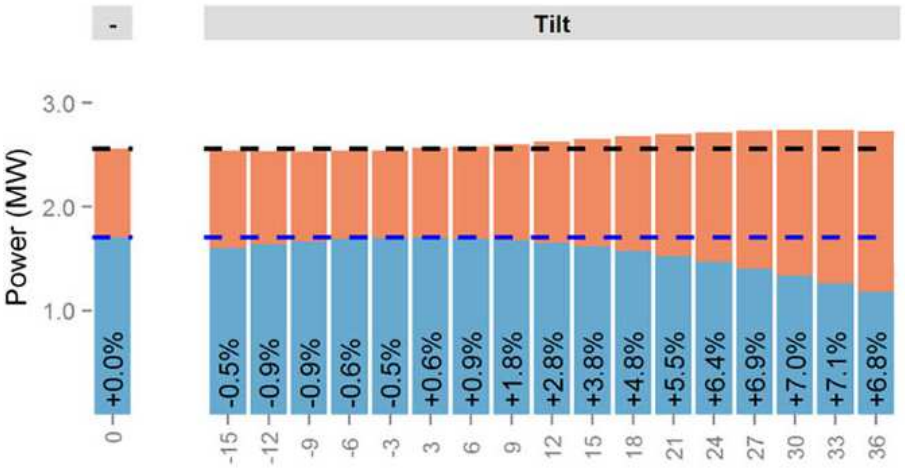

(b) Combined power output for tilt misalignment compared with the baseline case. Turbine 1 is blue, turbine 2 is orange.

Figure 2.3. Summary of the results of the two-turbine simulation. Thanks to Fleming et al. [23]

Furthermore, this method has been tested in wind tunnel experiments on a small-scale setup including 3 turbines [24]. However, certain results have not been provided for different reasons: firstly, using the constant torque control, measurements are also affected by the effect of axial induction making it hard to conclude anything with certainty about the influence of either of the variables. Finally, using greedy torque control with constant tip speed ratio makes the first turbine harvest more energy from the wind, causing stronger wake which negatively influences the other turbines. Instead, Jiménez et al. [25] have studied the consequences of yaw misalignment for different angles using a large eddy simulation (LES) model. It has been shown that yaw angles greater than 30° are unfeasible for yaw-misalignment. Finally, Gebraad et al. [26] have demonstrated that the control method applied increases the energy generation of the wind farm while reducing the loads of the turbines. However, benefits

might be smaller in real wind plants since the distances between the machines are far greater than in the setup study.
Although open-loop control has shown these advantages when compared with standard control approaches, some drawbacks can be identified:

- there is no guarantee that the wake is going to the desired direction because some of the assumptions (e.g. atmospheric conditions) might highly influence the overall control performance
- High sensitivity against disturbances influences the wake steering and therefore the desired performance

Consequently, some closed-loop methods have been proposed in order to overcome these intrinsic shortcomings. One of them consists of a controller which uses wake tracking information to set the new angle of the turbine's yaw actuator in order to steer the wake into the desired direction. It is based on two main tasks: the estimation and the control as shown in the Fig 2.4. The first one provides the wake position to the control using lidar measurements, whereas the latter commands the yaw angle to the machine minimising the error between the information gathered with the demanded one [27].

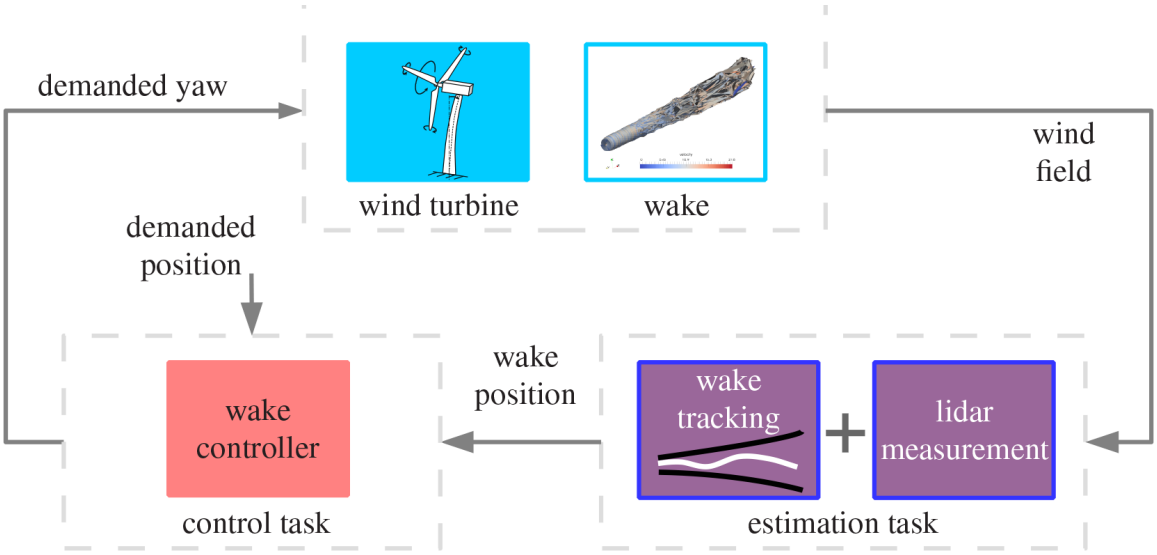

Figure 2.4. Closed loop wake steering architecture. Credit to Raach et al. [27].

This approach has demonstrated significant potential in a case study of nine turbines conducted by Doekemeijer et al. [28]. Increases in power production have been quantified for about 7% to 11% with respect to the greedy wind farm operations. Instead, the open-loop method has been accounted for an increase of power of around 3%.
Wake redirection can be also obtained by using a cyclically varying pitch input (IPC) to achieve a horizontal/vertical wake skew through the rise of a yaw or tilt moment as figured in Fig 2.5.

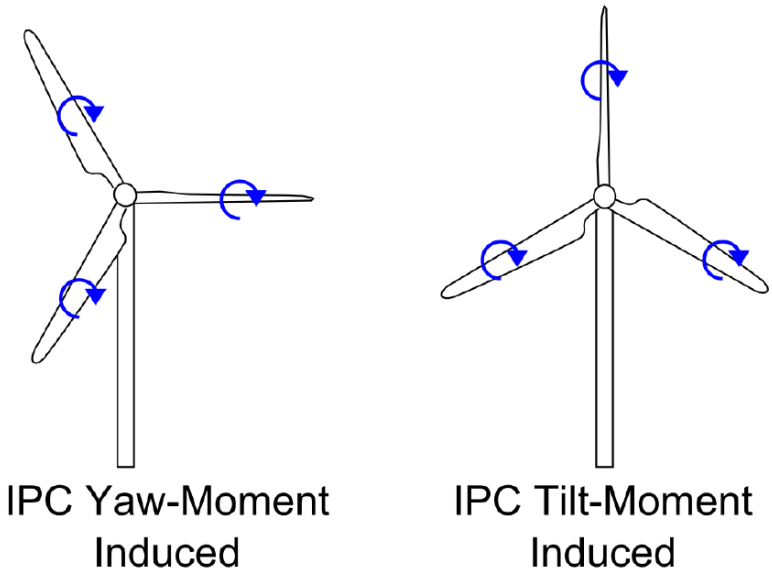

Figure 2.5. IPC techniques employed to steer the wake. Credit to Fleming et al. [29].

Experimental and numerical studies have shown the capability of this technique to achieve good results in steering the wakes. However, it is necessary to develop optimal algorithms to avoid substantial increases in blade loading which might prevent from the adoption of this technique even if it can be adjusted more quickly than yaw misalignment or tilt [29]. In particular, Wang et al. have demonstrated that the former is able to achieve more significant lateral wake displacement and power increase than the IPC while the latter might produce a faster wake recovery as shown in Fig 2.6.

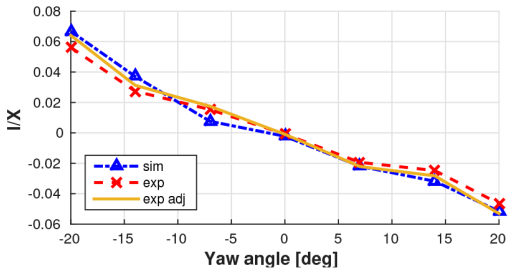

(a) Wake displacement obtained by yaw misalignment

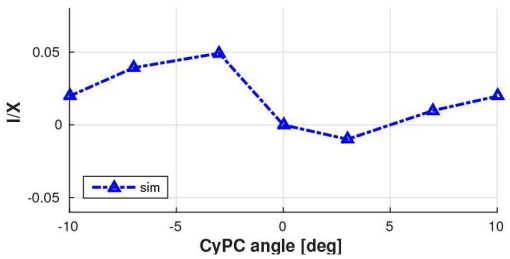

(b) Wake displacement provided by IPC

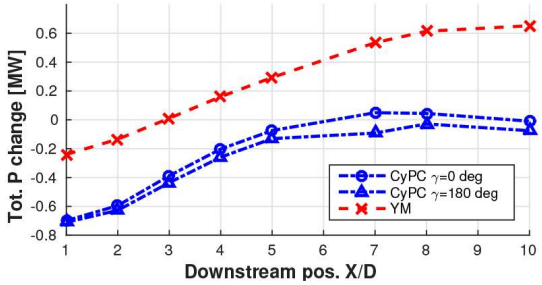

(c) Total power change

Figure 2.6. Final results of the study about the IPC strategy conducted by Wang et al. [30].

An interesting but rarely used approach is to use both the axial induction and the wake redirection control. Here [31], Park et al. have employed a simple model to capture wake dynamics with parameters tuned using data set from a high fidelity flow solver. The analyses carried out for different wind directions have shown that a power increase is achieved for all studied wind directions. However, the proposed control settings are not tested on a real wind farm nor on high fidelity flow solver.

2.3 Remarks concerning the state of art

Although several studies concerning wake steering by yaw-misalignment have been conducted, few researches try to investigate in detail what the consequence introduced on a single turbine could be. In fact, currently, researchers seem to be more interested in understanding the real benefit of a redirected wake without considering the potential drawbacks. In this regard, this Thesis wish to offer a stronger insight regarding the main implications caused by the aforementioned technique. In particular, this study attempt to grasp through highly detailed numerical models, if an existing turbine could be smoothly equipped with a similar strategy. Eventually, this work can be considered a trigger for further investigations about other novel wind farm control techniques, here neglected.

Chapter 3

Models and Tools

In this Chapter, we introduce the wind turbine models, their controllers and the tools employed in this work. The first Section deals with a complete overview of the reference turbines while the second one gives a brief description of their controllers. The third Section illustrates the tools used to develop the various activities presented in the Thesis. Finally, the last Section provides a detailed and consistent comparison between the benchmark and the novel controller to understand and embrace in detail the response of the latter.

3.1 Models

In this Section, the models of wind turbines employed for the present work are described. Since the goal of this study is to evaluate the overall impact of yaw-misalignment on existing turbines, we have decided to conduct the analyses on machines representing the current state of the art of technology so that we could obtain results that can be easily scaled to realistic and already developed solutions.

3.1.1 INNWIND.EU 10 MW

The first model is based on the DTU 10 MW RWT [32] turbine reference model, which is inspired by the NREL 5 MW [33] described in Subsection 3.1.2. It is often used to conduct a wide range of studies thanks to its peculiar characteristics:

- a traditional well-designed rotor with good aerodynamic performance and fairly low weight
- easy availability of the components used in the design process
- a full description of the aerodynamic, structure and control of the wind turbine is freely accessible so that the wind turbine model can be easily used as a baseline for further development

Key Parameters

The wind turbine has a rated power of 10MW, is designed for offshore siting for an IEC class 1A wind climate and is a traditional three-bladed, upwind wind turbine.

An overall description of the essential wind turbine features is provided in Table 3.1

Specifics	Values
Class and Category	IEC Class 1A
Rotor Orientation	Clockwise rotation - Upwind
Control	Variable Speed and Collective Pitch
Cut-In Wind Speed	4 m/s
Cut-Out Wind Speed	25 m/s
Rated Wind Speed	11.4 m/s
Rated Power	10 MW
Number of Blades	3
Rotor Diameters	178.3 m
Hub Diameter	5.6 m
Hub Height	119 m
Drivetrain	Medium Speed, Multiple-Stage Gearbox
Minimum Rotor Speed	6 rpm
Maximum Rotor Speed	9.6 rpm
Gearbox Ratio	50
Maximum Tip Speed	90 m/s
Rotor Precone Angle	4.65°
Nacelle Uptilt Angle	5°
Rotor Overhang	7.1 m
Rotor Mass	227962 kg

Table 3.1. Main characteristics of the INNWIND.EU 10 MW.

Blade

In order to design a relatively light-weight rotor, airfoils with high relative thickness have been selected to increase the angular mass so that the stiffness can increase. Since this model must be publicly available, the airfoils of the blade must meet this requirement. For this purpose, the FFA-W3-xxx airfoils are frequently used in modern wind turbine designs because their geometrical and aerodynamic characteristics are publicly available from the original paper [32]. However, since existing FFA airfoils are defined in a range of thickness between 21.1 % and 36.0 %, during the preliminary design operations additional airfoils have been created. In particular, due to the high request of flapwise stiffness related to the high length of the blade, a first airfoil with 48% thickness has been created from a simple multiplication of the normal-to-chord coordinates of the 36% airfoil. Afterwards, a transitional airfoil with thickness of 60% has been created through an interpolation between the 48% airfoil and the cylindrical root section. However, the 60% airfoil has not been considered in our reference model, since available polar data show unexpected jumps in the vicinity of the null angle of attack, triggering numerical instabilities in several simulations. Aerodynamic properties of the blade between the root and the first pivotal airfoil (48%) have been obtained by direct interpolation. Instead, the twist has a descending value from root

to tip, becoming negative from about 70% of the blade. A list of airfoils and their non-dimensional positions along the blade is reported in Table 3.2. In Fig 3.1 it is possible to observe the main aerodynamic parameters of the blade.

#	Airfoil	Thickness [%]	Twist	Spanwise position [%]
1	Cylinder	100	14.50°	0
2	Cylinder	100	14.50°	1.74
3	FFA-W3-480	48	10.08°	20.80
4	FFA-W3-360	36	7.3°	29.24
5	FFA-W3-301	30.1	5.75°	38.76
6	FFA-W3-241	24.1	0.1°	71.87
7	FFA-W3-241	24.1	−3.43°	100

Table 3.2. List of airfoils of the INNWIND.EU 10 MW.

Although a lot of wind tunnel measurements exist for the FFA-W3 airfoil series, only data for FFAW3-301 and FFA-W3-360 at Re = 1.6×10^6 are publicly available. However, the data needed for this rotor size are at Reynolds numbers between Re=6×10^6 and Re=1×10^7. To obtain reliable aerodynamic characteristics it has been decided to rely on a 2D computation plus a 3D correction according to Bak et al [34].

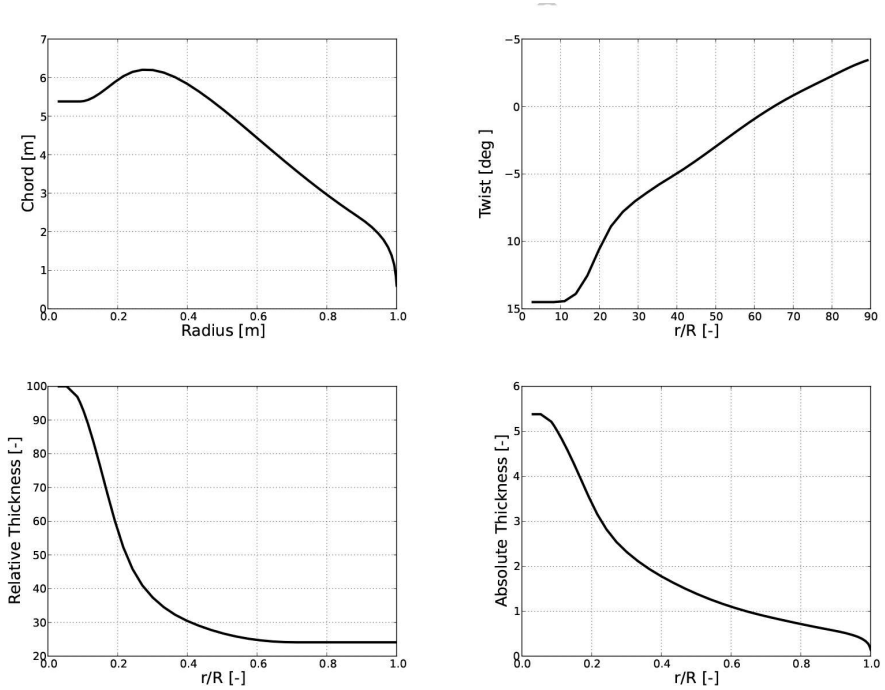

Figure 3.1. Blade planform aerodynamic parameters. Credit to DTU.

The cross section stiffness and mass properties of the blade have been computed using BECAS [35]. It determines the cross section stiffness and mass properties using a finite elements (FEM) approach. This tool handles arbitrary cross section geometries,

a wide number of arbitrarily oriented anisotropic materials, and correctly accounts for all geometrical and material induced couplings.

Tower

The tower is made from steel S355. However, the mass density has been increased to take into account the mass of secondary structures required for the calculation of its structural properties. The outer diameter varies linearly from 8.3 m at the bottom, to 5.5 m at the top. Finally, the tower has been equally divided into 10 sections with different properties.

Control

The model has been equipped with two different type of controllers: the Basic DTU Wind Energy Controller [36] and the OpenWitcon solution [37].

3.1.2 NREL 5 MW

The second model is based on the NREL 5MW reference model [33], a large wind turbine which is representative of typical utility-scale land- and sea-based multi megawatt turbines. The National Renewable Laboratory Energy (NREL) has decided to use the REpower 5M [38] prototype as a baseline to develop this model. However, since detailed information on these machines are not available they have decided to use WindPACT, RECOFF, and DOWEC [39–41] projects as conceptual models because much greater details are available. Their combination has led to the development of a final model which is as representative as possible of the machines installed in the offshore sector.

Key Parameters

The wind turbine has a rated power of 5MW, is designed for offshore siting for an IEC class 1B wind climate and is a traditional three-bladed, upwind wind turbine. An overall description of the essential wind turbine peculiarities is provided in Table 3.3

Specifics	Values
Class and Category	IEC Class 1B
Rotor Orientation	Clockwise rotation - Upwind
Control	Variable Speed and Collective Pitch
Cut-In Wind Speed	3 m/s
Cut-Out Wind Speed	25 m/s
Rated Wind Speed	11.4 m/s
Rated Power	5 MW
Number of Blades	3
Rotor Diameters	126 m
Hub Diameter	3 m
Hub Height	90 m
Drivetrain	High Speed, Multiple-Stage Gearbox
Minimum Rotor Speed	6.9 rpm
Maximum Rotor Speed	12.1 rpm
Maximum Tip Speed	80 m/s
Rotor Precone Angle	2.5°
Nacelle Uptilt Angle	5°
Rotor Overhang	5 m
Rotor Mass	110000 kg

Table 3.3. Main characteristics of the NREL 5 MW.

Blade

The structural and aerodynamic characteristics of the blades are based on those developed by LM Glasfiber [42] installed in the DOWEC 6MW wind turbine. However, the latter blade is slightly longer than the one mounted inside the REpower so that the structural characteristics have been scaled to satisfy the new length of 61.5 m. As far as aerodynamics is concerned, a similar approach has been followed. For this reason, the properties are based on the DOWEC solution. A list of airfoils and their non-dimensional positions along the blade is given in Table 3.4.

#	Airfoil	Thickness [%]	Twist	Spanwise position [%]
1	Cylinder	100	13.31°	0
2	Cylinder	100	13.31°	13.20
3	DU40_A17	40	13.25°	18.65
4	DU35_A17	35	11.3°	25.16
5	DU30_A17	30	9°	38.17
6	DU25_A17	25	7.7°	44.68
7	DU21_A17	21	5.25°	57.60
8	NACA64_A17	17	3.13°	70.71
9	NACA64_A17	17	0°	100

Table 3.4. List of airfoils of the NREL 5 MW.

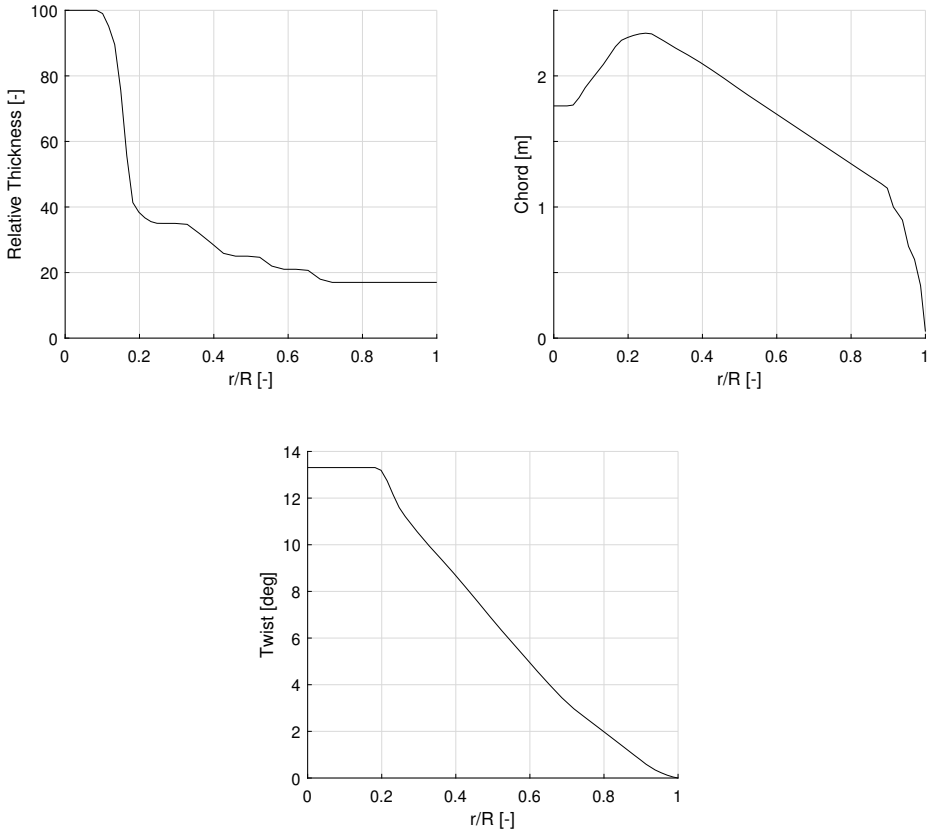

Figure 3.2. Blade planform aerodynamic parameters for the NREL 5MW

Tower

The properties of the tower for the reference model depend strongly on the installation site. For this model, a well-designed structure for land-based application has been considered, but it can be used as basis for further development for off-shore installations. As for the blade, the modelling of the tower has been made following the DOWEC turbine. The diameter varies linearly from 6 m at the bottom, to 3.87 m at the top of the tower. It has been divided into 10 sections of equal length but different properties.

The density of the steel has been increased above the typical value to take into account secondary structures.

Control

The model has been equipped with a LQR controller developed inside the POLI-WIND team [43].

3.2 Controllers

In this Section we describe the architecture of controllers with which reference turbine models have been equipped. The aim of this section is to stress potential differences or affinities to better understand their influence on the main results provided in the Thesis. The IK4 OpenWitcon is one of the wind turbine controller tool employed to achieve the requirements dictated by the several wind farm control strategies. In fact, these techniques require versatile tools able to guarantee a correct control of the turbine in relation to other players of the plant. Basically, it consists of a drivetrain damper and two different proportional–integral controllers which act on pitch angle and torque. Instead, a basic implementation of the DTU controller has been used as a benchmark to evaluate the response of the previous for validating its behaviour. Fundamentally, it is composed of one PID for the pitch angle, and a second PID for the torque regulation in both the II and $II_{\frac{1}{2}}$ region. The last controller provided is a Multi-Input Multi-Output (MIMO) linear quadratic regulator with integral state based on a model approach, which allows for a more accurate design of the control system.

3.2.1 DTU Controller

The controller features both partial (below rated power) and full (rated power) load operation capabilities and switching mechanisms which ensure smooth transition between the two modes of operation. The partial load controller is based on a classical K-$Omega^2$ strategy or on a PID controller to track constant tip speed ratio whereas the full load controller is also based on classical PID theory. It also includes drivetrain, tower dampers, a rotor speed exclusion zone and filters on the feedback signal. The torque reference $Q_{ref,k}$ is computed at each time step k based on a second order low-pass filtered LSS generator speed in order to avoid the feedback of higher frequency dynamics. Whenever the filtered rotational speed Ω_k is different from the minimum Ω_{min}, or the rated Ω_{rated}, the feedback is enforced by setting the torque limits for the PID controller to:

$$Q_{g,min,k} = Q_{g,max,k} = K\Omega_k \tag{3.1}$$

Instead, when the rotational speed approaches its bounds, these limits open according to the interpolation factors $\sigma_{min,k}$ and $\sigma_{max,k}$. These are based on how close the filtered generator speed is to the minimum and the rated speed. In this way, the torque reference is given by the PID controller accordingly to the error:

$$e_{Q,k} = \Omega_k - \Omega_{set,k} \tag{3.2}$$

where $\Omega_{set,k}$ can be the minimum, or the rated speed. Because the torque is bounded, the power loss can often be minimised adjusting the minimum pitch angle with an external look up table used as a reference at different wind speeds. In this manner, the reference pitch is maintained at a minimum value thanks to the power error feedback of pitch controller. In full load operation, the torque limits are defined by the selected power control strategy: constant power or constant torque. For this reason, the PID on the torque is not active anymore. As far as pitch is concerned, the reference angle is achieved from a combined PI feedback on the generator speed and power errors, and a possible differential feedback of the speed error. Both errors contribute to the same proportional and integral term, respectively $\theta_{P,k}$ and $\theta_{I,k}$, but the latter is more important because it ensures that the reference pitch angle is kept at the minimum pitch angle until rated power is reached if the gains have been well selected. If the reference power suddenly increases above rated, the controller will soon react forcing the minimum pitch limit on the reference in this way :

$$\theta_{ref,k} = max(\theta_{min,k}, \theta_{P,k} + \theta_{D,k} + \theta_{I,k}) \tag{3.3}$$

So, if the value of the reference pitch is at its minimum limit, the integral term for the next time step is recalculated according to:

$$\theta_{I,k} = \theta_{ref,k} - \theta_{P,k} - \theta_{D,k} \tag{3.4}$$

Below the rated power, the proportional term is negative because the rotational speed error is kept close to zero by the torque controller, thus the integral term will be positive. If the reference power becomes close to the rated, then the proportional term will approach zero, whereas the integral will still be positive and the resulting pitch reference angle will be positive, whereby large power and speed variations are avoided. The switching between partial and full load control of the generator torque is based on a filtered variable $\sigma_{\theta,k}$ that is driven by a function which uses the measured mean pitch angle.

3.2.2 IK4 Open Witcon

The IK4 OpenWitcon wind turbine controller code has been used as a basis for the development of a baseline controller with the objective of being used for the wind farm level control implementations. It is a generic and open source controller suitable for a wide range of wind turbine models by changing its parameters. It provides drivetrain damper and control loops for torque and collective pitch. The controller is characterised by both partial and full load operation capabilities. The partial load controller is based on a classical K-$Omega^2$ strategy or on a PI controller while the full load controllers are also based on classical PI control theory. It also includes other components such as filters, de-rating systems and individual pitch control to correctly implement wind farm control strategies. Basically, the torque controller is a PI characterised by negative gains in order to make the torque increase when the speed error is negative, and vice-versa. The speed feedback is filtered twice with a second order low-pass and notch filter to eliminate the first side-side tower mode. However, below rated wind speed, the torque controller uses a quadratic speed-torque curve:

$$Q = K_{opt}\Omega^2 \tag{3.5}$$

where the K_{opt} parameter can be calculated to fit the wind turbine employed. As for the pitch controller, it is a PI with the same logic explained before for the torque. Obviously, they do not share the same tuning parameters, in fact the pitch PI gains vary following a pitch-gain look-up table while the minimum pitch can change according to another table being dependent on the de-rating ratio.

3.2.3 POLI-WIND LQR

Linear quadratic regulators use a different approach with respect to the previous control laws:

- they are all based on a reduced and simple model of the wind turbine able to correctly capture the dynamics of the machine.
- it is possible to have a multi-input and multi-output control because the optimum can be evaluated for all closed loops at the same time.
- it is not necessary to distinguish the region in which the machine operates because the transition is managed in a very simple way.

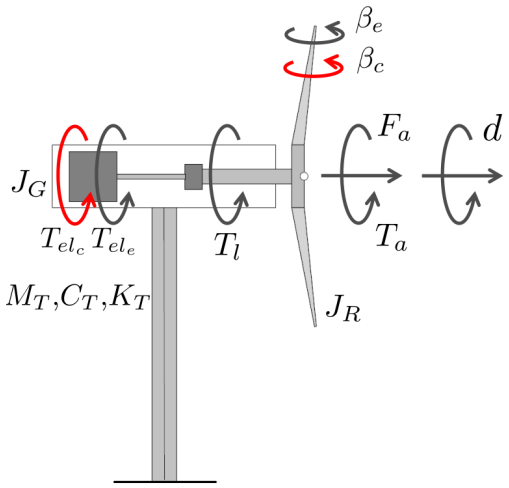

Figure 3.3. Scheme of the reduced order model.

Generally, the nonlinear model is based on the following set of equations:

$$(J_R + J_G)\,\dot{\Omega} + T_l(\Omega) + T_{el_e} - T_a\left(\Omega, \beta_e, V_w - \dot{d}, V_m\right) = 0 \tag{3.6a}$$

$$M_T\ddot{d} + C_T\dot{d} + K_T d - F_a\left(\Omega, \beta_e, V_w - \dot{d}, V_m\right) = 0 \tag{3.6b}$$

$$\ddot{\beta_e} + 2\xi\omega\dot{\beta_e} + \omega^2\left(\beta_e - \beta_c\right) = 0 \tag{3.6c}$$

$$\dot{T_{el_e}} + \frac{1}{\tau}\left(T_{el_e} - T_{el_c}\right) = 0 \tag{3.6d}$$

Equation 3.6a refers to drive-train dynamics.Equation 3.6b is the tower top fore-aft motion. Eqs. 3.6c and 3.6d represent the blade pitch and torque actuator. respectively. The states to consider will be the tower top displacement d, its first order derivative

$\dot{d}$, the effective pitch angle β_e, its first order derivative $\dot{\beta}_e$ and the effective electrical torque T_{el_e}. Instead, the inputs are the control pitch angle β_c and the control electrical torque T_{el_c}. However, given the presence of higher order dynamics, a numerical linearisation of Eqs. 3.6 around steady trimmed conditions is necessary. The rotor force and moment coefficients, F_a and T_a, are computed by using Eqs. 3.7:

$$T_a = \frac{1}{2}\rho\pi R^3 \frac{C_{P_e}(\lambda, \beta_e, V_m)}{\lambda}\left(V_w - \dot{d}\right)^2 \tag{3.7a}$$

$$F_a = \frac{1}{2}\rho\pi R^2 C_{F_e}(\lambda, \beta_e, V_m)\left(V_w - \dot{d}\right)^2 \tag{3.7b}$$

$$\lambda = \frac{\Omega R}{V_w - \dot{d}} \tag{3.7c}$$

where the term $V_w = V_m + V_t$ considers the mean and turbulent wind and $\dot{d}$ the tower dynamics. Moreover, aerodynamic coefficients C_{P_e} and C_{F_e} are evaluated off-line using the aero-elastic model of the turbine by means of an aero-elastic solver. Introducing the state vector $\underline{x} = \{d, \dot{d}, \beta_e, \dot{\beta}_e, T_{el_e}, \Omega\}$ and the control input vector $\underline{u} = \{\beta_c, T_{el_c}\}$, it is possible to write the system in matrix form combining it with the initial conditions, assuming the output to be proportional to the input, as shown in Eqs. 3.8. The final objective is to compute the gain matrix K.

$$\dot{\underline{x}} = f(\underline{x}, t) = A\,\underline{x} + B\,\underline{u} \tag{3.8a}$$

$$\underline{x}_0 = \underline{x}(0) \tag{3.8b}$$

$$\underline{u} = -K\underline{x} \tag{3.8c}$$

Generally, N values of V_m between cut-in and cut-off ($V_{cut-in} < V_i < V_{cut-out}$ with $i = 1 : N$) are taken into account, so that it's possible to linearise around N equilibrium and trimmed conditions : $\{\underline{x}^*, \underline{u}^*, V_m^*\}, V_t = 0$ with $\underline{x}^* = \underline{x}(V_m)$ and $\underline{u}^* = \underline{u}(V_m)$. The

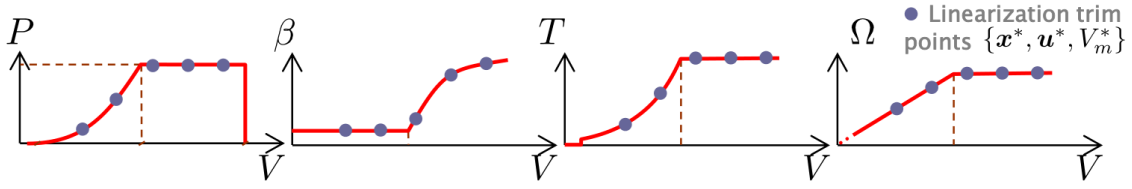

Figure 3.4. Qualitative trend of the parameters of interest as a function of V

linearisation can be done through different approaches, such as analytical methods or numerical ones (i.e. Finite Differences) but it is necessary to perturbate the equilibrium condition in all cases:

$$\Delta\dot{\underline{x}} = A(\underline{x}^*, \underline{u}^*, V_m)\,\Delta\underline{x} + B(\underline{x}^*, \underline{u}^*, V_m)\,\Delta\underline{u} \tag{3.9a}$$

$$\Delta\underline{x} = \underline{x} - \underline{x}^* \tag{3.9b}$$

$$\Delta\underline{u} = \underline{u} - \underline{u}^* \tag{3.9c}$$

With Eqs. 3.9 we can write the quadratic merit index that must be minimised to define the characteristics of the LQR:

$$J = \frac{1}{2}\int_0^\infty \left(\underline{x}^T Q\,\underline{x} + \underline{u}^T R\,\underline{u}\right) dt \tag{3.10}$$

Equation 3.10 must be constrained to meet the dynamics of the reduced models, through the technique of the Lagrange multipliers $\underline{\lambda}$, so can rewrite it in this manner:

$$\hat{J} = \frac{1}{2}\int_0^\infty \left(\underline{x}^T\, Q\, \underline{x} + \underline{u}^T\, R\, \underline{u}\right)\, dt - \int_0^\infty \underline{\lambda}^T(\dot{\underline{x}} - A\,\underline{u} - B\,\underline{u})\, dt - \underline{\lambda}^T(0)\,(\underline{x}(0) - \underline{x}_0) \quad (3.11)$$

Perturbing it, imposing zero at every contribute which multiplies $\delta\underline{x}, \delta\underline{u}$ e $\delta\underline{\lambda}$ and exploiting the fundamental theorem of calculus we obtain a system of five equations:

$$\begin{aligned}
\dot{\underline{x}} &= A\underline{x} + B\underline{u} && (3.12a)\\
\dot{\underline{\lambda}} &= -Q\underline{x} - A^T\underline{\lambda} && (3.12b)\\
\dot{\underline{u}} &= -R^{-1}\, B^T\underline{\lambda} && (3.12c)\\
\underline{x}(0) &= \underline{x}_0 && (3.12d)\\
\underline{\lambda}(\infty) &= 0 && (3.12e)
\end{aligned}$$

Eqs. 3.12a and 3.12c are the dynamic equations. Equation 3.12b deals with the evolution of Lagrange multipliers while Equations 3.12d and 3.12e are related to the initial conditions. At this point, we assume that $\underline{\lambda}$ is proportional to the states: $\underline{\lambda} = -P\underline{x}$ and $\dot{\underline{\lambda}} = P\dot{\underline{x}} + \dot{P}\underline{x}$. Now, after a series of mathematical steps, we can write everything as a function of the states. In order to verify the relation, it is necessary that the term which multiply $\underline{x}$ is null. In this way we obtain the Riccati equation (Eqs. 3.13) that in case of stationary conditions becomes algebraic.

$$\begin{aligned}
\dot{P} &= -Q - A^TP - PA + PBR^{-1}B^TP && (3.13a)\\
0 &= -Q - A^TP - PA + PBR^{-1}B^TP && (3.13b)
\end{aligned}$$

The matrices A and B derive from the system reduced to the states while Q and R represent the matrices of index merits of the original problem. They represent the degrees of freedom of the control system and must be defined positive. Tt is possible to compute P which allows to obtain R, the gain matrix that we were looking for, from Equation 3.13b, . Finally, the control law can be formulated as reported here:

$$\begin{aligned}
\underline{\lambda} = P\underline{x} \Rightarrow \underline{u} &= -R^{-1}B^T\underline{\lambda} = -R^{-1}B^TP\underline{x} = -K\underline{x}\\
\Delta\underline{u} &= -R^{-1}B^TP\Delta\underline{x} = -K\Delta\underline{x} && (3.14)
\end{aligned}$$

In this way we have built a MIMO LQR that does not require high computational calculus because the wind turbine control system will carry out only the last calculation. In fact, matrices Q and R are evaluated off-line. It is possible to assign different weights of the inputs for each speed considered, in order to give different priorities on torque and pitch with respect to the others. A similar approach is called wind scheduling.

3.2.4 Comparison between DTU and IK4 controller

This Section provides the most significant results of the comparison between the DTU and the IK4 controller. To perform a coherent analysis, we have decided to use the INNWIND.EU 10 MW as reference turbine equipping it with both controllers. Exploiting the fact that the DTU controller is revised and tuned specifically for

this machine, we have an ideal benchmark for the direct comparison. Such an approach allows to easily evaluate and understand in detail the response of the OpenWitcon controller. However, configuration parameters of the benchmark controller have not been optimised during this study since it is not the purpose of this study. The comparison has been conducted performing several simulations which represent different design load cases (DLC's), as listed in Tab 3.5, so that we could evaluate the response of the machine in different operative conditions. However, although international guidelines suggest the use of six seeds, the research has been carried out using only one seed to limit the computational time, keeping in mind that this is a comparative analysis and not a design to be certified.

Design situation	DLC	Wind	Safety Factor	Faults
Power production	1.1	NTM	1.35	No
	1.3	ETM	1.35	No
	1.4	ECD	1.35	No
	1.5	EWS	1.35	No
Power production plus faults	2.2a	NTM	1.1	Grid loss Freeze on Pitch
	2.2b	NTM	1.1	Grid loss Mechanical Brake
	2.2f	NTM	1.1	Pitch runaway
	2.3b	EOG	1.1	Grid loss
Parked	6.1	EWM	1.1	No
	6.2	EWM	1.1	Grid loss

Table 3.5. DLC's analysed during the comparison.

In subsequent results, the power curves and the control parameters (rotor speed, pitch and torque) evaluated with normal turbulent wind and extreme coherent gust will be compared to show differences or similarities between the two controllers. Finally, both ultimate and fatigue loads will be considered to highlight the consequence of the different control approaches. However, while the former will be evaluated taking into account all the DLC's, the latter will be obtained only from DLC1.1, since it represents the normal operative conditions of the turbine.

General results

Figure 3.5 illustrates the different power curves provided by both controllers. It is possible to observe that they are capable of generating similar power. As a consequence, the Annual Energy Production (AEP) will be very similar between the two solutions. In fact, Table 3.6 shows that the IK4 controller guarantees a small increase of 0.23% with respect to the DTU controller. Furthermore, different parameters defining the controller performances are analyzed at two different mean wind speed conditions: below-rated (7 m/s) and above-rated (15 m/s). Finally, they are also examined in relation to an extreme coherent gust with direction change at rated condition, to

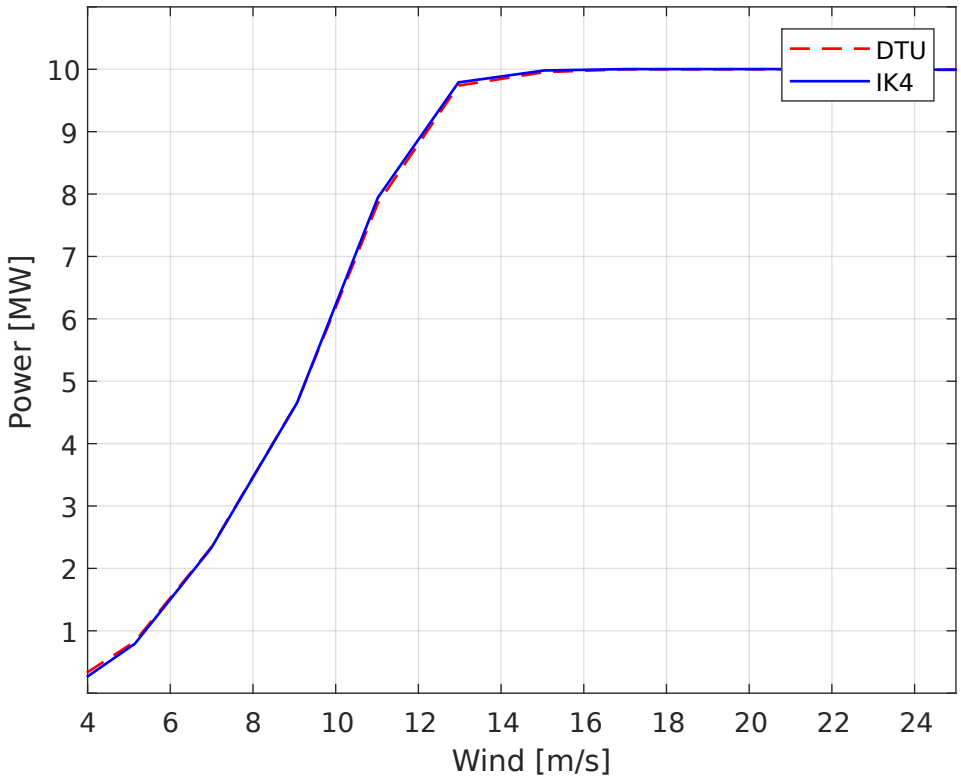

Figure 3.5. Comparison between the power curves.

	AEP [GWh/y]	Variation [%]
DTU	46.1751	
IK4	46.2842	0.23

Table 3.6. AEP for both controllers.

observe how controllers manage such a hard situation. Figure 3.6 shows the trend of control parameters in the below-rated region. As far as power is concerned, there is almost no difference between both controllers. The pursuit of maximum power is accomplished by keeping pitch angle in its optimal value, while the rotor speed is controlled by imposing the electrical torque of the generator. The OpenWitcon controller maintains the pitch angle at 0°, while the DTU shows some variations up to more than 1.6°, when the wind speed is low. The OpenWitcon rotor speed is generally a little lower with respect to the DTU but consequently the torque is higher to achieve the maximum power available.
In full-load region, as shown in Fig 3.7, the blade pitch angle is used to control the rotor speed whose results are quite similar between both solutions. The main differences can be noticed comparing torque and power. In fact, the OpenWitcon controller reduces consistently the torque oscillations about the nominal value with respect to the DTU. As a consequence, the latter controller provides less power because the

rotor speed can not compensate such a big drop in the torque provided. This is due to the fact that both controllers use different approaches in terms of control logic: Ikerlan's controller assumes constant torque unlike DTU's solution constant power. This choice leads to reduce potentially shaft and generator loads in full-load region, providing less long-term fatigue damages on the whole turbine.
The control parameters displayed in Figure 3.8 highlight different performances during an extreme coherent gust with direction change. In fact, as soon as the gust approaches the rotor, the OpenWitcon controller starts to increase the pitch more quickly than DTU. Simultaneously, a stronger oscillation of the rotor speed and torque is provided by the latter resulting in more power but greater loads on the machine. This response is caused by a different tuning of controller parameters with less conservative gains provided by the OpenWitcon.

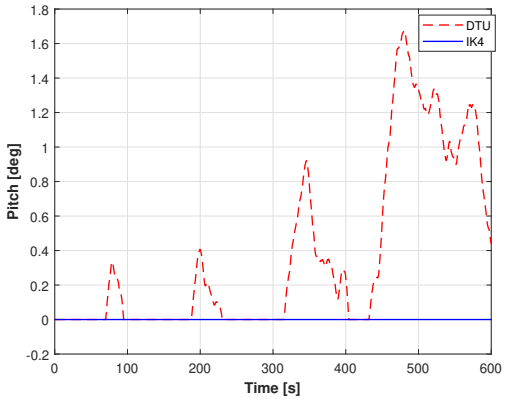

(a) Blade 1 pitch.

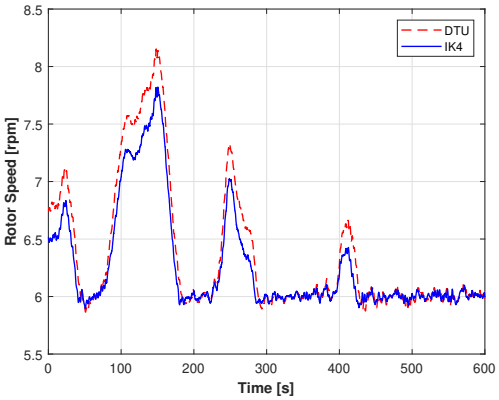

(b) Rotor speed.

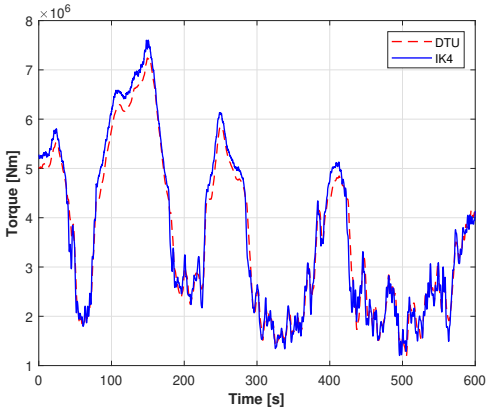

(c) Torque.

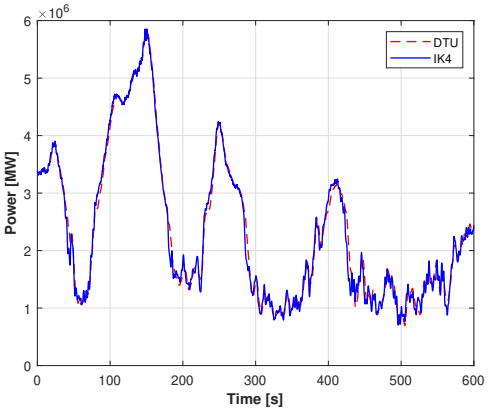

(d) Power.

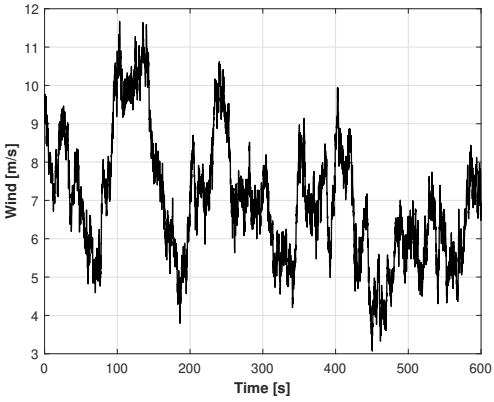

(e) Wind filtered.

Figure 3.6. Control parameters in partial-load operations @7m/s.

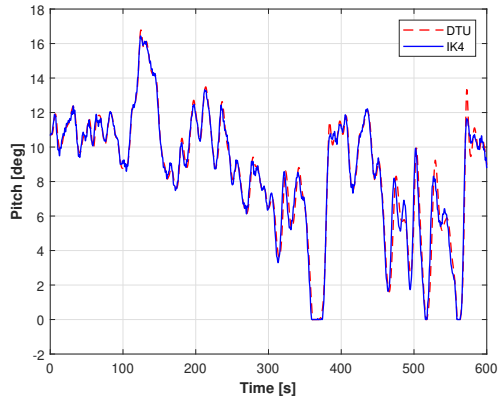

(a) Blade 1 pitch.

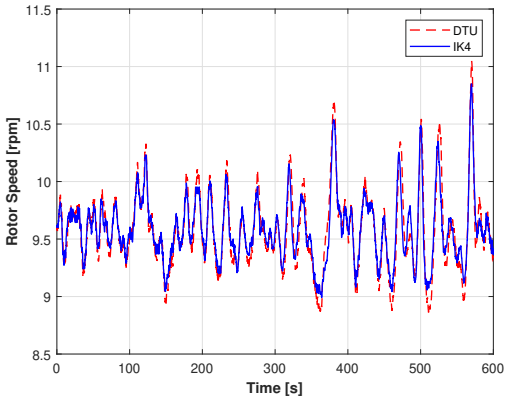

(b) Rotor speed.

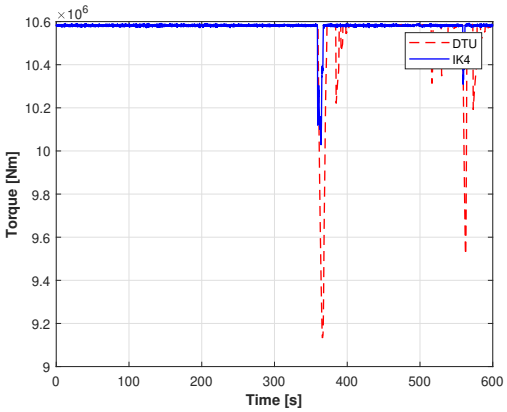

(c) Torque.

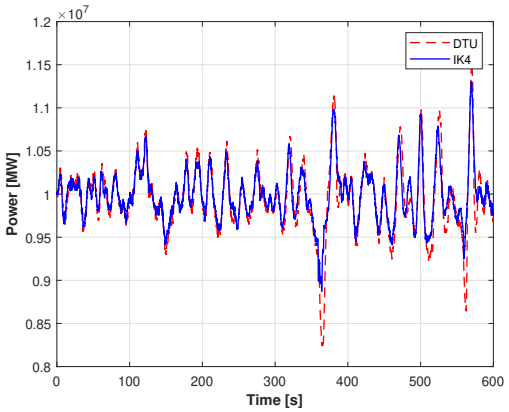

(d) Power.

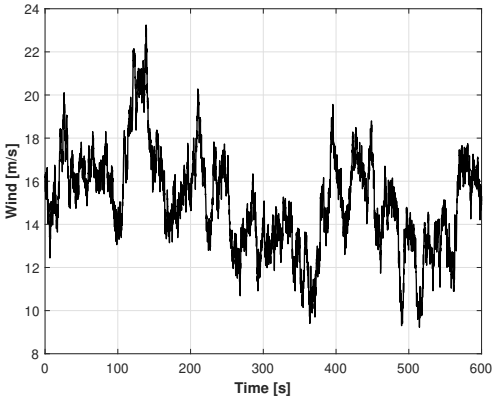

(e) Wind filtered.

Figure 3.7. Control parameters in full-load operations @15m/s.

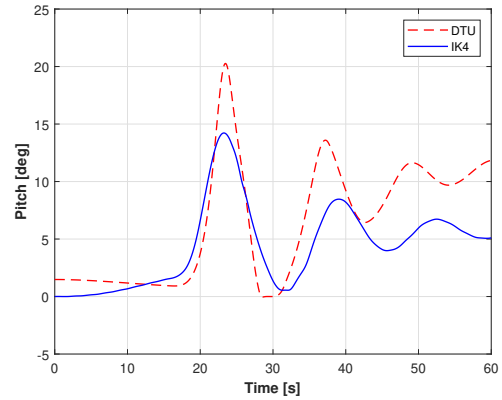

(a) Blade 1 pitch.

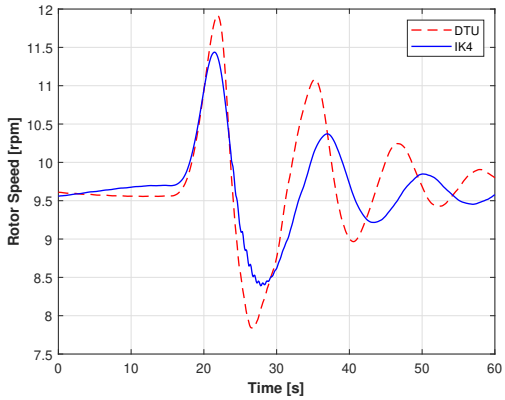

(b) Rotor speed.

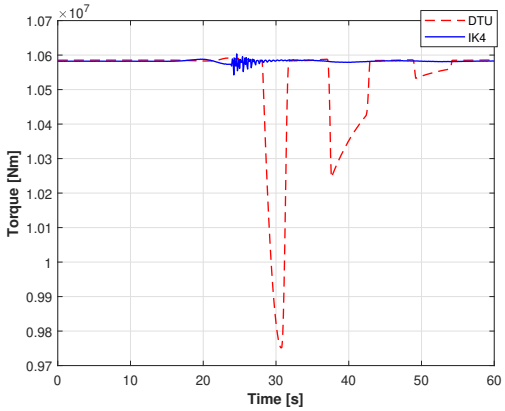

(c) Torque.

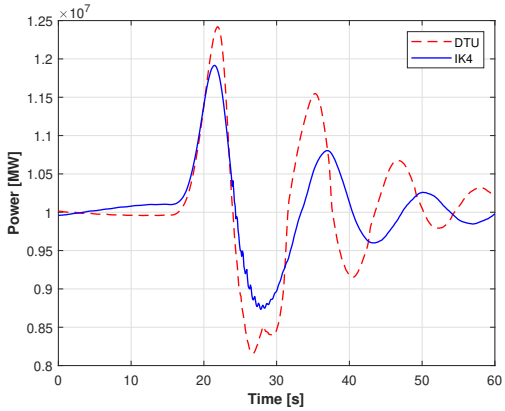

(d) Power.

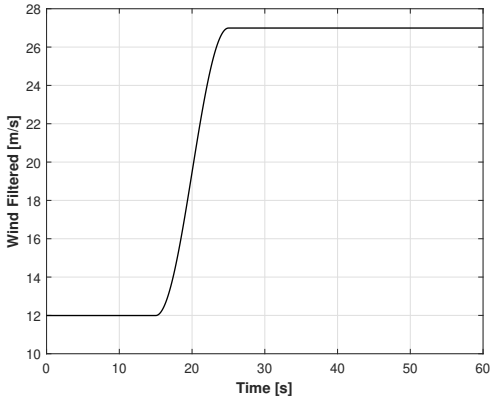

(e) Wind filtered.

Figure 3.8. Control parameters during an ECD @rated.

Ultimate loads

During the evaluation of the performance of different control systems, it is fundamental to analyse the ultimate loads returned by the machine. Obviously, the controller able to provide lower loads represents the optimal choice allowing the turbine to work more efficiently.
The analysis of the loads has been conducted evaluating the envelope loads of the machine using both controllers. The wide range of DLC's considered allows to have an extended variety of conditions from which the ultimate loads can be computed. In the following Figures the maximum loads of different parts of the turbine are compared between the two controllers, scaling the values obtained by the OpenWitcon controller with respect to the DTU. Following this approach, it is possible to catch immediately the main differences provided by both solutions. Finally, as summary, tables containing the exact value of loads and their relative DLC's are provided.
As far as the root of the blade is concerned, we have selected the greatest value for each load component amongst the three blades since it is an analysis of ultimate loads. In Figure 3.9 the percent increments of flapwise, edgewise and combined loads are represented. Here, it is possible to note that although the OpenWitcon controller makes the flapwise increase slightly, it guarantees a considerable reduction of edgewise load, experienced in an extreme operating gust with grid loss. In particular we obtain a reduction of about 25% with respect to the DTU, as shown in Tab 3.7. This result can be justified from the fact that the solution proposed by Ikerlan tends to control the torque better, reducing oscillations consistently, which may have an impact on this load. Instead, the limited increment of combined load is a direct reflex of the small increase of flapwise, since the latter contributes more effectively to the combined flapwise/edgewise moment.

	DTU Value	IK4's percent increment [%]
Flapwise	75444 KNm (DLC13 15m/s)	1.62 (DLC13 15m/s)
Edgewise	39890 KNm (DLC14 at rated)	-24.8 (DLC23b at cut-out)
Combined	75449 KNm (DLC13 15m/s)	1.67 (DLC13 15m/s)

Table 3.7. Blade root ultimate loads values.

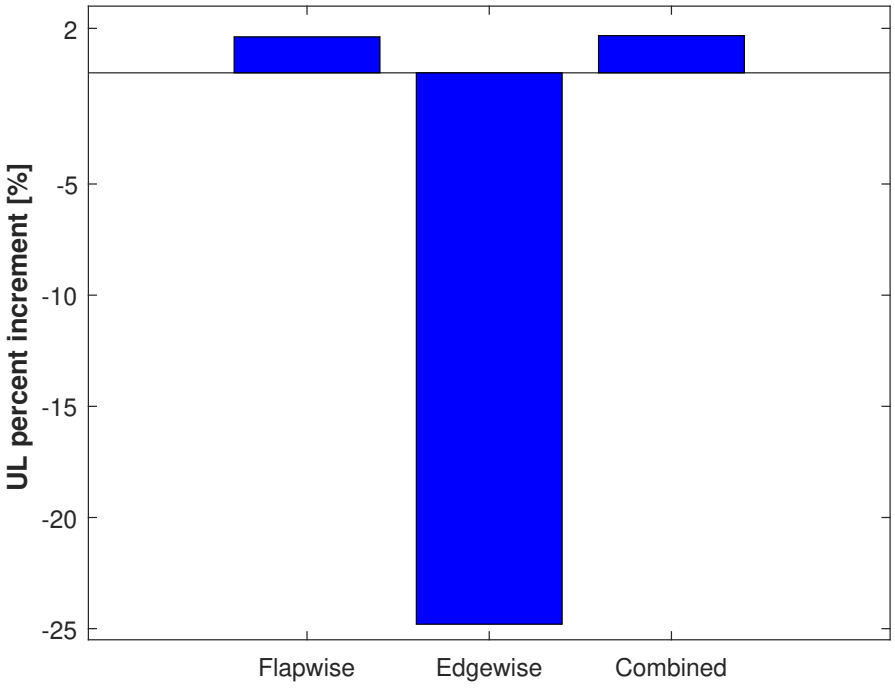

Figure 3.9. Blade root ultimate loads percent increments.

Furthermore, the top and the base of tower are considered in Figures 3.10 and 3.11. We can point out immediately the main differences between both controllers. In fact, as listed in Tab 3.8 and 3.9, the OpenWitcon provides a significant decrease of fore-aft loads due to different tuning of pitch controller which results in obtaining lower thrust acting on the rotor; therefore, the load transmitted to the tower is lower. Instead, side-side loads are identical because the maximum is found when the machine is parked without producing electricity, so that the control is irrelevant. Finally, the fore-aft/side-side combined load provides the same information of fore-aft load because order of magnitudes are clearly different between the two components.

	DTU Value	IK4's percent increment [%]
Fore-aft	78316 KNm (DLC22f 23 m/s)	-14.94 (DLC22a 11 m/s)
Side-side	25023 KNm (DLC62 60 deg)	0 (DLC62 60 deg)
Torsion	68752 KNm (DLC22f 19 m/s)	-0.94 (DLC22f 15 m/s)
Combined	78785 KNm (DLC22f 23 m/s)	-15.44 (DLC22a 11 m/s)

Table 3.8. Tower top ultimate loads values.

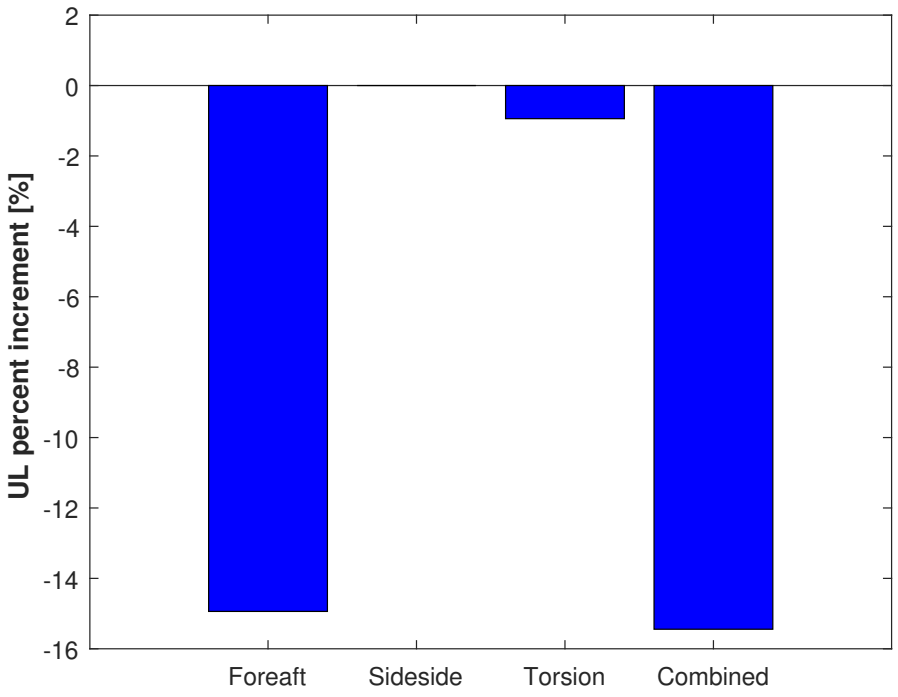

Figure 3.10. Tower top ultimate loads.

	DTU Value	IK4's percent increment [%]
Fore-aft	473603 KNm (DLC14 at rated)	-7.84 (DLC62 120 deg)
Side-side	350158 KNm (DLC62 8 deg)	0 (DLC62 8 deg)
Torsion	69053 KNm (DLC22f 19 m/s)	-1.24 (DLC22f 15 m/s)
Combined	478126 KNm (DLC14 at rated)	-1.51 (DLC62 -60 deg)

Table 3.9. Tower root ultimate loads values.

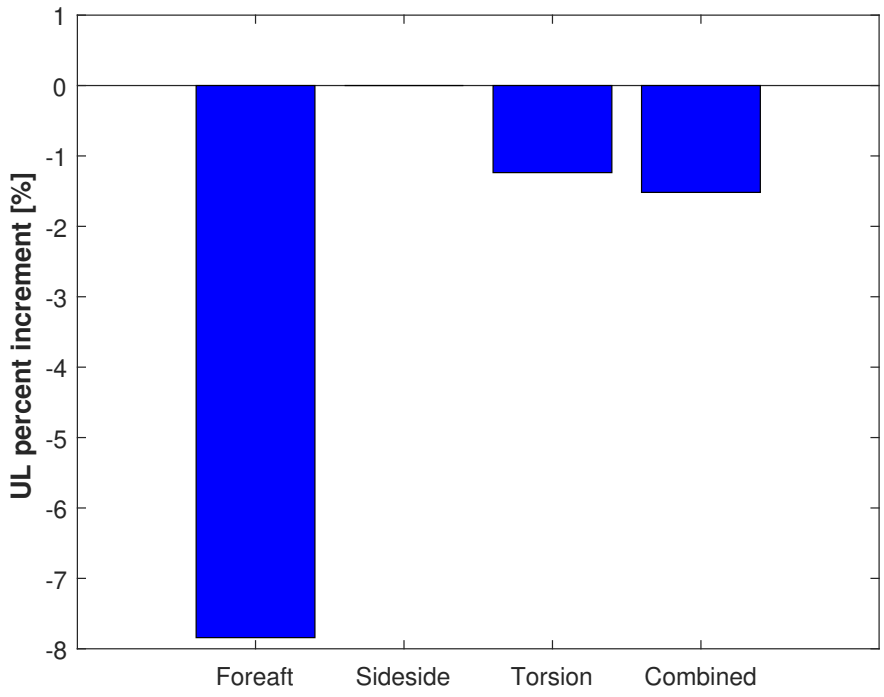

Figure 3.11. Tower root ultimate loads.

Lastly, ultimate loads on hub are studied. Figure 3.12 shows percent increments of nodding, yawing and combined loads, while Table 3.10 lists the corresponding values. It is possible to note an overall decrease of all loads under analysis. The reason behind this trend might be found in the different regulation followed by both controllers. In fact, the constant torque approach provided by the OpenWitcon allows for a minor imbalance of the rotor, which reflects on lower loads experienced by the hub.

	DTU Value	IK4's percent increment [%]
Nodding	77479 KNm (DLC22f 23 m/s)	-22.98 (DLC22a 11 m/s)
Yawing	70293 KNm (DLC22f 19 m/s)	-5.05 (DLC22f 21 m/s)
Combined	80636 KNm (DLC22f 23 m/s)	-8.28 (DLC22f 21 m/s)

Table 3.10. Hub ultimate loads values.

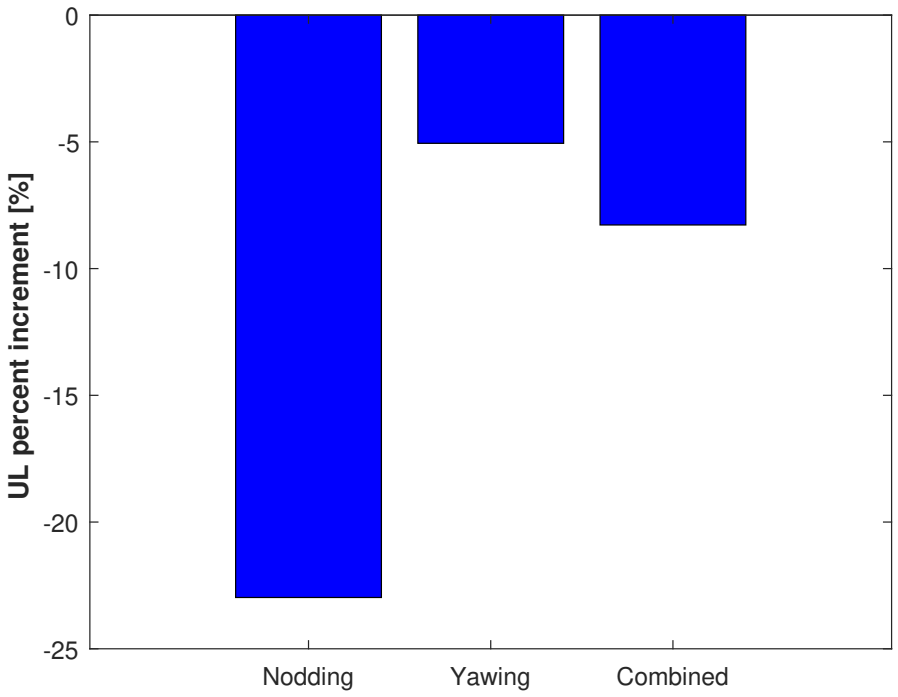

Figure 3.12. Hub ultimate loads.

Fatigue loads

Another fundamental performance indicator of a controller is the Damage Equivalent Load (DEL). In this context, we provide the results connected to a full fatigue analysis performed on the wind turbine using both controllers. The study is conducted by applying a rainflow counting algorithm on the required set of DLC, according to the IEC requirements [44]. For each load considered, a figure showing the DEL values is given. Finally, the Table 3.11 reports the value of these loads cumulated with the Weibull wind distribution. The blade flapwise DEL is considered in Figure 3.13. The general trend shows a different behaviour of both controllers between partial and full load regions. In fact, below rated, the OpenWitcon provides lower loads with respect to the DTU but above rated the situation is opposite. The cause of this particular trend might be found in a lower level of the activity of the OpenWitcon pitch controller in partial load region providing minor loads. Consequently, the cumulated DEL is slightly lower than the DTU since the Weibull wind distribution is centered around the rated value.

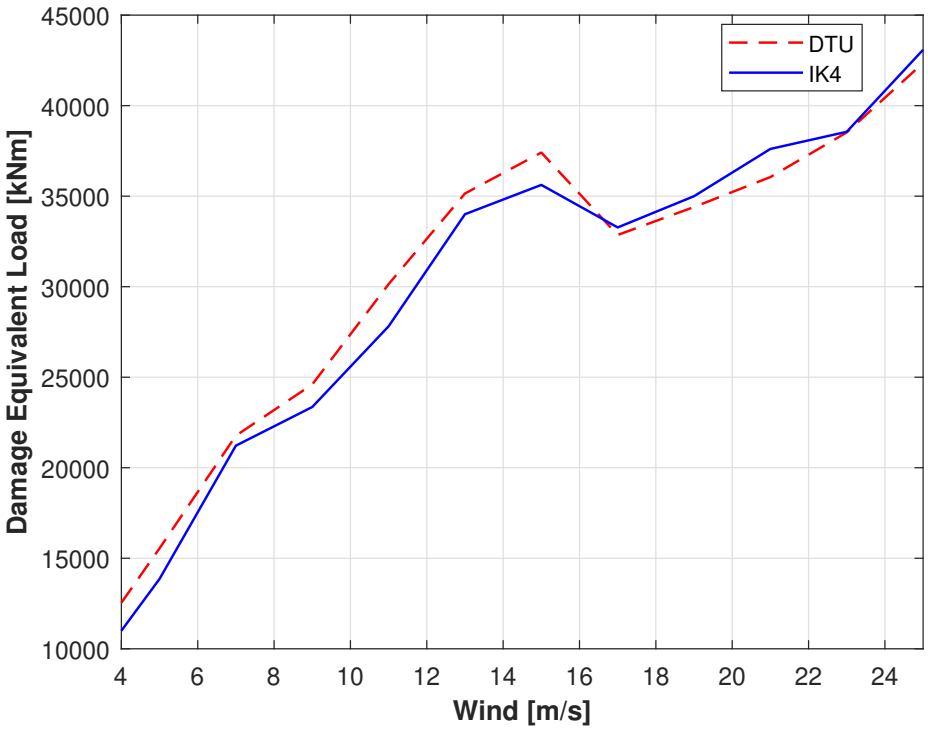

Figure 3.13. Blade flapwise fatigue load.

Figures 3.14 to 3.15 are referred to the fore-aft fatigue load of the tower. As far as tip is concerned, both controllers provide similar results. However, the root of the tower gives different outcomes. In fact, the OpenWitcon controller achieves lower values with respect to the DTU. Even in this case, the lower thrust acting on the rotor is the responsible of these results. Clearly, this behaviour affects the cumulated values: the controller developed by IK4 guarantees a decrease of about 10% with respect to the benchmark controller.

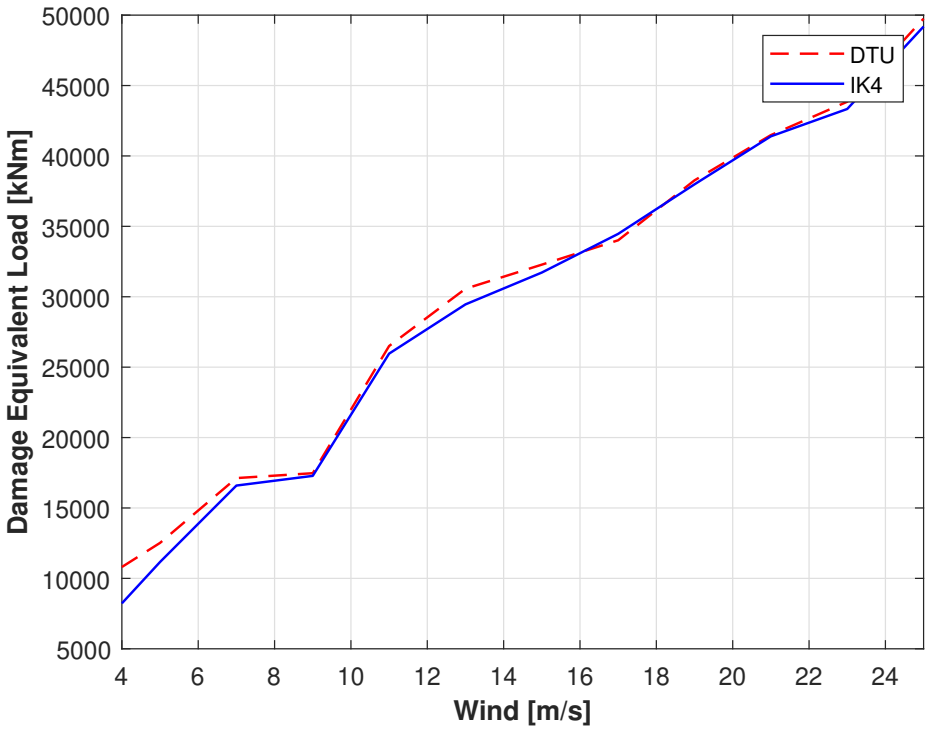

Figure 3.14. Tower top fore-aft DEL.

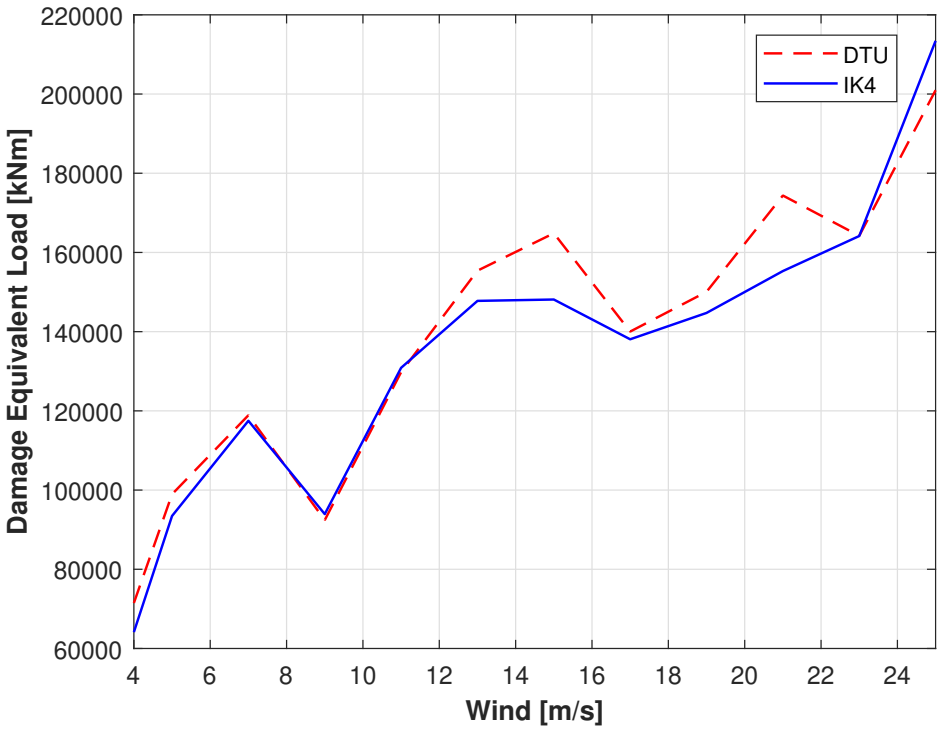

Figure 3.15. Tower root fore-aft DEL.

Finally, we can observe results obtained for the hub nodding and yawing from Figures 3.16 to 3.17. Basically, both controllers provide very similar results but the DTU performs slightly better with regard to yaw moment.

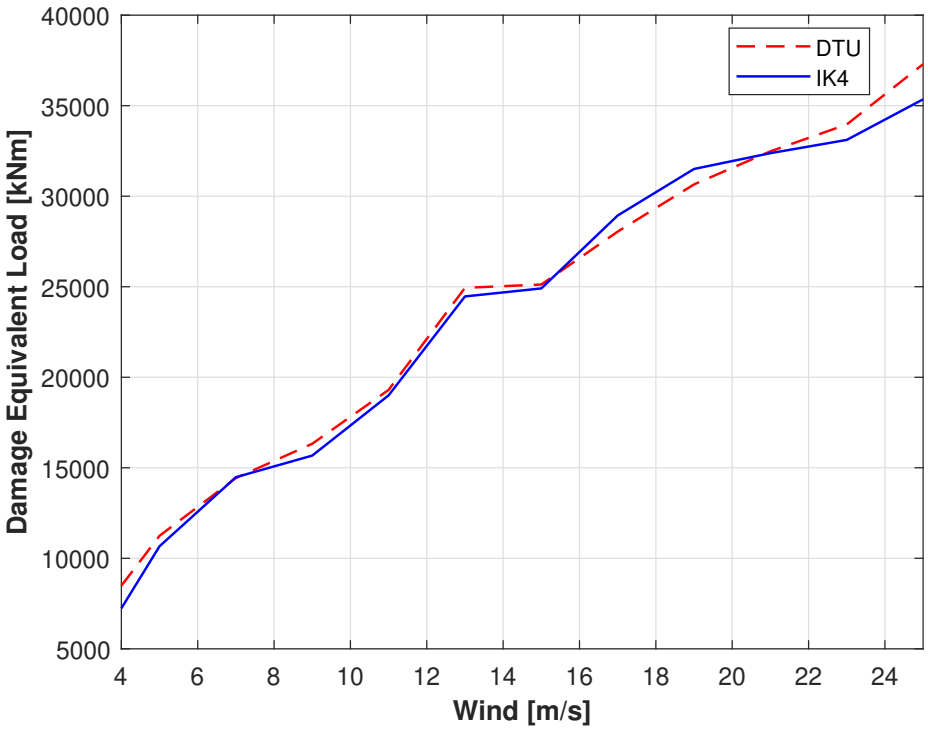

Figure 3.16. Hub nodding DEL.

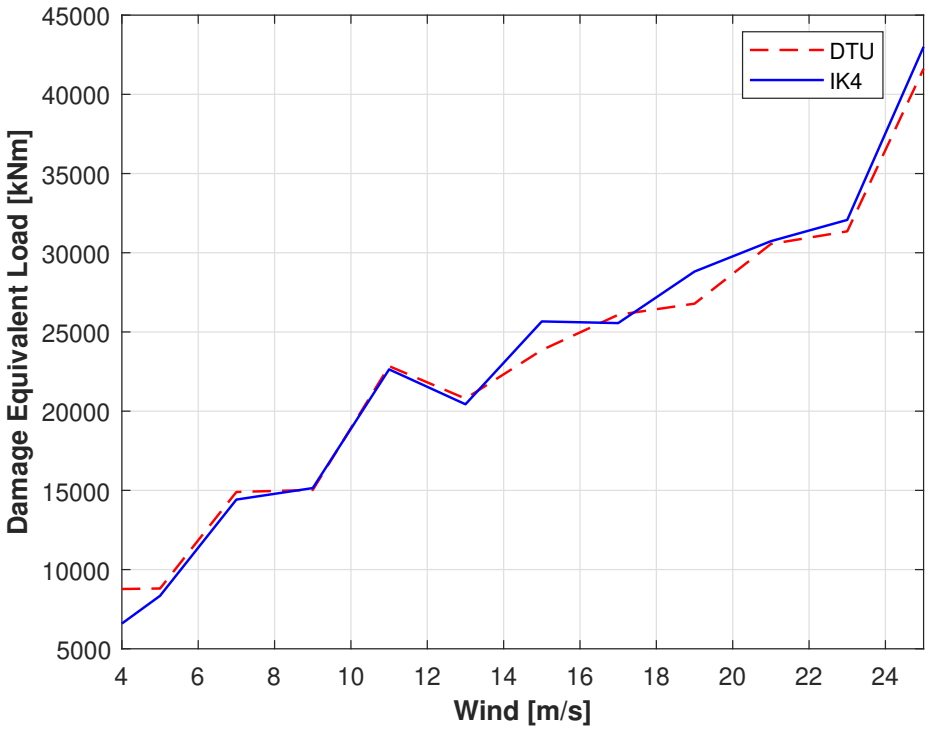

Figure 3.17. Hub yawing DEL.

	DTU Cumulated Value	IK4's percent increment [%]
Blade flapwise	32413 KNm	-1.88
Tower top fore aft	26135 KNm	-0.81
Tower root fore aft	142681 KNm	-10.28
Hub nodding	26034 KNm	-0.48
Hub yawing	26021 KNm	2.99

Table 3.11. DEL's cumulated values.

3.3 Tools

3.3.1 Cp-Lambda

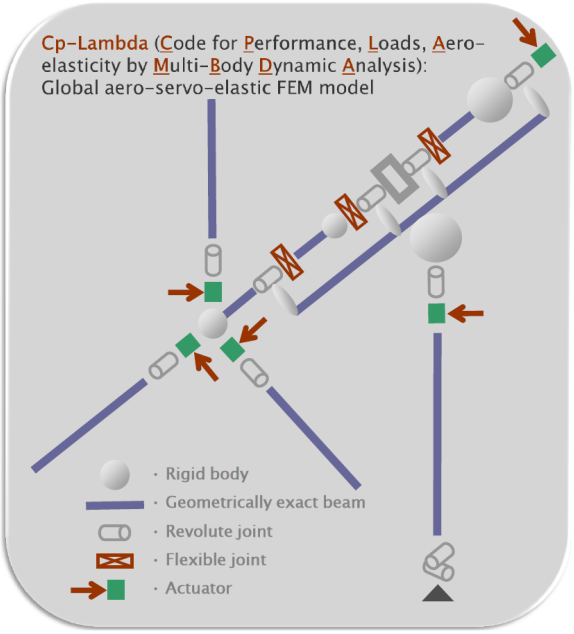

Figure 3.18. An example of a modelled wind turbine through a multi-body approach.

The aeroelastic simulations of the wind turbines have been performed through Cp-Lambda [45], a nonlinear code based on a multi-body finite element method solver developed by the Department of Aerospace Engineering at Politecnico di Milano. It has been validated with both aeroelastic codes and experimental data. Initially the code has been developed for applications to helicopters, but it has been implemented for wind turbine analysis under standard or exceptional operating conditions due to its versatility. With the multi-body approach, it is possible to model a structure taking items from a library containing both rigid and flexible elements such as beams, joints, actuators, sensors, as it can be seen in the example in 3.18 figure. In particular:

Beams can be modelled geometrically exact letting the user define also composite materials. From a structural point of view, they are described by a 6x6 stiffness matrix which allows for a complete aeroelastic description of the problem. Furthermore, reference lines can be curved and twisted because they are represented with NURBS.

Joints can be rigid or flexible and are enforced by Lagrange multipliers. They consist of springs, dampers, backlashs and frictions which can be cylindrical, prismatic, revolute, spherical and so on.

Actuators can be linear or rotational and are described by both the first or second order dynamic.

Sensors and control elements are used together to measure quantities such as loads, displacements, etc in order to apply changes to actuators. The position of the sensors must be specified by the user as input before running the simulation.

As far as aerodynamic is concerned, the blade-element momentum theory is implemented, letting the user associate lifting lines to every type of items using a 2D strip theory. The BEMT is enriched with corrections in order to take into account tip losses, radial and unsteady flows and dynamic stalls. Even if geometrical properties of airfoils are not required, aerodynamic coefficients (Cl,Cd, Cm) of the airfoils must be given as input to evaluate loads acting on the blades. To perform aeroelastic analysis, the wind must be considered. The code requires its time history for the total duration of the simulation. A possible way is to use Turbsim [46] which uses flow field information to generate a grid. Another possibility is to exploit wind time histories coming from computational fluid dynamics or other type of aerodynamic analysis.

3.3.2 Cp Max

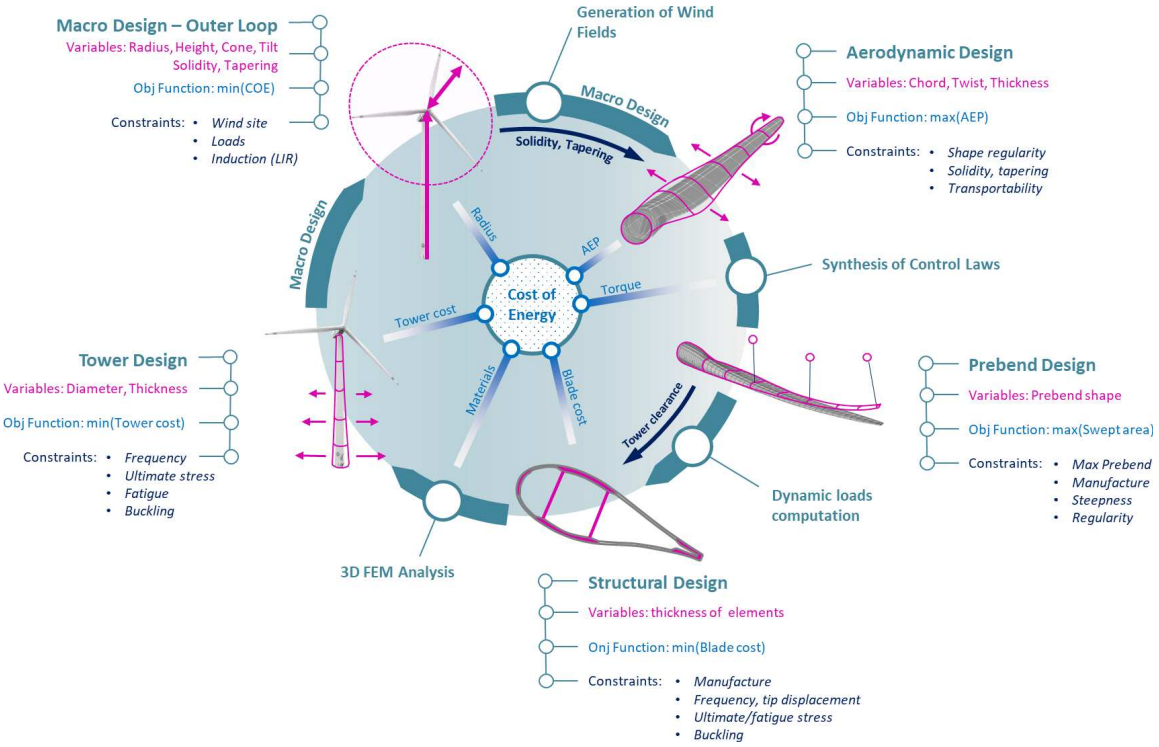

Figure 3.19. Architecture of Cp-Max.

Cp-Max [47] is a wind turbine design tool based on the combination of highly detailed numerical models and a dedicated multi-level optimisation framework. The objective of this code is to provide a system able to consider a full set of DLC's inside the optimisation scheme so that it is possible to rely on realistic loads from the beginning of the design procedure. The algorithm is based on a multi-level architecture: an external loop controls the optimisation of some fundamental characteristics of the turbine while a wide range of different submodules performs the design of specific components

satisfying merit functions and constraints. In this light, the overall workflow can be seen as a branched sequence of individual optimisation problems influencing and sharing information each other. By proceeding with a similar methodology, these functions work together to achieve the minimisation of the cost of energy defined at an external level. However, such a similar approach has to be accompanied by an appropriate number of simulations in order to be able to gather information useful to design the turbine. These are computed by Cp-Lambda which is briefly described in Section 3.3.1.

Architecture of the program

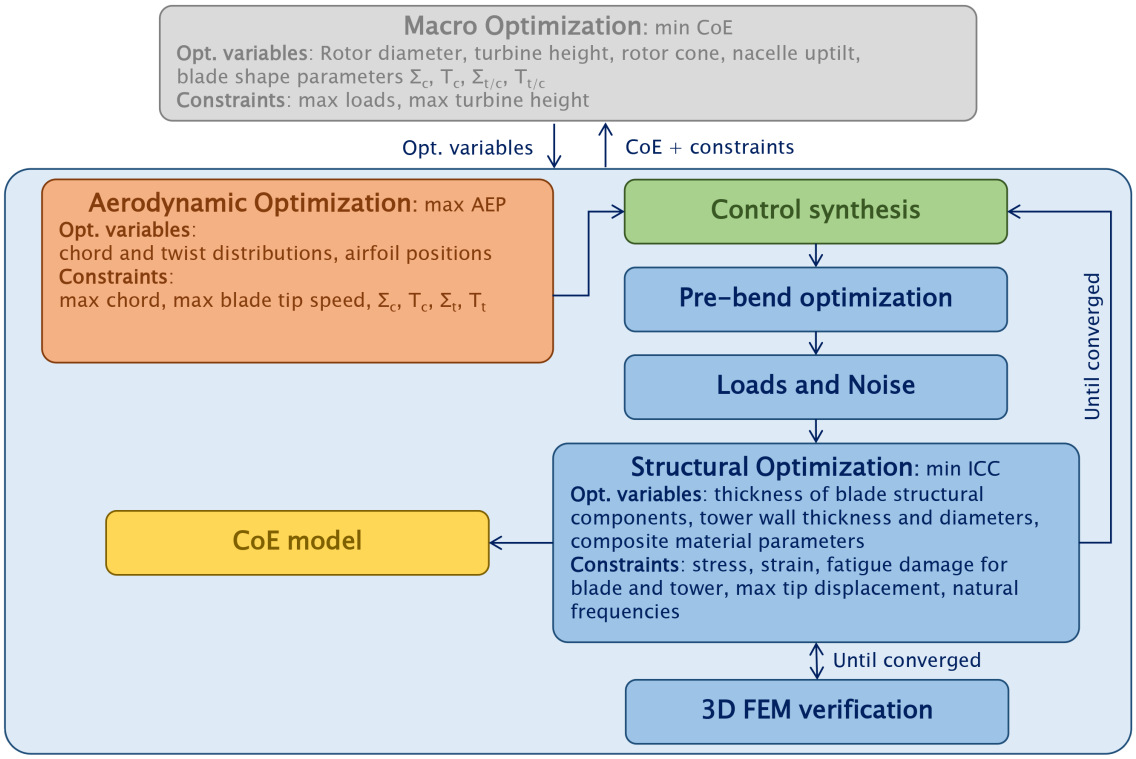

Figure 3.20. Architecture of the Macro Design Loop of Cp-Max.

The main idea behind the architecture of this program is to interface two different levels of design: the one dedicated to the preliminary aeroelastic optimisation, the other developed as a series of individual modules able to provide a detailed design of subcomponents of the turbine. It is fundamental that the two levels work together in the same direction to prevent the single module from evolving independently from the macro level. With this approach, it is possible to put together the highly detailed simulations computed by the aero-elastic solver with a big number of design variables typical of aero-structural problems. However, these heterogeneous quantities are not all treated at the same level, but are organised in order to form a hierarchy providing better sensitivity to the optimisation scheme.
The key part of Cp-Max is the Macro Design Loop (MDL). It represents the interface between the various submodules managing the global optimisation of the machine.

Basically, it performs a preliminary design, selecting some macro parameters to optimises, trying to minimise the COE. During the loop, these values are perturbed letting the submodules involved perform the detailed design of the wind turbine at an inner level.
The algorithm of the structure takes as input the array of the aerodynamic, prebend, structural and global parameters and conducts the individual optimisation separately. The first three are optimised by the individual submodules while the latter by the MDL. In addition to this, a set of fixed input parameters, containing quantities such as power rating, wind turbine class, topological data of the blade and tower and DLC's involved, are collected together being frozen during the design procedure. The global optimisation variables include a little number of fundamental features of the wind turbine which have a significant impact on the cost of energy. In particular, the rotor radius because the cost of several elements of the turbine scales with it. Other important macro variables are the rotor tilt, the coning angles and the nominal hub height since they directly affect the AEP and the structural design of the whole turbine. Finally, the array contains additional four-shape parameters whose function is to connect the macro loop design with the individual aerodynamic submodules, keeping its design within certain limits. This is essential to avoid bad positionings of the MDL optimisation due to the fact that the aerodynamic sub-module is completely independent from the underlying structure.
The work-flow of the macro design loop is explained in the following lines. After a perturbation of the global design array, the CoE of the solution is computed by a specific subroutine. However, there are several submodules called sequentially within it: firstly, the Aerodynamic Submodule, whose aim is to provide the optimal combination of the aerodynamic design variables necessary to the next operations. Secondly, the Control Synthesis Tool evaluates the regulation trajectory of the turbine following the chosen control strategy. Subsequently, starting from the control law, the Prebend Design Submodule gives the optimal spanwise prebend preserving the AEP. Finally, the Structural Design Submodule is responsible for the optimisation of the blade and tower structure trying to minimise the Initial Capital Cost (ICC). Inside this micro-loop, the significant ultimate and fatigue loads and displacement are continually updated by running an arbitrarily set of DLC's in order to provide a coherent structure. The problem is solved when all constraints are fully satisfied. After the end of the loop, the AEP is recomputed to consider the several changes occurred during the optimisation. The whole problem is solved by means of a Sequential Quadratic Programming (SQP) algorithm, exploiting gradients computed through finite differences. It must be stressed that boundaries and constraints must be wisely defined before the start of the optimisation process, to set the right path to follow according to the user's guidelines. These precautions allow to define a well-posed problem, aiming to find a feasible solution and trying to avoid the occurrence of non-physical configurations.
Since the optimisation of a wind turbine must be based on the CoE, Cp-Max supports different cost models which can be selected at the beginning of the optimisation.
Such a so conceived architecture enables the use the tool in several modes: automatic macro design, parametric macro design and individual component design. The first mode is widely used to conduct a complete design or redesign of a wind turbine but might be demanding in terms of time and computational costs. The second one is

capable of highlighting the effects of specific parameters during the design of the machine. On the contrary, the last mode is often used for detailed component design or when some specific limits exist making it a typical industrial application. Each module, including the MDL, can be activated or not, according to specifications and necessity of the work in question, allowing to perform complete or specific design of some components of the machine.

Aerodynamic Submodule

This module is able to find the blade aerodynamic shape for a fixed structure of the rotor which shows the highest annual energy production (AEP). The four-shape parameters defined externally make sure that the results of this stage do not conflict with the global strategy to minimise the CoE.
We can shortly represent the aerodynamic optimisation function in this manner:

$$Function\ (\boldsymbol{p_a^*}, AEP^*) = MaxAEP(\boldsymbol{p_a}, \boldsymbol{p_b}, \boldsymbol{p_s}, \boldsymbol{p_g}, \boldsymbol{D}) \tag{3.15a}$$

$$with$$

$$\boldsymbol{p_a} = [\boldsymbol{p_{ac}}, \boldsymbol{p_{a\theta}}, \boldsymbol{p_{at}}] \tag{3.15b}$$

$$s.t.:$$

$$\boldsymbol{g_a}(\boldsymbol{p_a}, \boldsymbol{p_g}) \leq 0 \tag{3.15c}$$

$$v_{tip} \leq v_{tip_{max}} \tag{3.15d}$$

This module provides as output both the optimised aerodynamic variables $\boldsymbol{p_a^*}$ and the optimal value of the AEP*, inserting $\boldsymbol{p_a}, \boldsymbol{p_b}, \boldsymbol{p_s}, \boldsymbol{p_g}$ which represent the arrays of aerodynamic, prebend, structural and global parameters. In particular, Equation 3.15b indicates that $\boldsymbol{p_a}$ is constituted by parameters associated to the chord, thickness distribution and twist. $\boldsymbol{D}$ is made up of data which include the quantities which remain frozen during the loops.
The final objective of this loop is to maximise the AEP. At this point, it is computed for each variation of the aerodynamic parameters $\boldsymbol{p_a}$ by integrating the product of the power curve with the Weibull wind distribution, as shown in Equation 3.16:

$$AEP = Y \int_{V_{in}}^{V_{out}} P(V)\, f_w(V)\, dV \tag{3.16a}$$

$$Y = 8760 \text{ hours/years} \tag{3.16b}$$

At the end of the MDL, the annual energy production is recomputed using turbulent simulations.

Control Synthesis Tool

During dynamic simulations, the wind turbine is equipped with a certain control system able to meet the required performance and protection in case of gusts or faults. In view of this, Cp-Max supports different control strategies based on the assumption of variable-speed wind turbine with pitch and torque actuators. Consequently, the CST evaluates the necessary control laws, according to the selected strategy, extrapolating parameters from the Cp-Lambda curves.

Prebend Submodule

The main goal of this submodule is to optimise the blade prebend in order to maximise the rotor swept area. A successful optimisation is necessary: although a certain amount of prebend can relax the tip blade deflection constraint, it is obvious that large deformations might result in a reduction of the energy production of the turbine. So, the objective is to find a compromise between these two contrasting concepts.
It is important to note that all the constraints are defined at a local level, so the MDL has no direct feedback on the outcomes of this optimisation. For this reason, a limit on the total prebend at tip has been inserted through a non-linear constraint to avoid problems in the conditioning of the Macro Design Loop. This is justified by the fact that this value is often a design constraint by manufacturing requirements.
The deformation of the blade is computed through static aero-elastic analyses of the complete turbine model, where the rotor is subjected to aerodynamic and centrifugal forces corresponding to the rated operational condition. So, the optimal prebend is calculated minimizing the out-of-plane blade deflection according to this condition. Static simulations are employed because of the notable reduction of the computational time. To identify the best prebend distribution, the curvature is modeled through Bezier curves [48] of arbitrary degree, so that the control points are the unknowns of the optimisation algorithm. A set of nonlinear constraints limits the maximum and minimum values, the steepness and shape regularity of the prebend.

Structural Submodule

This part of Cp-Max allows for a fully and feasible structural optimisation of blades and tower minimizing the ICC. The design variables are sized exploiting loads obtained from a set of customisable set of DLC's in order to automatically satisfy the international guidelines in terms of wind turbine design. It is necessary to keep in mind that running a wide range of dynamic simulations might be too time consuming becoming the real bottleneck alongside the whole optimisation process. Basically, the goal of this tool is to optimise the thicknesses of the structural components of the blade and tower defined alongside the sectional arrangements for a given aerodynamic shape and prebend. The algorithm of the structural optimisation function is illustrated in Equation 3.17:

$$Function\ (\boldsymbol{p_s^*}, ICC^*) = MinICC(\boldsymbol{p_a}, \boldsymbol{p_b}, \boldsymbol{p_s}, \boldsymbol{p_g}, \boldsymbol{D}, \boldsymbol{r_\epsilon}) \tag{3.17a}$$

$$with$$

$$\boldsymbol{p_s} = [\boldsymbol{t_b^{Fabrics}}, \boldsymbol{t_b^{Core}}, \boldsymbol{t_s}, \boldsymbol{\rho_t}] \tag{3.17b}$$

$$s.t.:$$

$$\boldsymbol{g_s}(\boldsymbol{p_b}, \boldsymbol{p_s}, \boldsymbol{p_g}) \leq 0 \tag{3.17c}$$

Equation 3.17a takes as input all the design variables from the MDL and from the aerodynamic and prebend submodule, as well as the array of known information $\boldsymbol{D}$. The control laws $\boldsymbol{r_\epsilon}$ define the control strategy adopted by the machine during the dynamic simulations. Equation 3.17b shows the array of the structural design variables containing the thicknesses of composite fabrics $\boldsymbol{t_b^{Fabrics}}$, the various fillers $\boldsymbol{t_b^{Core}}$ included in sandwich layups, the thickness $\boldsymbol{t_s}$ and diameter $\boldsymbol{\rho_t}$ of the tower

segments. At the beginning of the loop, the structural definition of the model is updated with the actualised variable $\boldsymbol{p_s}$ containing the above-mentioned thicknesses. To correctly run the required set of simulations, the knowledge of the structural properties along the axis of the beam is required to compute the ultimate and fatigue loads and displacements. These are computed by means of ANBA developed by Giavotto et al [49]. Once the multi-body model is correctly updated, DLC's are launched in order to extrapolate sizing loads and displacements. Fatigue is evaluated through a Rainflow-counting algorithm while the ultimate displacements are computed with an equivalent loading system to decrease the computational time. Finally, the structural optimisation starts, sizing the variables to minimise the ICC through sequential design steps. At the end of the structural optimisation, if the desired tolerance is violated, the assumption of frozen loads is not guaranteed anymore and the whole process must be repeated until convergence to obtain a solution coherent with its own loading system.
Blade and tower must satisfy all the constraints applied to the sub-module to obtain a realistic design. In particular, it is possible to divide them in two types: global constraints which rule the whole system, and local ones which are related to each section of the blade and the tower. A complete list of constraints has been defined by Sartori [50].

Chapter 4

Parametric analysis of the reference turbines with wind farm control

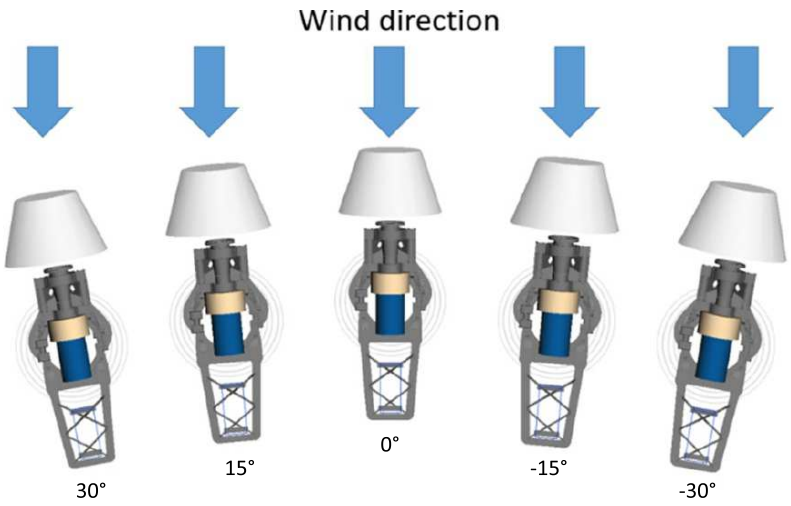

Figure 4.1. Nacelle positions relative to wind direction as seen from above. Credit to Cardaun et al. [52].

In this Chapter we conduct a parametric analysis of the reference turbines with yaw-based wind farm control. The ultimate aim is to provide a better understanding of the phenomenon which may lead to discover, possibly, the impact of the application of this strategy on wind turbines. The study has been carried out following international guidelines for an individual turbine because, currently, there are no defined standards which rule the wind farm design, being a novel topic in wind energy. In this view, we have decided to rely on a broad set of DLC listed in Table 4.1 which are representative of some of design load cases fixed by the International Electrotechnical Commission [44]. In this way, we should be able to include realistic load conditions to verify if the chosen strategy can be directly applied to existing wind turbines or if, on the contrary, a certain turbine must account for the controller from the beginning. Hence, we have performed our investigation on both the INNWIND.EU 10MW and the NREL 5MW references (see Section 3.1) because they well exhibit the characteristics of actual and next-generation wind turbine concepts. Both machines have been equipped

with controllers which are able to satisfy the requirements dictated by the wind farm control studied. In fact, we have decided to provide the OpenWitcon controller and the POLI-WIND LQR to the first and second turbine, respectively (see Section 3.2). The organisation of the work follows this outline:

- firstly, to successfully implement the wind farm control, both turbines have been rotated by a set of yaw angle: $\theta = [-30°, -15°, 0°, 15°, 30°]$ according to the reference frame shown in Fig 4.1;
- secondly, aeroelastic simulations representing the DLC's have been performed for each of the yaw angles. However, given the potential ineffectiveness of wake steering above 15 m/s, we have decided to exclude from the study all cases in which the machine is yaw-misaligned above that speed;
- finally, we have post-processed the outputs of the simulations rigorously identifying the key performance indicators for both turbines.

Design situation	DLC	Wind	Safety Factor	Faults
Power production	1.1	NTM	1.35	No
	1.3	ETM	1.35	No
	1.4	ECD	1.35	No
	1.5	EWS	1.35	No
Power production plus faults	2.2a	NTM	1.1	Grid loss Freeze on Pitch
	2.2b	NTM	1.1	Grid loss Mechanical Brake
	2.2f	NTM	1.1	Pitch runaway
	2.3b	EOG	1.1	Grid loss
Parked	6.1	EWM	1.1	No
	6.2	EWM	1.1	Grid loss

Table 4.1. Selected DLC's for the parametric analysis.

4.1 Key Performance Indicators

The outcomes of the simulations have been analysed and selected accurately with a critical spirit in order to provide reliable data representative as much as possible of the physics of the phenomenon. In this light, we have decided to evaluate the impact of wake steering by yaw-misalignment by providing the Key Performance Indicators (KPI), which will be shown with a parametric representation, so that the influence of wind farm control can be appreciated immediately. They consist of: power production, ultimate and fatigue loads.

4.1.1 Power production

Power production is studied by means of power curve, a powerful tool able to estimate the power extraction process of wind turbines. In this regard, Figures 4.2 and 4.4 reveal the power curves achieved by applying the wind farm control. They have been computed following the procedures defined by IEC [51] exploiting data coming from DLC11, which represents the normal operative conditions of wind turbines. In this performance, both turbines display a similar trend, in fact it is quite clear that yaw-misalignment implies an overall reduction of the power extracted. From a physical point of view, this is an expected outcome because the incoming wind is not perpendicular to the rotor plane, which is rotated by θ. As a consequence, power output is proportional to $(V \cos\theta)^3$. In Figure 4.3 and 4.5 the decrease of AEP for each of the yaw angles examined is quantified. It is an unsurprising result since power production impacts directly the AEP according to Eq. 3.16.

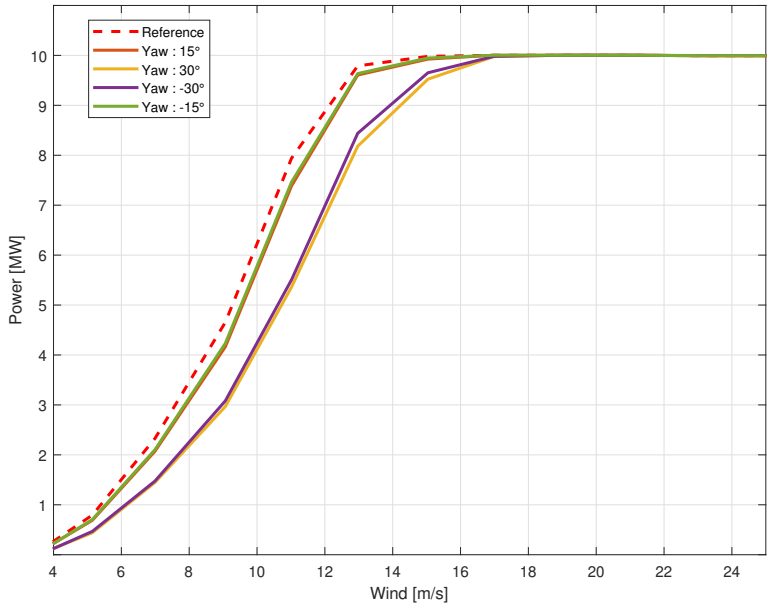

Figure 4.2. Comparison between the power curves for each of the yaw angles for the INNWIND.EU 10 MW.

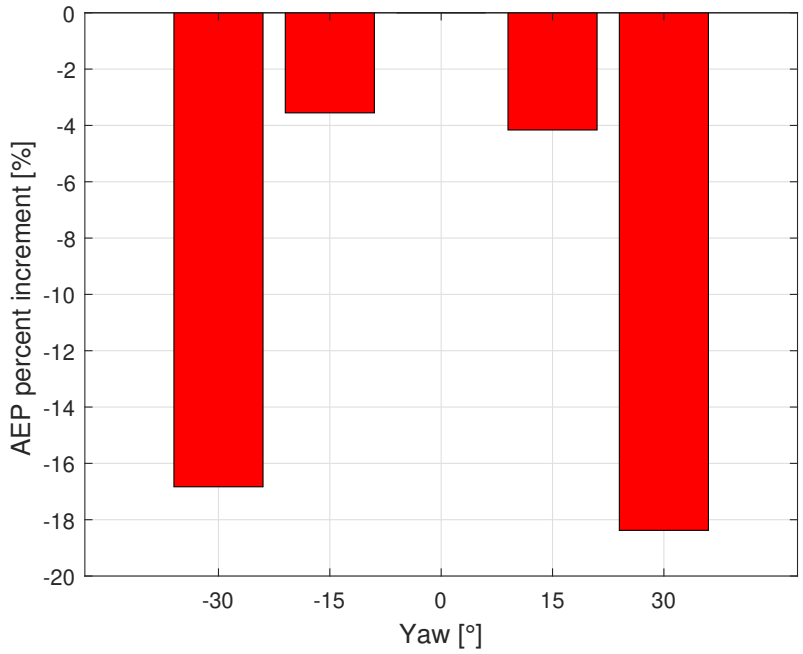

Figure 4.3. AEP percent increments for each of the yaw angles for the INNWIND.EU 10 MW.

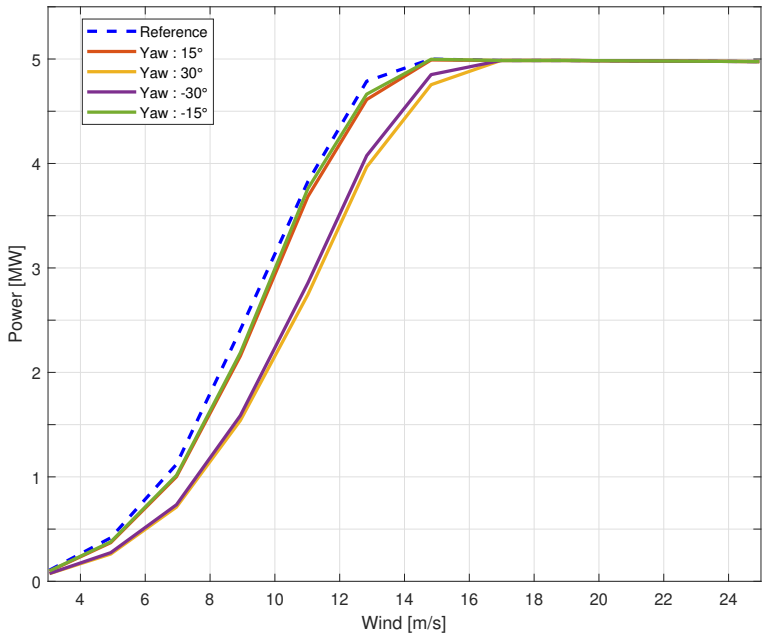

Figure 4.4. Comparison between the power curves for each of the yaw angles for the NREL 5 MW.

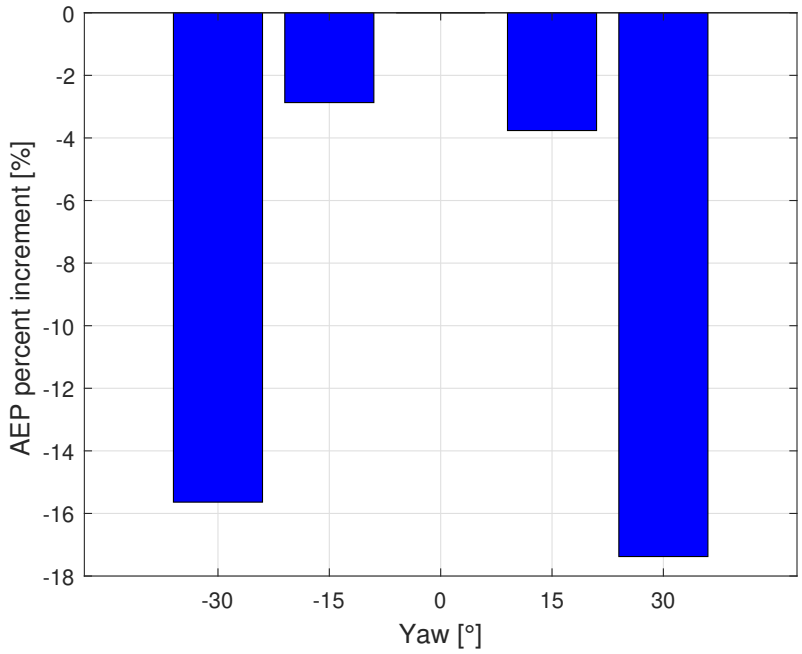

Figure 4.5. AEP percent increments for each of the yaw angles for the NREL 5 MW.

4.1.2 Ultimate loads

Ultimate loads play a fundamental role on wind turbines driving their design. It is, therefore, essential to understand how wind farm control may impact the envelope loads and ultimate displacements of a single turbine. In this Section, we present the outcomes of the parametric analysis performed on both turbines showing the most significant maximum loads of different parts of the turbine. Clearly, the broad set of DLC's performed allows for an extended variety of conditions from which the ultimate loads can be computed, setting an optimal benchmark to understand the incidence of this control strategy on existing turbines. In following figures, maximum loads have been scaled with respect to the configuration in which the machine is not yawed ($\theta = 0°$) to simplify further the viewing.
Figures 4.6 and 4.7 consider the blade root, showing the percentage increments of flapwise, edgewise and combined loads for both turbines. From a qualitative point of view, it is evident that both machines exhibit similar trends. Focusing on flapwise, loads on blade show a clear asymmetry between $\theta = 30°$ and $\theta = -30°$, registering, respectively, an increase and a decrease. Furthermore, as far as edgewise load is concerned, it is possible to note a general and substantial increase for both turbines. However, since the flapwise contributes more to the combined flapwise/edgewise moment, the trend of the latter matches the flapwise bending. It is important to highlight that maximum loads are extracted from DLC1.4 for both turbines. This design load case represents an extreme coherent gust with direction change. However, the turbines are initially yawed so that the incoming wind is not fully perpendicular to the rotor but as soon as the gust arrives, the wind starts to change direction approaching and eventually overcoming the yaw angle of the machine. In this way, combining this effect with the coherent increase in magnitude of wind, the turbines

experience an extreme situation where the supervisor switches off the machines to preserve the structural integrity. For example, this behaviour can be observed during the simulation at V_{r-2} by the INNWIND.EU 10 MW as shown in Fig 4.10. Likewise, a similar attitude can be shown for the other machine. Another fundamental aspect that drives the performance of a blade is its tip displacement. In fact, it is fundamental to avoid improper deflection which leads to collision with the tower. From Figure 4.8 and 4.9 it is possible to note that the abovementioned DLC affects consistently also the maximum tip displacement. This result will assume a key-role in our subsequent redesign study, as it drives the blade sizing.

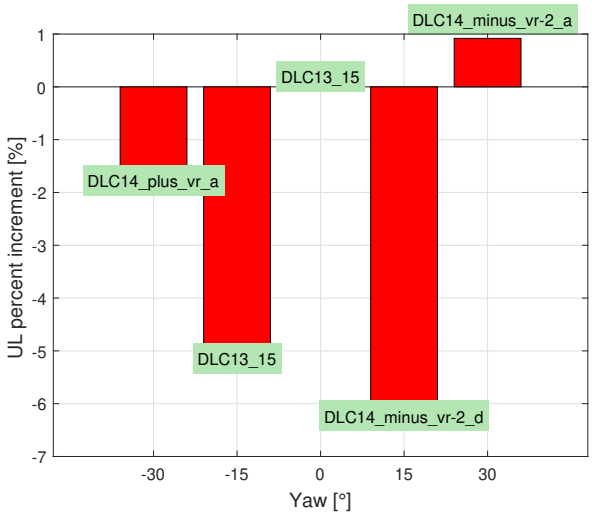

(a) Blade root flapwise.

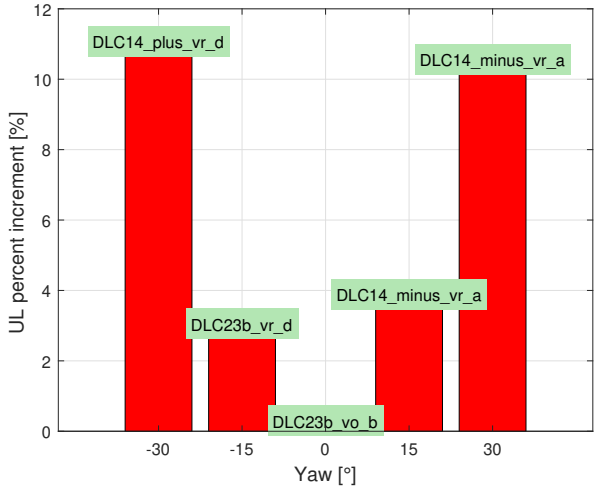

(b) Blade root edgewise.

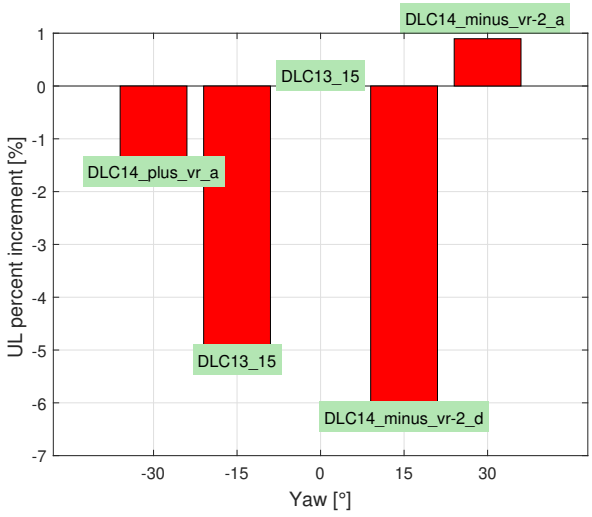

(c) Blade root combined load.

Figure 4.6. Blade root ultimate loads percent increments for each of the yaw angles for the INNWIND.EU 10 MW.

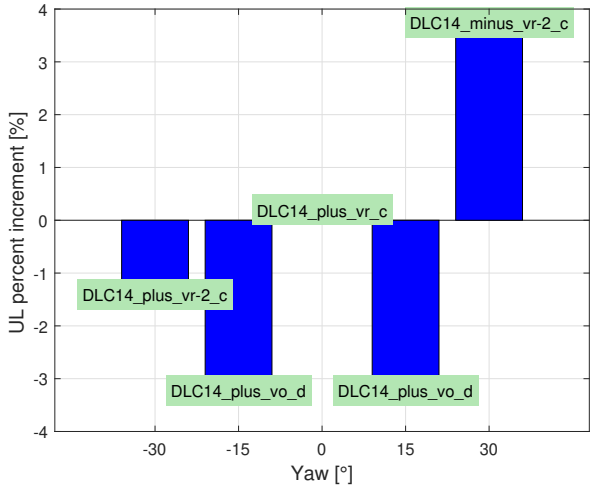

(a) Blade root flapwise.

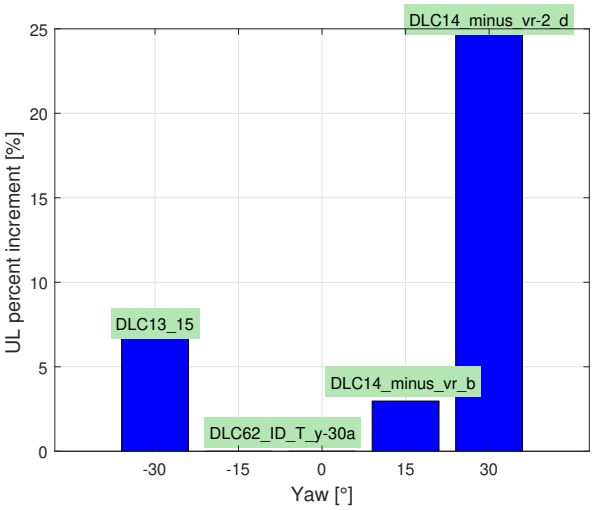

(b) Blade root edgewise.

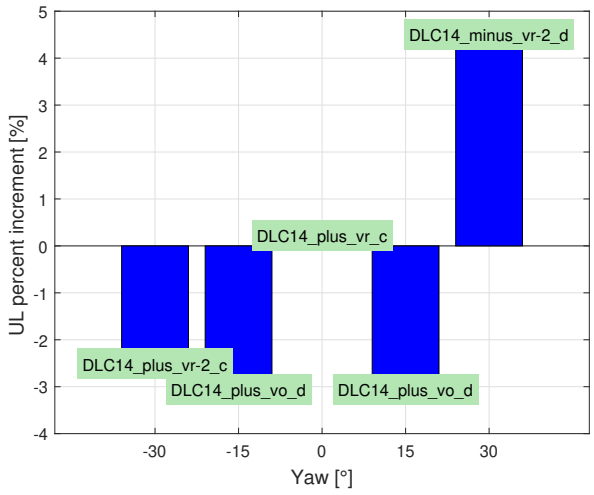

(c) Blade root combined load.

Figure 4.7. Blade root ultimate loads percent increments for each of the yaw angles for the NREL 5 MW.

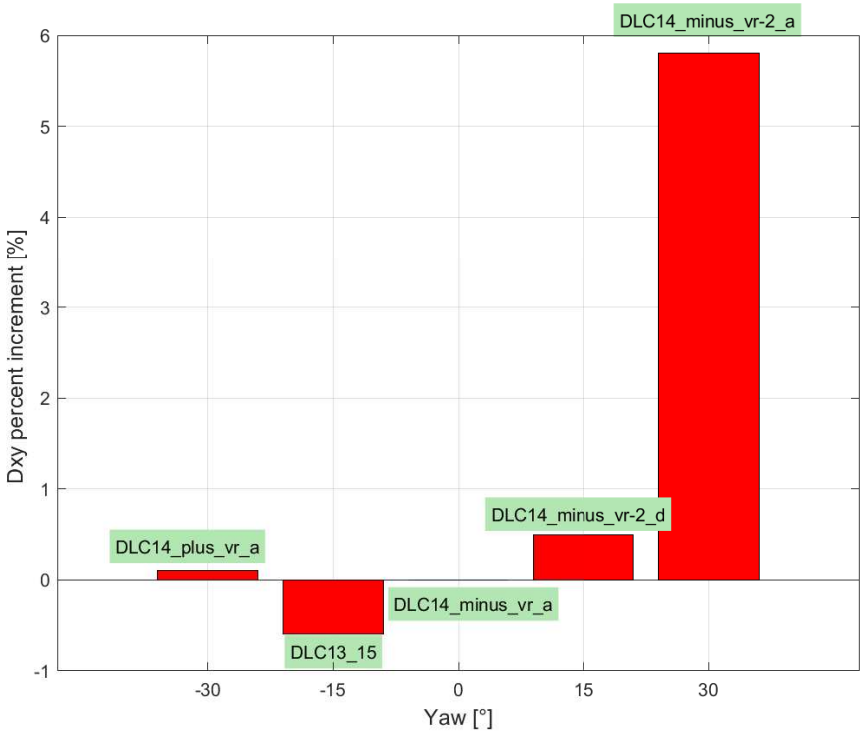

Figure 4.8. Blade tip displacement for the INNWIND.EU 10 MW.

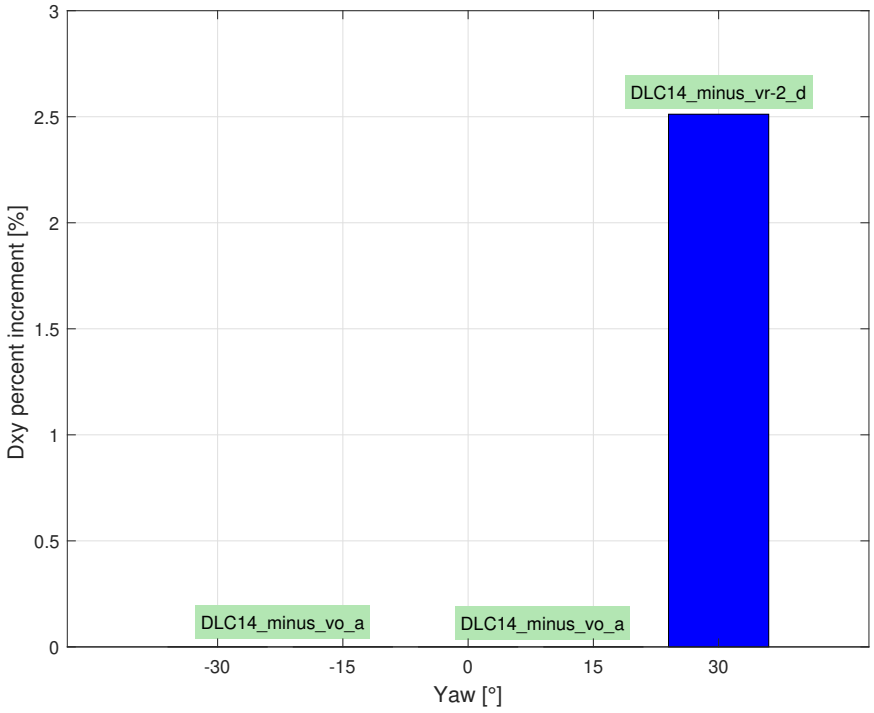

Figure 4.9. Blade tip displacement for the NREL 5 MW.

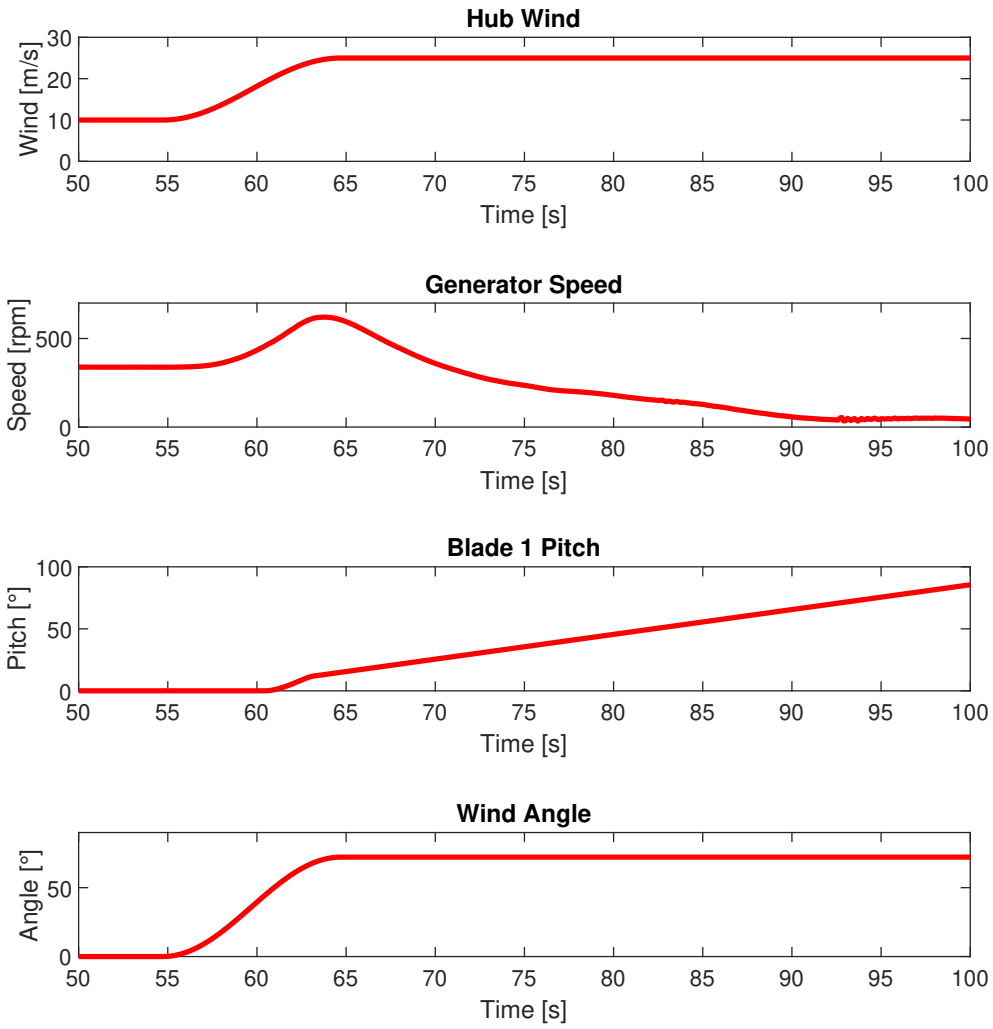

Figure 4.10. Effect of ECD on the INNWIND.EU 10 MW at minus V_{r-2}.

The results of the tower are displayed in Figure 4.11 and 4.12. We have decided to display only the flapwise/side-side combined load because sensors, designated to measure the bending moments of the tower, are not rotating according to the wind turbine. As a consequence, when the machine is yawed, they measure loads in different frames so that an equal comparison cannot be provided by showing the fore-aft and the side-side individually. The ECD seems to play still a fundamental role returning for both machines higher loads with respect to the reference conditions. Although they exhibit similar trends in terms of tower base, the percentage increase is clearly different: the NREL shows an higher increment of one order of magnitude with respect to INNWIND.EU. As far as tower top is concerned, it is not possible to evidence a similar trend between both turbines since their load spectra is clearly different.

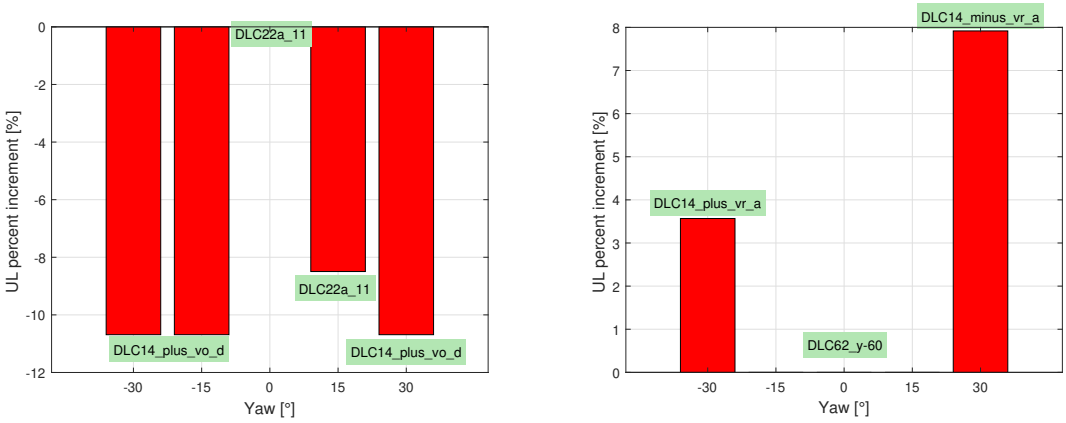

(a) Tower top combined load.

(b) Tower base combined loads.

Figure 4.11. Tower ultimate load percent increments for each of the yaw angles for the INNWIND.EU 10 MW.

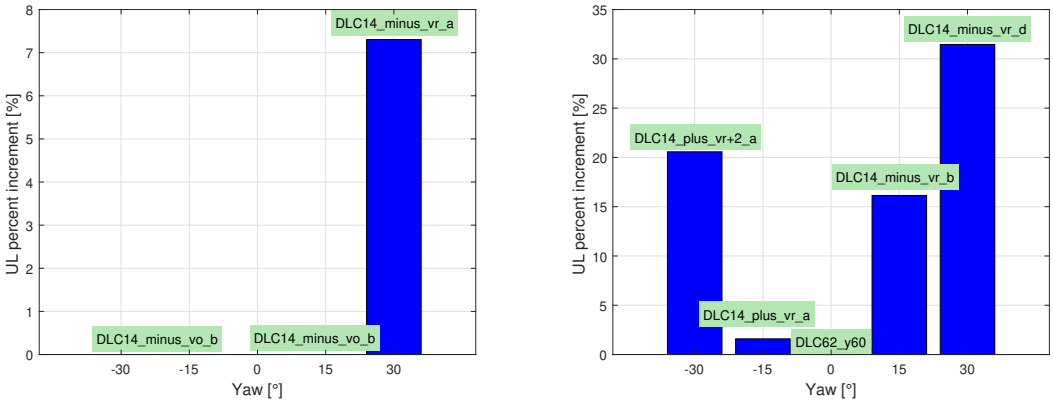

(a) Tower top combined load.

(b) Tower base combined load.

Figure 4.12. Tower ultimate load percent increments for each of the yaw angles for the NREL 5 MW.

Figure 4.12 shows the hub nodding/yawing combined load for the NREL 5 MW. In the analysed case, wind farm control seems to have an impact at $-30°$. This result can be justified by the yaw-misalignment and the vertical wind shear coupling, giving rise to a load increase of about 3.5%. However, as far as the INNWIND.EU is concerned, no relevant outcomes have been obtained.

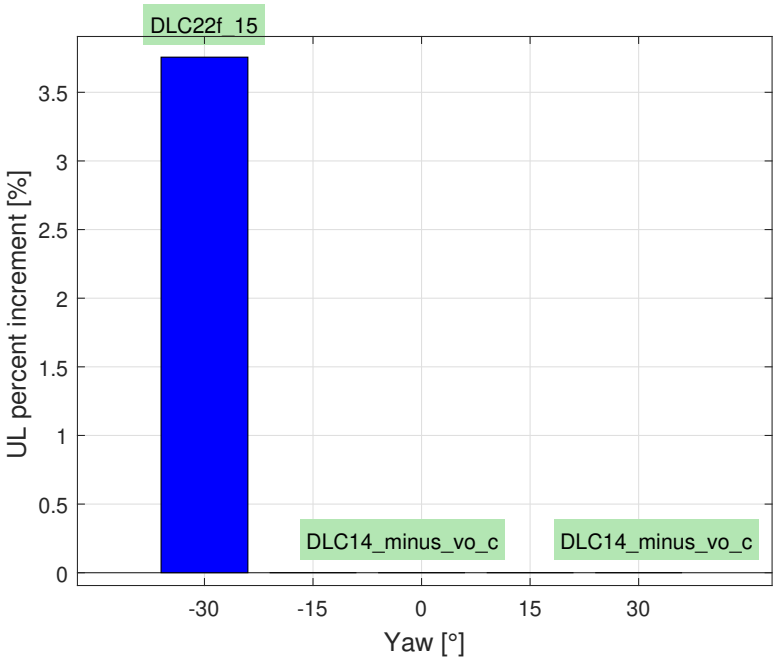

Figure 4.13. Hub combined load percent increments for each of the yaw angles for the NREL 5 MW.

4.1.3 Fatigue loads

Fatigue constitutes a fundamental performance indicator because it provides a lifetime evaluation of wind turbine components. In this context, the study has been carried out differently compared to the ultimate loads. In fact, the usual way to measure bending loads on shafts, blades, and towers is to use two sensors placed at 90°. However, when the shaft is bent, it is not necessarily bent purely in the direction of one of the sensors, but at some angle in between. However, the sensors measure only the bending moments in those two directions. For ultimate loads, it is possible to consider the combined, but when trying to determine the fatigue damage, it is not reasonable to calculate the damage of the loads measured by the two sensors because it is unlikely that either orientation represents the most heavily loaded one. In this regard, a load roses might be necessary before computing the rainflow analysis to determine the fatigue damage for each of the load rose's orientations. Anyway, since a similar procedure is time-consuming and implementing is not the scope of our research, a different approach between tower base and blade root has been followed. Considering that sensors of blade root rotate according the machine, we have assumed that it is reasonable to compare values from rainflow analysis without using load roses. On the contrary, as for tower base, this procedure has been implemented for each of yaw angles θ:

- the time history of foreaft load has been rotated by an angle ϕ defined in the same reference frame of θ, from 0° to 180°;
- for each of ϕ values, a rainflow analysis has been performed;

- the most heavily loaded orientation has been extracted for each of the angle ϕ, by selecting the maximum value among the cumulated DEL

The fatigue analysis carried out on blade root for both models is shown in Figure 4.14 and 4.15. Basically, it is possible to note that the trend of the flapwise and the edgewise DEL are comparable. However, as for the first machine, we can observe that for $\theta = -15°$, the flapwise DEL is slightly higher than the case with null yaw angle leading to a higher cumulated load. Instead, the NREL turbine exhibits nothing relevant. As far as the tower base is concerned, the above-mentioned procedure has been followed so that the most heavily loaded orientation has been found to be in agreement with the yaw angle of the turbine. The results are shown in Fig 4.14 and Fig 4.17.

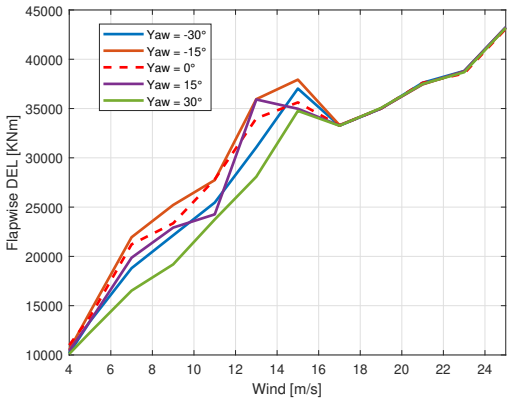

(a) Blade flapwise DEL.

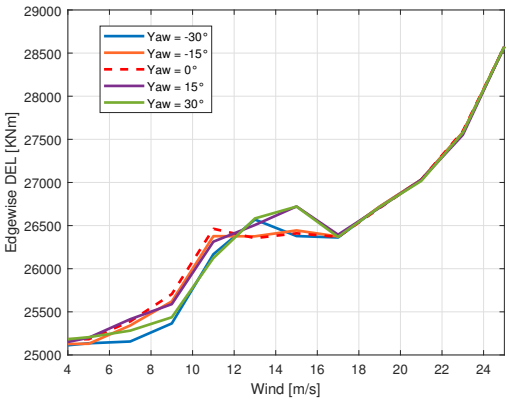

(b) Blade edgewise DEL.

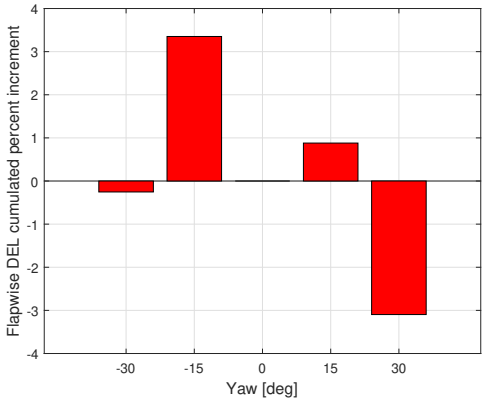

(c) Blade flapwise DEL's cumulated percent increments.

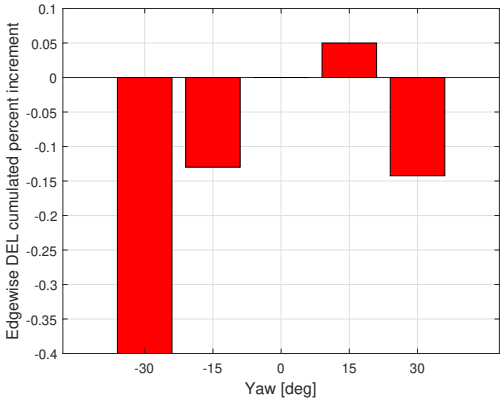

(d) Blade edgewise DEL's cumulated percent increments.

Figure 4.14. Fatigue analyses on blade root for the INNWIND.EU 10 MW

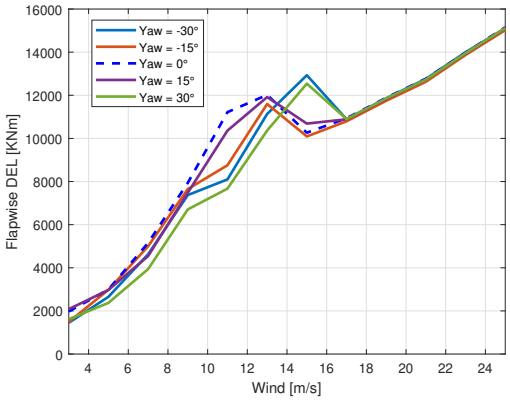

(a) Blade flapwise DEL.

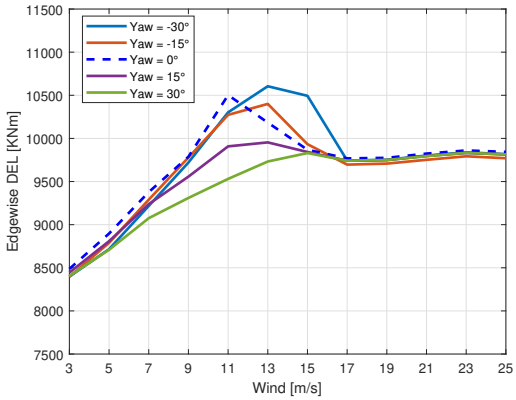

(b) Blade edgewise DEL.

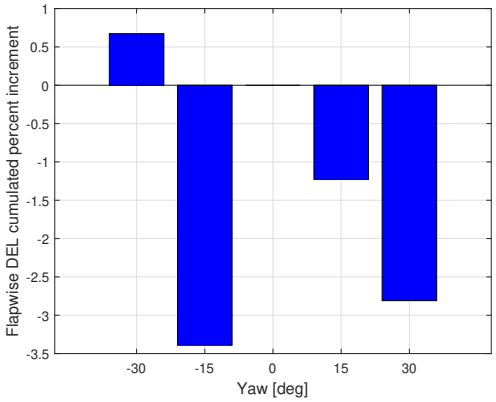

(c) Blade flapwise DEL's cumulated percent increments.

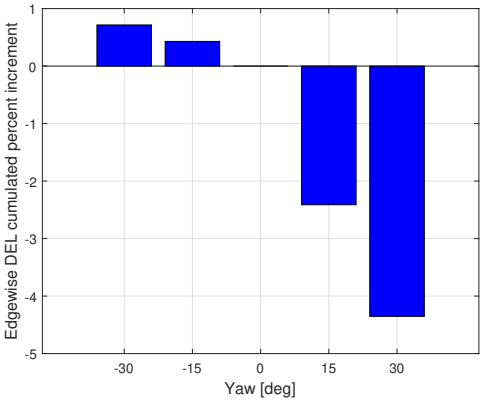

(d) Blade edgewise DEL's cumulated percent increments.

Figure 4.15. Fatigue analyses on blade root for the NREL 5 MW.

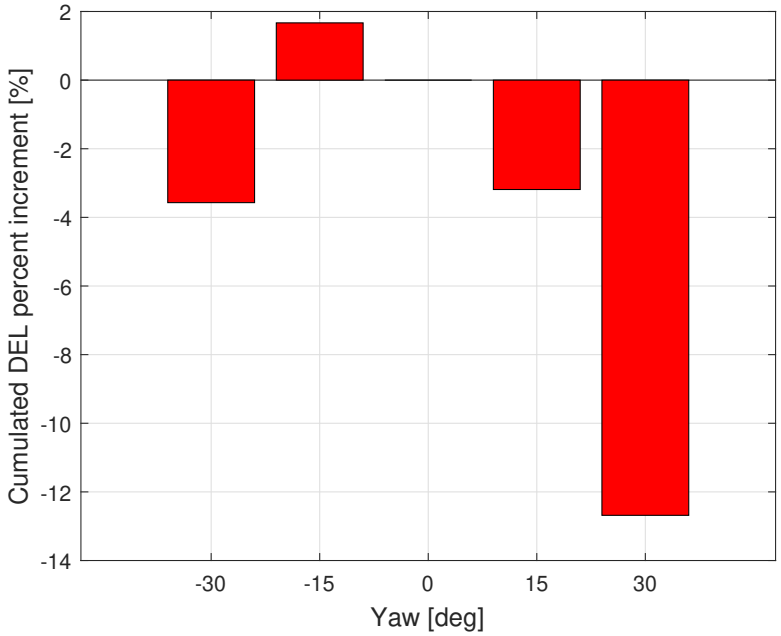

Figure 4.16. Tower foreaft DEL's cumulated percent increments for the INNWIND.EU 10 MW.

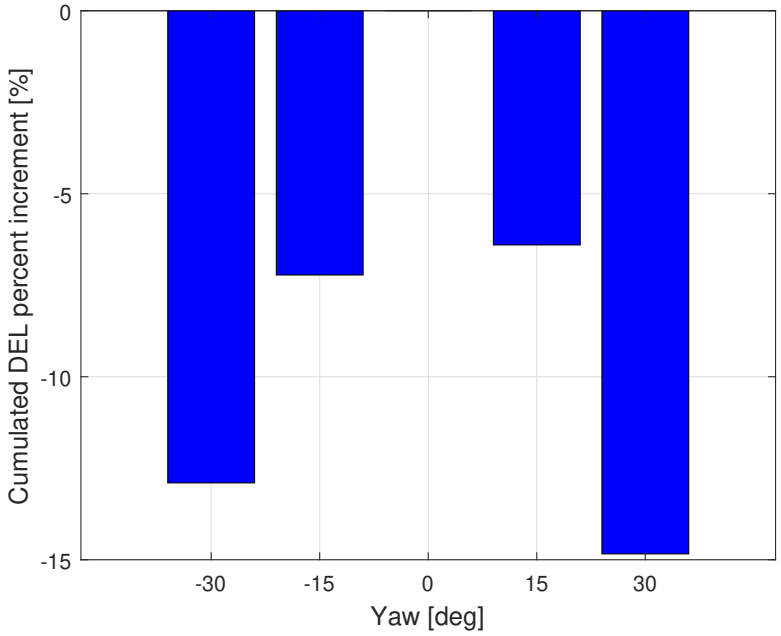

Figure 4.17. Tower foreaft DEL's cumulated percent increments for the NREL 5 MW.

4.2 Main outcomes

This section provides a brief overview of the fundamental achievements of this analysis. Firstly, power production is clearly reduced for both machines, however, since the

scope of wake steering is driving the wake, this result should be evaluated bearing in mind the possible benefit experienced by downwind turbines. However, this is far beyond the scope of the Thesis. As far as ultimate loads are concerned, even though loads spectra are wind turbine dependents, our research has discovered a common trend between both turbines. In fact, we have noted a significant increment of the blade multi-directional combined load for $\theta = 30°$ which has been triggered by an extreme coherent gust with wind direction changes. As a consequence, this impacts also the behaviour of the ultimate displacements which exhibit a similar trend. These results indicate that the application of the studied WF control must be carefully evaluated according to the structural peculiarities of the turbines. For example, in our investigation, both the 10MW and the 5MW feature fiberglass blades. Therefore, it might be necessary to examine if the increase of blade tip displacement could represent a problem, inspecting the tip clearance. However, this is not the purpose of this stage, in fact this will be studied in Chapter 5 during the redesign. Alternatively, one could limit the range of yaw angles causing a likely decrease of wake steering effectiveness. Likewise, a similar trend is observed for the tower. This consequence suggests conducting a preventive analysis before applying the investigated WF control to avoid potential detriments. Although the performed fatigue analysis presents potential limits, it seems not to constitute a serious problem to the life-cycle of both turbines, considering the fact that turbines equipped with the studied WF control don't operate constantly with yaw-misalignment. In this context, results should be further weighted through a probability density function to take into account this aspect, here neglected.

Chapter 5

Redesign of a 10 MW turbine

In this Chapter we provide a redesign activity to evaluate the impact of the wind farm control upon the structure of a wind turbine. In particular, we are interested in understanding if a resizing of a blade is unavoidable to withstand the higher loads and displacements introduced by the investigated WF control, as we have reported in Section 4.2. The ideal tool for reaching this goal is Cp-Max, as it offers the possibility to provide a high-fidelity conceptual design meeting the constraint enforced by the international guidelines (see Section 3.3.2). In this regard, it is primarily necessary to obtain a baseline which is correctly sized so that the effects of a subsequent resizing may be caused only by the introduction of the wind farm control and not by the fact that the first configuration proves incorrectly sized. As a consequence, we have employed as a reference turbine the INNWIND.EU 10 MW (see Section 3.1.1) and subsequently, used the SDS sub-module of Cp-Max to optimise the rotor structure in order to attain the baseline. At this stage, we have decided to consider the same set of DLC's proposed for the parametric analysis as they are already well-representative of a broad design situation. In a later phase, we have introduced simulations in which the baseline is yawed by the angle θ into the redesign procedure in order to implement the investigated WF control strategy. Finally, a sub-set of DLC's has been built to speed up the work due to the excessive computational cost without neglecting all the cases which return the most severe loads and displacements.

5.1 Definition of the baseline

In a first step, a preliminary design of the internal structural layout of the blades has been performed to identify a feasible sizing of the structural components trying to meet the properties of the reference turbine. In this light, an internal structural topology has been defined to reach the above-mentioned goal before starting with the optimization procedure provided by the SDS of Cp-Max. The definition of the structural topology of the blade has been carried out using a typical arrangement based on a spar-box containing two spar-caps and two identical shear webs bonded together to form the main box. However, a third shear web has been introduced to reduce the free length of the shell panels and to retard the onset of buckling because of the wide chord of the rotor. The description of the sections of the blade requires the definition of equivalent panels, or sectional elements, associated to a certain

lamination sequence. The internal blade layout consists of: four shell panels, two spar caps (suction side and pressure side), three main shear webs, leading edge and trailing edge panels which can all be observed in Fig 5.1. Conversely, Tab 5.1 lists the mechanical properties of the material which have been defined according to the reference model.

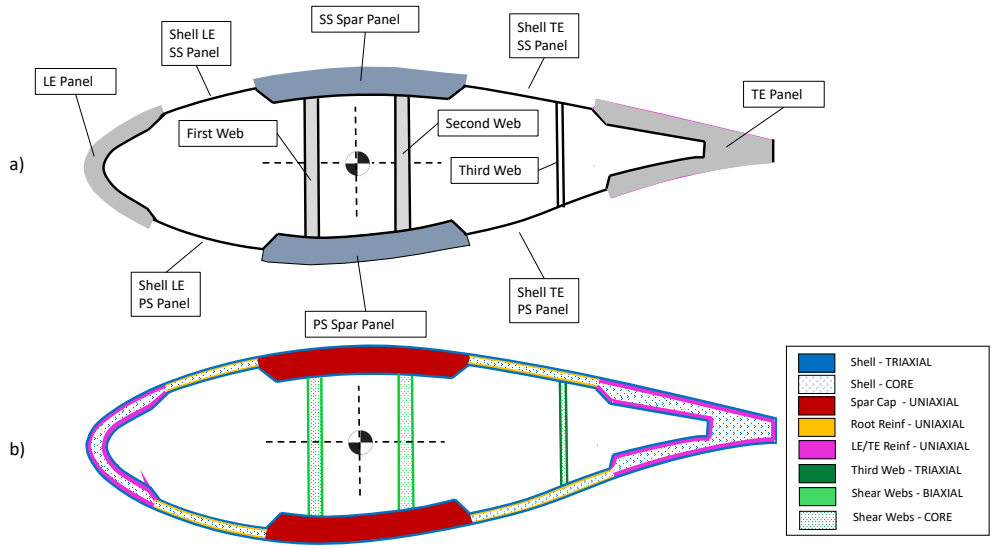

Figure 5.1. Model of the section : Sectional elements (a) and structural components (b).

Each of these sectional elements of the blade has its purpose inside the blade layout:

- shell panels maintain the shape of the aerodynamic airfoils absorbing torsional loads;
- webs withstand torsional and shear loads and reduce the buckling;
- spar caps are responsible for bearing the flapwise bending;
- root reinforcement grants a better redistribution of the loads;
- leading and trailing edge panels bear edgewise bending and reinforce the in-plane stiffness;

Figure 5.2 shows the blade planform and thus the position of the elements inside the section. The x-axis represents the blade axis, while the y-axis goes from the leading edge to the trailing edge.

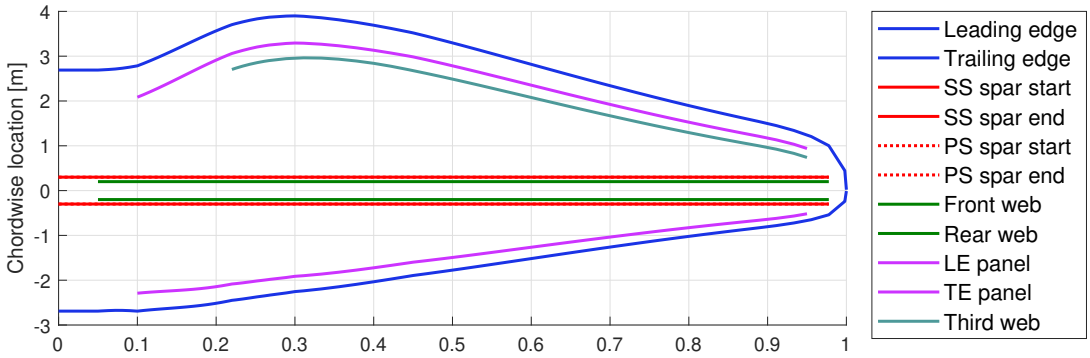

Figure 5.2. Blade planform of the baseline.

Property		Unidirectional	Biaxial	Triaxial
E_{11}	$[GPa]$	42	13.92	21.79
E_{22}	$[GPa]$	12.3	13.92	14.67
ν_{12}	$[-]$	0.31	0.53	0.5
G_{12}	$[GPa]$	3.47	11.5	9.413
ρ	$[Kg/m^3]$	1940	1845	1845
σ_{max}	$[MPa]$	868	223.2	480.4
σ_{min}	$[MPa]$	869	209.2	393

Table 5.1. Mechanical properties of the materials.

The thicknesses of each structural component represent the optimisation variables employed in the design process. They are defined at 16 significant sections along the blade span. Generally, each element can be sized independently, however, considering the high number of DLC's involved in the work, some topological assumptions have been considered to reduce the number of unknowns. Specifically, the four shell panels and the two main webs are linked, while the third web and the root reinforcement can evolve independently. Eventually, the leading and trailing reinforcements are not enforced to evolve together while the two spar caps are assumed to be identical. This choice is justifiable since glass solutions are mainly constrained by the maximum tip deflection, and in this view it would make no sense to decouple the two spar caps. The optimal value of each structural components is given in Table 5.2. The final characterisation of the blade is obtained interpolating both thicknesses and bounds defined at 77 sections.

η	t_{shell}	t_{spar}	t_{webs}	$t_{3_{rd}web}$	t^{LE}_{strip}	t^{TE}_{strip}	t_{rr}
0.000	50.00	-	-	-	-	-	15.00
0.010	50.00	-	-	-	-	-	15.00
0.025	30.00	-	-	-	-	-	15.00
0.050	12.00	1.00	1.00	-	-	-	8.50
0.100	5.00	10.34	1.00	-	0.10	1.00	8.35
0.153	4.00	60.00	2.50	-	4.06	7.00	5.36
0.220	3.00	103.61	5.00	4.50	3.50	9.00	3.54
0.268	3.02	119.23	5.50	5.00	3.51	11.00	2.41
0.355	3.09	114.88	6.09	6.00	3.20	11.00	2.65
0.450	3.70	111.70	7.12	7.00	3.00	6.00	-
0.555	3.23	93.24	7.62	4.50	3.07	5.00	-
0.650	2.41	69.15	8.00	4.00	4.42	3.31	-
0.800	1.08	30.38	8.34	3.75	0.75	1.64	-
0.900	1.00	20.00	6.00	3.50	0.10	0.10	-
0.950	1.57	5.69	5.00	3.00	0.10	0.10	-
0.977	1.42	4.86	3.50	-	-	-	-

Table 5.2. Spanwise values of the design variables.

The lamination sequence of the blade elements is provided in Figure 5.3. It must be highlighted that although the unidirectionals show different colours, all the components are based on the same material. The main performances of the rotor, reported in Table 5.3, are: the first flapwise frequency of the isolated clamped blade, the maximum tip displacement, the total blade mass, the AEP computed from the DLC1.1 and the corresponding CoE. Instead, Tables 5.4 and 5.5 report the ultimate loads and fatigue equivalent loads. All these values will be employed as reference values in the redesign activity described in the next section.

Frequency	Displacement	Blade mass	AEP	CoE
0.58 Hz	15.94 m	40637 kg	45.86 GWh	89.43 €/MWh

Table 5.3. KPI of the baseline rotor.

Sensor	Load	Value	
Blade root	Combined	73.62	[MNm]
Hub	Thrust	3.76	[MN]
	Combined	81.454	[MNm]
Tower Top	Combined	77.45	[MNm]
Tower Base	Combined	1178	[MNm]

Table 5.4. Ultimate loads provided by the baseline.

Sensor	Load	Value	
Blade root	Flapwise	34.91	[MNm]
Hub	Nodding	26.60	[MN]
	Yawing	24.74	[MNm]
Tower Top	Fore Aft	26.37	[MNm]
Tower Base	Fore Aft	134.95	[MNm]

Table 5.5. DEL's provided by the baseline.

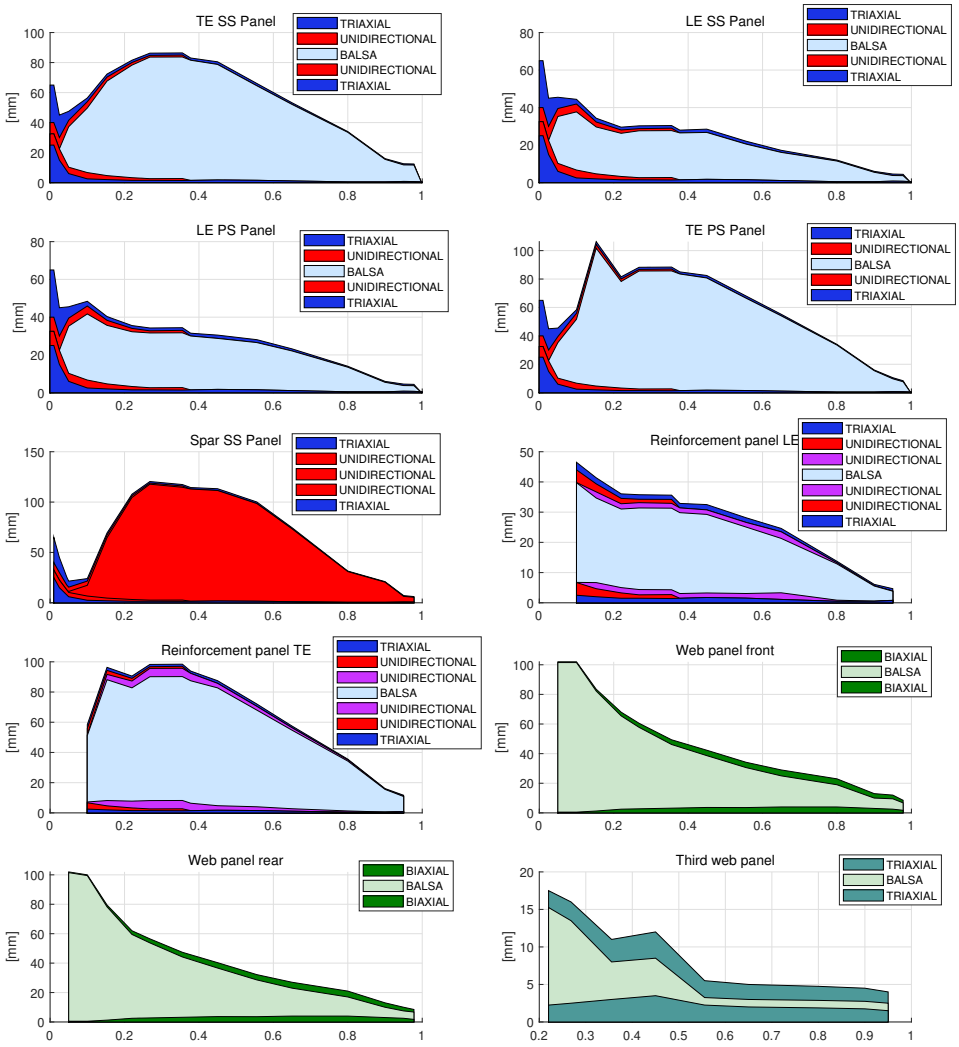

Figure 5.3. Lamination sequence of the sectional elements of the blade.

5.2 Redesign procedure

Once the baseline has been defined, we have conducted a series of redesign steps with the aim of providing a turbine which is able to withstand the severe loads and displacement returned by the studied WF control. However, the aerodynamic optimisation has been excluded from the overall loop as we are interested in observing the evolution of the blade structure as a direct consequence of WF control and not by the fact that the aforementioned optimisation has been performed. In view of the aim, we have initially added the complete set of DLC's accounting for yaw misalignment to the list of performed simulations. However, we have decided to build a sub-set of simulations in the following steps to drastically reduce the computational time, without losing the effects caused by the implementation of the WF control strategy. In fact, the most significant design situations in terms of ultimate loads and displacements have been considered so that the final number of sizing DLC's has been reduced to approximately 100, as listed in Tab 5.6. Finally, it must be clear that the overall design has been limited to the rotor neglecting the tower and other components of the turbine. Furthermore, we have decided to exclude the yaw-misalignment from the fatigue sizing being supported by the results achieved in the parametric analysis carried out in Chapter 4. Results of the last iteration of the redesign will be discussed and compared with the baseline to explore the consequence of the activity.

DLC	Wind	Speed [m/s]	Yaw [°]	Safety Factor	Faults
1.1	NTM	4 : 25	0	1.35	No
1.3	ETM	4 : 25	0	1.35	No
1.4	ECD	4 : 25	0	1.35	No
1.5	EWS	4 : 25	0	1.35	No
2.2a	NTM	4 : 25	0	1.1	Grid loss Freeze on Pitch
2.2b	NTM	4 : 25	0	1.1	Grid loss Mechanical Brake
2.2f	NTM	4 : 25	0	1.1	Pitch runaway
2.3b	EOG	4 : 25	0	1.1	Grid loss
6.1	EWM	4 : 25	0	1.1	No
6.2	EWM	4 : 25	0	1.1	Grid loss
1.3	ETM	4 : 15	[-30,-15,15,30]	1.35	No
1.4	ECD	4 : 15	[-30,-15,15,30]	1.35	No

Table 5.6. Sub-set of DLC's employed during the subsequent stages of the redesign.

5.2.1 Results

In this Subsection, we present the main results of the work. An overview of some of the key performance indicators is given in Tab 5.7 in terms of blade mass, AEP and CoE. The most significant result is the substantial increase of the blade mass which directly affects the cost of energy, considering that the AEP is similar between the two

rotors. However, this is a predictable result due to the fact that the baseline already constitutes an optimal starting point. In this regard, the optimisation procedure has evolved towards a solution able to comply with the constraints which have been violated after the introduction of the WF control. In particular, the maximum tip displacement has driven the whole design loop to a consistent increment of the thicknesses of the sectional element of the blade, with particular regard to spar caps, as shown in Figure 5.4.

	Blade Mass [Kg]	AEP [GWh/year]	CoE [€/MWh]
Baseline	40637	45.86	89.43
Yaw control	45766	45.87	89.78
Increment [%]	12.62	0.04	0.4

Table 5.7. Performance comparison between the two solutions.

The higher thicknesses of the sectional elements allow for a stiffer blade, as displayed in Fig 5.5, capable of withstanding the loads provided by the WF control. Consequently, the two compared blades show a similar trend in terms of blade spanwise displacement, as illustrated in Fig 5.6. Figures 5.7 and 5.8 show respectively the variations of the most representative ultimate and fatigue loads experienced by both turbines. The results are normalised with respect to the baseline so that the loads of the latter are equal to 1. BR means blade root, TT and TB indicate the top and the root of the tower while HC signifies the hub center. The edg, flp, tors, cmb components represent the edgewise, flapwise, torsion and combined while yaw and nod are the yawing and nodding components at the hub. The tower bendings are represented by FA and SS which stand for fore-aft and side-side, respectly. The redesigned turbine experiences generally much higher loads than the baseline in terms of ultimate and fatigue loads. However, as far as the blades are concerned, this trend should not raise concerns because the employed procedure provides a solution which automatically meets the enforced constraints. On the contrary, the behaviour of the tower and the hub should be further investigated because they have been excluded from the overall design loop. In this perspective, it would be interesting to understand in detail whether a redesign of both turbine elements is necessary.

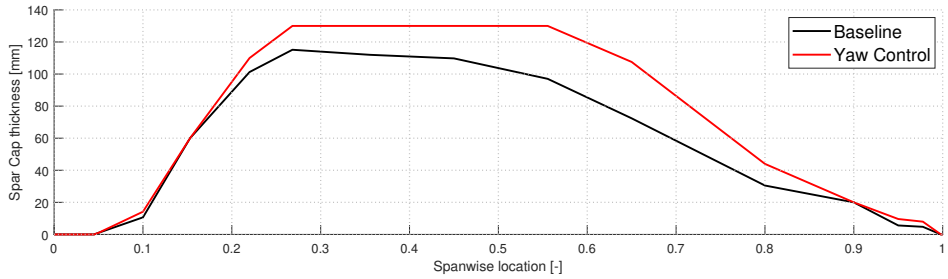

(a) Spar caps.

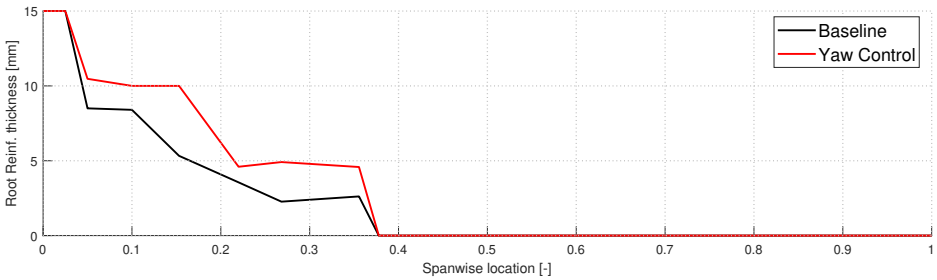

(b) Root reinforcement.

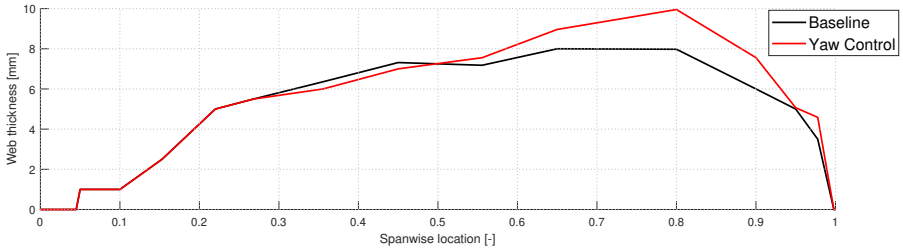

(c) Main webs.

Figure 5.4. Comparison of mainly changed sectional elements between the two solutions.

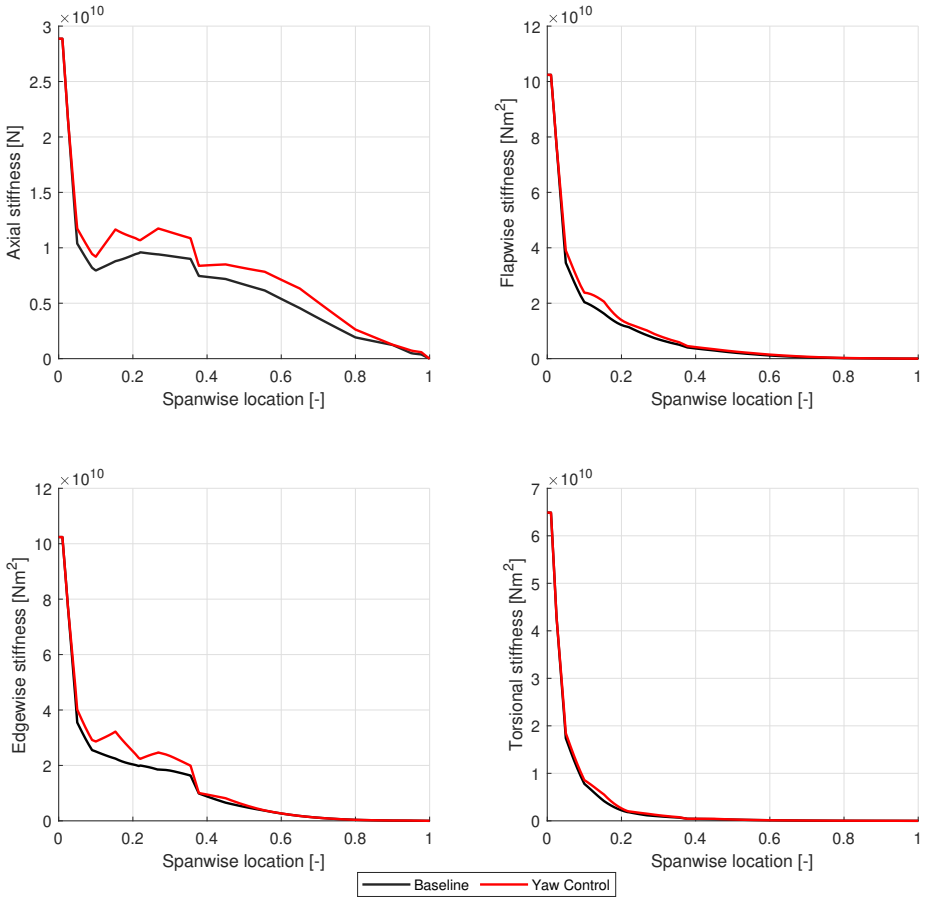

Figure 5.5. Comparison of blade stiffness between the two solutions.

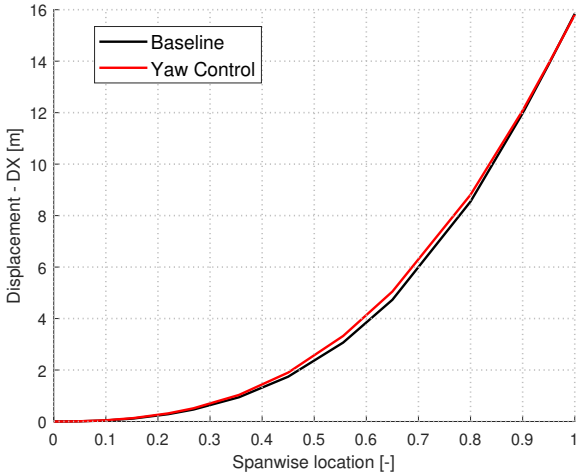

Figure 5.6. Comparison of blade spanwise DX displacement between the two solutions.

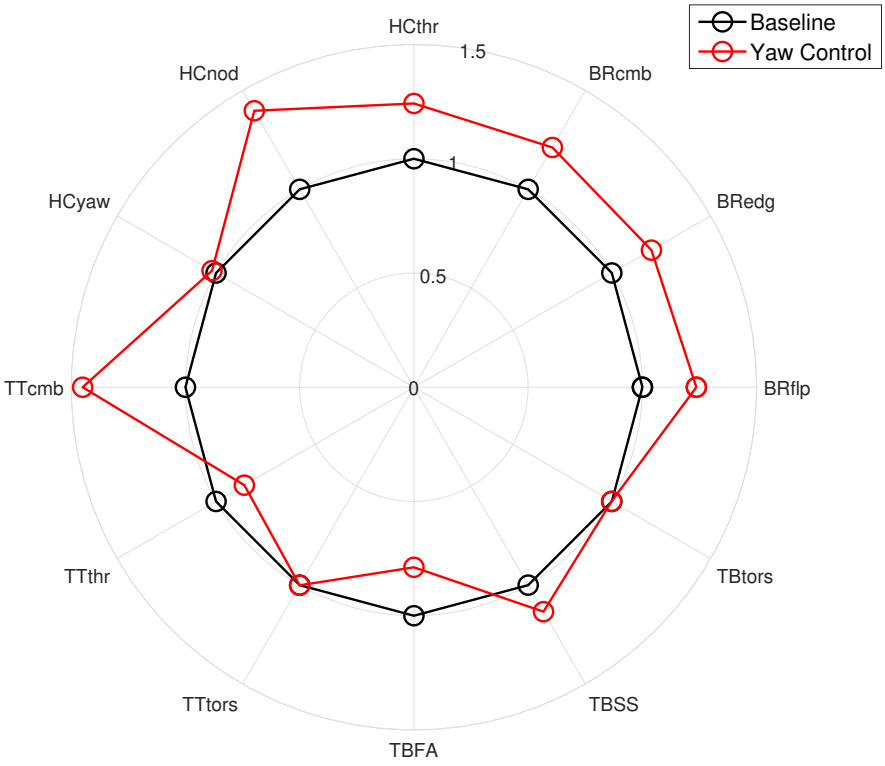

Figure 5.7. Comparison of ultimate loads between the two solutions.

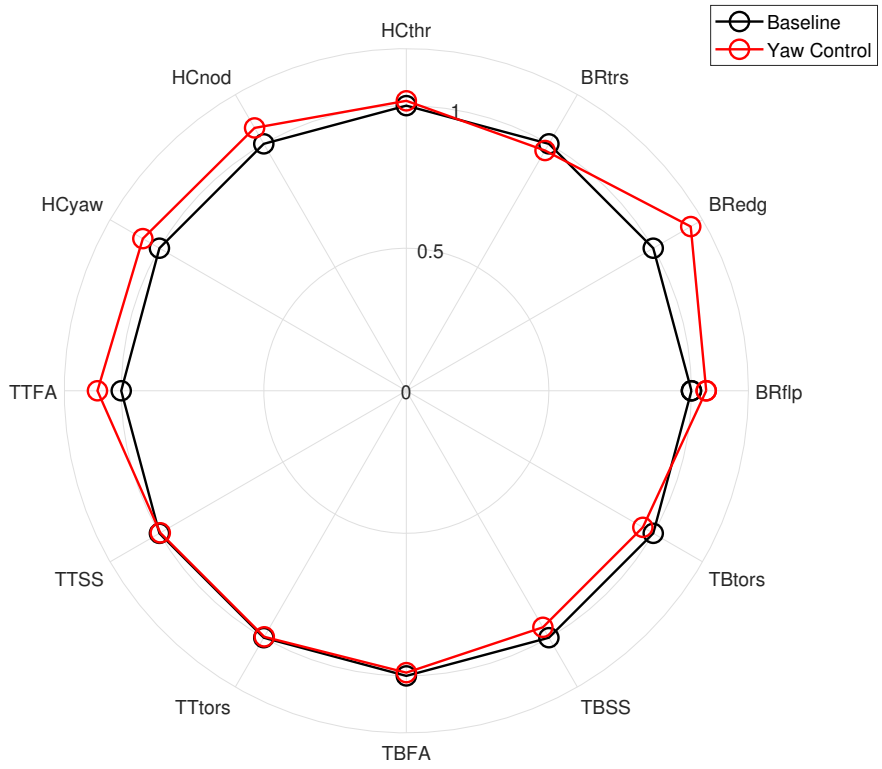

Figure 5.8. Comparison of the fatigue loads between the two solutions.

Chapter 6

Conclusions and future developments

This Thesis investigates the effects of the wake steering by yaw-misalignment on the upwind active turbine to evaluate its impacts on the key performance indicators (KPI) in terms of power productions and loads. In this light, it has been decided to employ mathematical models representing the state of the art for what concerns the design of wind turbines taking into account the current guidelines. Thus, we have performed parametric analyses on two reference turbines having different sizes to understand how the investigated control strategy impacts them to show if possible common trends exist between the two models and if would be possible to draw generalised conclusions from this study. As a first step, we have performed a full comparison between a specific controller (OpenWitcon) employed for the use of wind farm operations with a benchmark controller (DTU) to evaluate the response of the former. This has been necessary because wind farm controllers are relatively new and their use in highly-detailed numerical models is still fairly unexplored. Results have clearly shown that there are no substantial differences between the two solutions, validating indeed the OpenWitcon controller. At the end of this phase, we have started our parametric analysis upon the INWIND.EU 10 MW and NREL 5 MW reference turbines, in order to extract key performance indicators of the turbines. This task has been achieved by applying different yaw angles θ on the upwind turbine and, then, performing a wide range of design load cases. The main results provided by both turbines are briefly listed below:

- a predictable reduction of power production;
- an increase of flapwise-edgewise combined load for the blade (about 1% for the INWIND.EU and 4% for the NREL) and multi directional combined load for the tower root (about 8% for the INWIND.EU and 30% for the NREL);
- a considerable rise of blade tip displacement (about 6% for the INWIND.EU and 2.5% for the NREL);
- a lower impact of fatigue loads on the life-cycle of both turbines.

The key role apparently played by the increase of blade tip displacements on the overall machine behaviour has highlighted the possibility to explore a conceptual redesign of blade to understand if and how such control impacts on its structural integrity.

In this regard, in the final step of the study, we have provided a structural redesign of a 10 MW rotor equipped with WF control comparing characteristics and main performances of the two solutions:

- the redesigned blade shows higher thickness of sectional elements resulting in a 12% increment of mass;
- the final turbine shows about 0.4% increment of Cost of Energy;
- both turbines experience the same blade tip displacement showing that it is an active constraint during the whole structural design of the machine;
- a substantial increase of tower top and hub centre loads.

The study has shown the fundamental need to provide a conceptual redesign of the blade, and plausibly of other components of the turbine, once the original wind turbine has been retrofitted with the investigated WF control strategy. Despite this, it should be emphasised that the work has been carried out in accordance with the regulations currently in force regarding individual turbines because dedicated standards for the wind farm design have still not been issued at present. It should therefore be assessed whether using current guidelines constitutes a serious limitation in the overall evaluation of the validity of the study. For example, design load cases such as DLC 1.4 have been found to be very penalising in all the studied conditions. However, these cases model an unlikely gusty wind which is relatively rare to occur and might possibly be avoided using novel closed-loop detection techniques. Consequently, as a future project it would be interesting to understand how and whether to change the current regulations by defining laws that provide for these aspects. In any case, these considerations do not affect the consistency of the results obtained in the Thesis. In this light, it must be clear that to carry out a rigorous and systematic study it is necessary to use consistent methodologies from the initial definition of the work. It is in this perspective that we have decided to use current guidelines. Furthermore, the study could also be enriched by considering other conceptual designs of turbines, including cases of carbon blades, for which, typically, the main design driver is not the ultimate displacement. This could highlight that results might vary according to different design configurations. Another possible future development could be investigating other wind farm control techniques, as illustrated in Chapter 2, to understand which ones are able to provide more convincing results. From this perspective, it would be interesting to understand what actually happens downstream of a turbine. The need for a redesign has emerged, but considering the development of a new wind farm, it is essential to know if driving and re-energizing the wake can still be cost-effective. However, this entails the implementation of mathematical models that allow for the correct modelling of the wake and the development of cost models able to consider the mutual interaction existing in wind plants. It would therefore be engaging to investigate the real possibilities of expanding Cp-Max by implementing a collective rather than an individual turbine design. Another possibility to explore is that of creating physical and mathematical predictive models able to foresee the behaviour of the loads on the turbines. In this way, we could quickly evaluate the countermeasures to adopt in order to avoid potential problems. Lastly, several numerical instabilities

have often arisen throughout the study delaying the outcomes of the simulations. In this regard, it would be helpful to analyse the reasons in detail. However, these are likely to be caused by the implemented aerodynamic model (BEMT). Therefore, a possible future development could involve understanding if more refined techniques are necessary to represent yaw-misalignment in greater details.

Bibliography

[1] *Advantages and Challenges of Wind Energy*. Office of energy efficiency and renewable-energy. URL: https://www.energy.gov/eere/wind/advantages-and-challenges-wind-energy (cit. on p. 1).

[2] *Annual Statistics*. 2018. URL: https://windeurope.org/wp-content/uploads/files/about-wind/statistics/WindEurope-Annual-Statistics-2018.pdf (cit. on p. 1).

[3] *Closed Loop Wind Farm Control*. Cl-Windcon. URL: http://www.clwindcon.eu (cit. on p. 2).

[4] T. Göçmen et al. "Wind turbine wake models developed at the technical university of Denmark: A review". In: *Renewable and Sustainable Energy Reviews* 60 (July 2016), pp. 752–769 (cit. on p. 2).

[5] T. Burton et al. *Wind Energy Handbook*. 2011 (cit. on p. 2).

[6] R. Barthelmie et al. "Modelling the impact of wakes on power output at Nysted and Horns Rev". In: *European Wind Energy Conference and Exhibition 2009, EWEC 2009* 2 (Jan. 2009) (cit. on pp. 2, 6).

[7] P. Fleming et al. "Initial results from a field campaign of wake steering applied at a commercial wind farm – Part 1". In: *Wind Energy Science* 4 (May 2019), pp. 273–285 (cit. on p. 3).

[8] P. Gebraad and J.W. Wingerden. "Maximum power-point tracking control for wind farms". In: *Wind Energy* 18 (Feb. 2014) (cit. on p. 2).

[9] M. Dijk et al. "Yaw-Misalignment and its Impact on Wind Turbine Loads and Wind Farm Power Output". In: *Journal of Physics: Conference Series* 753 (Sept. 2016), p. 062013 (cit. on p. 2).

[10] *Global Warming of 1.5 °C*. 2018. URL: https://report.ipcc.ch/sr15/pdf/sr15_spm_final.pdf (cit. on p. 5).

[11] J. Rogelj et al. "Paris Agreement climate proposals need a boost to keep warming well below 2 °C". In: *Nature* 534 (June 2016), pp. 631–639 (cit. on p. 5).

[12] *Annual Energy Outlook*. 2018. URL: https://www.eia.gov/outlooks/aeo/pdf/AEO2018.pdf (cit. on p. 5).

[13] C.L. Archer and M. Jacobson. "Evaluation of global wind power". In: *Journal of Geophysical Research* 110 (June 2005) (cit. on p. 5).

[14] K.E. Johnson and N. Thomas. "Wind farm control: Addressing the aerodynamic interaction among wind turbines". In: July 2009, pp. 2104–2109 (cit. on p. 5).

[15] J.K. Lundquist et al. “Publisher Correction: Costs and consequences of wind turbine wake effects arising from uncoordinated wind energy development”. In: *Nature Energy* 4 (Mar. 2019) (cit. on p. 6).

[16] J.Å. Dahlberg. “Load/fatigue effects on a wind turbine generator in a wind farm”. In: *Journal of Wind Engineering and Industrial Aerodynamics - J WIND ENG IND AERODYN* 39 (Dec. 1992), pp. 199–209 (cit. on p. 6).

[17] V. Spudic T. Horvat and M. Baotic. “Proceedings of the 35th International Convention MIPRO”. In: 2012, pp. 829–834 (cit. on p. 7).

[18] J. Lee. In: *Renewable Energy* 54 (2013), pp. 124–130 (cit. on p. 7).

[19] J. Annoni et al. “Analysis of axial-induction-based wind plant control using an engineering and a high-order wind plant model”. In: *Wind Energy* 19 (Aug. 2015) (cit. on p. 7).

[20] J. Bartl and L. Sætran. “Experimental testing of axial induction based control strategies for wake control and wind farm optimization”. In: *Journal of Physics: Conference Series* 753 (Sept. 2016), p. 032035 (cit. on pp. 7, 8).

[21] C. Santoni et al. “Development of a high fidelity CFD code for wind farm control”. In: *Proceedings of the American Control Conference* 2015 (July 2015), pp. 1715–1720 (cit. on p. 8).

[22] P. Gebraad et al. “A Data-Driven Model for Wind Plant Power Optimization by Yaw Control”. In: June 2014 (cit. on p. 9).

[23] P. Fleming et al. “Simulation comparison of wake mitigation control strategies for a two-turbine case”. In: *Wind Energy* 18 (Oct. 2014) (cit. on pp. 9, 10).

[24] J.T.Heinen et al. “Wake-steering demonstration model. Scaled demonstration model to show the effects of wake steering within a wind farm.” PhD thesis. June 2018 (cit. on p. 10).

[25] A. Jimenez and A. Crespoand E. Migoya. “Application of a LES technique to characterize the wake deflection of a wind turbine in yaw”. In: *Wind Energy* 13 (Sept. 2009), pp. 559–572 (cit. on p. 10).

[26] P. Gebraad et al. “Wind plant power optimization through yaw control using a parametric model for wake effects—A CFD simulation study”. In: *Wind Energy* (Dec. 2014) (cit. on p. 10).

[27] S. Raach, D. Schlipf, and P.W. Cheng. “Lidar-based wake tracking for closed-loop wind farm control”. In: *Journal of Physics: Conference Series* 753 (Sept. 2016), p. 052009 (cit. on p. 11).

[28] M. Bart, P. Fleming, and J. van Wingerden. “A tutorial on the synthesis and validation of a closed-loop wind farm controller using a steady-state surrogate model”. In: *ArXiv* abs/1810.12066 (2018) (cit. on p. 11).

[29] P. Fleming et al. “Evaluating techniques for redirecting turbine wake using SOWFA”. In: *Renewable Energy* 70 (Oct. 2014), pp. 211–218 (cit. on p. 12).

[30] J. Wang, C. Bottasso, and F. Campagnolo. “Wake redirection: comparison of analytical, numerical and experimental models”. In: *Journal of Physics: Conference Series* 753 (Sept. 2016), p. 032064 (cit. on p. 12).

[31] J. Park and K.H. Law. "Cooperative wind turbine control for maximizing wind farm power using sequential convex programming". In: *Energy Conversion and Management* 101 (Sept. 2015) (cit. on p. 13).

[32] C. Bak, R. Bitsche, and A. Yde. *The DTU 10-MW Reference Wind Turbine*. 2013 (cit. on pp. 14, 15).

[33] J. Jonkman et al. "Definition of a 5MW Reference Wind Turbine for Offshore System Development". In: *National Renewable Energy Laboratory (NREL)* (Jan. 2009) (cit. on pp. 14, 17).

[34] C. Bak, J. Johansen, and P. Andersen. "Three-Dimensional Corrections of Airfoil Characteristics Based on Pressure Distributions". In: (Jan. 2006) (cit. on p. 16).

[35] J.P. Blasques. "User's Manual for BECAS: A cross section analysis tool for anisotropic and inhomogeneous beam sections of arbitrary geometry". In: 2012 (cit. on p. 16).

[36] M.H Hansen and L.C Henriksen. *Basic DTU Wind Energy controller*. English. Denmark: DTU Wind Energy, 2013 (cit. on p. 17).

[37] Ikerlan. *OpenDiscon*. `https://github.com/ielorza/OpenDiscon`. 2017 (cit. on p. 17).

[38] *REpower 5M*. 2005. URL: `http://www.repower.de/typo3/fileadmin/download/produkte/5m_uk.pdf` (cit. on p. 17).

[39] D. Griffin. "WindPACT Turbine Design Scaling Studies Technical Area 1Composite Blades for 80- to 120Meter Rotor". In: (Jan. 2001) (cit. on p. 17).

[40] Niels Jacob Tarp-Johansen's. *RECOFF Home Page*. 2004. URL: `gttp://www.risoe.dk/vea/recoff/` (cit. on p. 17).

[41] H. Hendriks et al. "DOWEC concept study; evaluation of wind turbine concepts for large scale offshore application". In: (Jan. 2000) (cit. on p. 17).

[42] *Wind Turbine Blades*. LM Glasfiber Group. URL: `https://www.lmwindpower.com/` (cit. on p. 18).

[43] C. Riboldi. "Advanced control laws for variable-speed wind turbines and supporting enabling technologies". PhD thesis. Politecnico di Milano, 2012 (cit. on p. 20).

[44] International Electrotechnical Commission. *IEC 61400-1 Wind Turbines - Part 1: Design Requirements*. 2006 (cit. on pp. 35, 47).

[45] A. Croce, C. Bottasso, and B. Savini. "Aero-servo-elastic modeling and control of wind turbines using finite-element multibody procedures". In: *Multibody System Dynamics* 16 (Oct. 2006), pp. 291–308 (cit. on p. 40).

[46] B. Jonkman and B. Jr. "TurbSim User's Guide". In: (Jan. 2007) (cit. on p. 41).

[47] C. Bottasso, F. Campagnolo, and A. Croce. "Multi-disciplinary constraint optimization of wind turbines". In: *Multibody System Dynamics* 27 (July 2012), pp. 21–53 (cit. on p. 41).

[48] S. Jaiswal. "Shape Parameterization of Airfoil Shapes Using Bezier Curves". In: Sept. 2017, pp. 79–85. ISBN: 978-981-10-1770-4 (cit. on p. 45).

[49] V. Giavotto, M. Borri, and P. Mantegazza. “Anisotropic beam theory and applications”. In: *Computers and Structures* 16 (Dec. 1983), pp. 403–413 (cit. on p. 46).

[50] L. Sartori. “System design of lightweight windturbine rotors”. PhD thesis. Politecnico di Milano, 2019 (cit. on p. 46).

[51] International Electrotechnical Commission. *IEC 61400-12-1 Wind Turbines - Power performance measurements of electricity producing wind turbines*. 2005 (cit. on p. 49).

[52] M.Cardaun et al. “Analysis of Wind-Turbine Main Bearing Loads Due to Constant Yaw Misalignments over a 20 Years Timespan”. In: *Energies* 12 (May 2019), p. 1768 (cit. on p. 47).